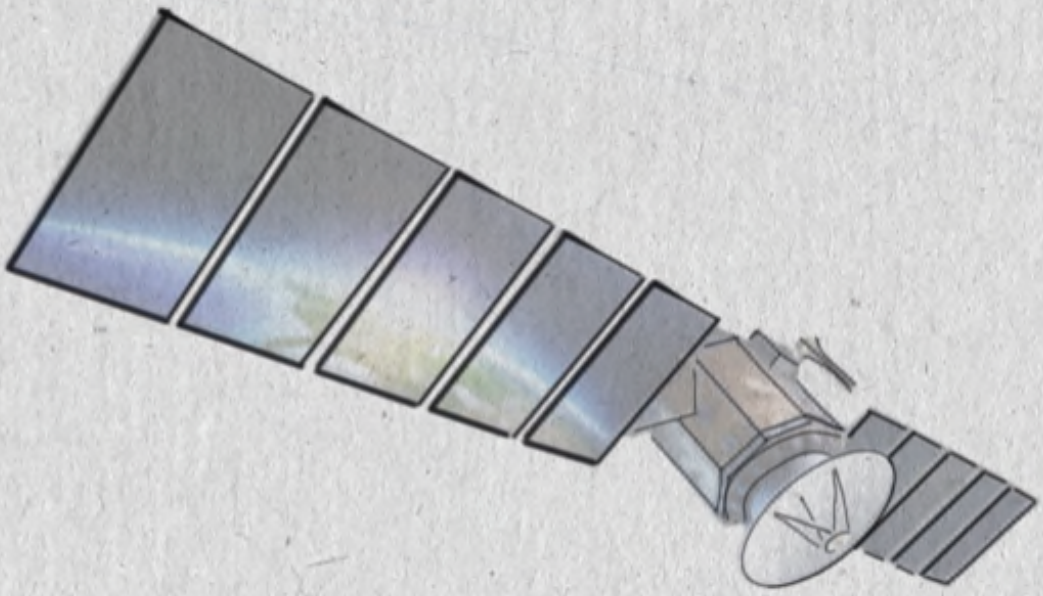

Satellite Soil Moisture Retrieval

Validation and Analysis of Satellite Retrieved Soil Moisture in the Tropics, a case study in Myanmar

MSc. Thesis I.H. de Kat

VanderSat

TU Delft

Satellite Soil Moisture Retrieval

Validation and Analysis of Satellite Retrieved Soil Moisture in the Tropics, a case study in Myanmar

by

I.H.(Ileen) de Kat

to obtain the degree of Master of Science
at the Delft University of Technology,
to be defended publicly on March 19^{th} 2021 at 14:00.

Student number:	4224647	
Project duration:	January, 2020 – xx, 2021	
Thesis committee:	Dr. T.A. Bogaard,	TU Delft, supervisor
	Prof. Dr. ir. S. Steele-Dunne,	TU Delft
	Dr. M.A. Schleiss,	TU Delft
	Ir. T. van der Horst.	VanderSat

This thesis is confidential and cannot be made public until March 19^{th} *2021*

TU Delft

Preface

While writing this report, *Satellite Soil Moisture Retrieval, a case study in Myanmar*, I can reflect on an experience with many up and downs. With a bag full of equipment I went to Myanmar in February 2020, and right from the start I was warmly welcomed by the friendly Myanmar People. Although the trip was cut short by two months due to the corona virus, I have learned a lot during the month that I was there. I have installed the sensors with the help of the staff at the Irrigation Technology Centre and they have continuously given data ever since. I want to thank VP Delta for the opportunity to go here. Furthermore I would like to thank the Irrigation Technology Centre for their hospitality and support, especially staff officer Sai Wunna for his guidance during and after the fieldwork.

This thesis is the final product of my master thesis in Environmental Engineering at the Delft University of Technology. This research would not have been possible without the equipment and datasets that were provided by VP Delta and Vandersat. Four brand new dataloggers that I installed in Myanmar and that connected to the cloud to provide me with constant information. The satellite products of VanderSat that were made available, and the code in python for Land Parameter Retrieval Model that was used for the parameterisation.

I am very grateful for those who helped me during the writing of my thesis. First of all I would like to thank the committee members of my thesis. Many thanks to my supervisor Thom Bogaard, who guided me from the start, during the first week in Myanmar to the bi-weekly zoom meetings and the small but important deadlines near the end. I want to thank Teije van der Horst, my supervisor from VanderSat, who extensively mentored me during the course of this research. He was always available when needed and helped my out with any question ranging from programming to report set up. My sincerest gratitude goes out to Susan Steele-Dunne, who was the one that got me interested in this subject and connected me to VanderSat. Thank you for the sharp feedback and showing me to the right direction in the endless amount of literature on the subject. I would like to thank Marc Schleiss for the new insights and fresh perspective on the report, while I was buried into the subject. Finally I would like to thank all my committee members for the time and support they gave me during the difficult time in my family.

Last but not least, I would like to thank the people that supported me during the ups and downs op this entire process. First of all I would like to thank my mother for the endless support, love and encouragement, but also for reading and correcting and giving me new insights. I would like to thank my father for his support and the beautiful front page he created. Many thanks to my brother for the the endless calls and use of his office as a study cave in weeks with deadlines and my sister for the reading and cooking and always being ready to listen. A special thanks goes out to my boyfriend, Marijn, who has dragged me through my entire thesis, who was always there for me and gave me love and support throughout the entire process.

I would like to end this preface with a note on the current situation in Myanmar. As of the first of February 2021 a military coup took place in Myanmar. The leader Aung San Suu Kyi was arrested and the military is in charge and declared a year-long state of emergency. Many large-scale protest have been organised and some ended deadly. My heart goes out to all the people in Myanmar and I sincerely hope a democratic regime will be reestablished soon.

Ileen de Kat
Rotterdam, March 12^{th} *2021*

Abstract

The validation of satellite retrieved soil moisture over a tropical region (Bago, Myanmar) has been conducted in this research. The downscaled soil moisture products of VanderSat using the Land Parameter Retrieval Model, were compared with an in-situ soil moisture network that operated between 2017 and 2018 and a newly placed network installed during a fieldwork trip early 2020. Soil moisture is a key variable in the hydrological cycle, but the understanding of soil moisture content in tropical areas like Myanmar is substandard. This study provides new insights, being one of the first of its kind in the tropics. The reliability of both in-situ soil moisture networks was analysed and indicated that the 2017 network could be used for the validation, and the 2020 network for a visual comparison, with a focus on the soil temperature as a source of error. The results of the validation showed high correlation with Pearson's R ranging between 0.70 and 0.89. The highest correlations were found for the L-band, between 0.78 and 0.89 and for the location Hpayargyi. The root mean square difference (RMSD), unbiased RMSD and bias indicated that the accuracy and precision need improvement. For the ubRMSD values between 0.059 m^3/m^3 and 0.129 m^3/m^3 are found. The best result is found for the L-band at Hpayargyi, which is the only location/band combination that meets the target accuracy of 0.06 m^3/m^3 that is often set for SMAP satellite retrieval. The visual comparison of the 2020 network showed good agreement for the soil moisture measurement. When the in-situ soil temperature measurements were compared with the satellite retrieved land surface temperature measurement, however, this resulted in a large bias of approximately 15 degrees Celsius. To evaluate possible improvements for the validation result, several sources of errors were explored. Two sources concerning the in-situ network indicated the challenges of an in-situ network in a remote tropical area. The first showed that re-calibration of the sensor is necessary to improve representation of the ground truth. The second discussed the spatial mismatch between the point scale in-situ measurement and the downscaled satellite products, with a pixel size of 100x100m. The sparse in-situ network with four stations cannot represent the entire area and can therefore result in errors. The other sources of errors that were discussed originated from the retrieval algorithm of the Land Parameter Retrieval Model. A parameterisation was performed to assess the sensitivity of the ubRMSD to the polarisation mixing factor (Q), the single scattering albedo (ω) and the roughness parameters (h1 and h2). The parameters were optimised to achieve the lowest ubRMSD, the result indicated that an improvement of the ubRMSD up to 40% can be achieved. However the evidence that linked the optimised parameters to the tropics was not found and it was concluded that the optimising could be covering the large temperature bias, that is a direct input in the Land Parameter Retrieval Model. The large bias in the temperature was evaluated as a source of error. The bias can partially be explained by the masking of water bodies, where the dynamic effect of the tropical monsoon on the water bodies is not taken into account. Another explanation for the bias could potentially be found in the emissivity that is determined by optimising the ΔT, which can cause imperfections in the prediction of the temperature. It was concluded that the satellite retrieved soil moisture products show good correlation but need improvement in accuracy and precision. This can be accomplished by updating the in-situ soil moisture network, creating new water masks, solving the retrieval algorithm for the temperature bias and then optimising tropical specific location parameters.

Ileen de Kat
Rotterdam, March 12^{th} *2021*

Contents

List of Figures

List of Tables

Abbreviations

AMSR	Advanced Microwave Scanning Radiometer (for Earth Observation system)
CCI	Climate Change Initiative
CDZ	Central Dry Zone
DMH	Department of Meteorology and Hydrology
ESA	European Space Agency
FLDAS	Famine Early Warning Systems Network Land Data Assimilation System
GDP	Gross Domestic Product
HWSD	Harmonised World Soil Database
ITC	Irrigation Technology Centre
LPRM	Land Parameter Retrieval Model
MERRA	Modern-Era Retrospective analysis for Research and Applications
MODIS	Moderate Resolution Imaging Spectroradiometer
MPDI	Microwave Polarisation Difference Index
NASA	National Aeronautics and Space Administration
NDVI	Normalized Difference vegetation Index
RMSD	Root Mean Squared Difference
RMSE	Root Mean Squared Error
RSS	Residual Sum of Squares
SMAP	Soil Moisture Active Passive
SMOS	Soil Moisture and Ocean Salinity
ubRMSD	unbiased Root Mean Squared Difference
VOD	Vegetation Optical Depth

1

Introduction

The yearly Thingyan festival, a water festival to celebrate their new year, shows that Myanmar is a country in which water plays a central role. Along their large coasts and many long rivers their water resources are well provided. The delta plains have fertile soil in which agriculture such as rice fields thrive. The weather in Myanmar is affected by the monsoon climate. During the wet season almost 90% of the annual rainfall pours down (Naing, 2007). This means that the country is highly reliant on both the weather and irrigation to distribute the water. The government has invested in dams and other water regulating structures to limit the dependency on the rain. The Ministry of Agriculture, Livestock and Irrigation is in charge of the water regulation, and each of the township's Agriculture Coordinating Committee manages it's local irrigation systems. To construct irrigation schemes or decide which crops to grow, soil moisture is of great importance. The long dry periods that Myanmar experiences each year lead to a shortage of soil moisture, and thereby affect the crop productivity. Which means soil moisture is a very important factor, and more knowledge on the distribution could be of large value.

Soil moisture is the water stored in the unsaturated soil zone, which is the part of the soil that is above the groundwater table. Precipitation is the main source of water in the unsaturated soil zone. The water retention capacity depends on texture of the soil. " Soil moisture is an important link between the exchange of water and energy at the soil-atmosphere phase" (de Jeu, 2003). The incoming radiation of the sun leaves the soil in latent heat. The latent heat creates evaporation. This means that water from the soil moves into the atmosphere. This evaporation of water results in an energy flux that is controlled by the soil moisture content. This way soil moisture can have an impact on weather patterns and climate variability, even though it only represents a small amount of the fresh water cycle in the atmosphere. Therefore, soil moisture is a crucial variable in a wide variety of processes and applications, including numerical weather prediction, flood forecasting, agricultural drought assessment, water resources management, greenhouse gas accounting, civil protection, and epidemiological modeling of water-borne diseases (Dorigo et al., 2013). Soil moisture measurements have been conducted since years and several methods have been used, such as in-situ soil moisture networks and remotely sensed soil moisture. Unfortunately the amount of in-situ soil moisture sensors in tropical areas like Myanmar is extremely low. This results in the fact that the understanding of the soil moisture content in these areas is substandard.

During this research a soil moisture network was installed in Bago, Myanmar. This network and a previous network were compared with satellite retrieved soil moisture products. The measured in-situ data was compared to the satellite products from a Dutch company: "VanderSat". VanderSat uses microwave satellites to measure soil moisture levels. The set of data is very detailed and has daily availability. The accuracy of satellite soil moisture measurement is still a challenge, but the large scale of the measurements creates many possibilities. These satellite measurements cover larger areas and are not in need of placement and maintenance. However the measurements of the satellite need to be validated to create a reliable product. To validate and improve the satellite retrieved soil moisture a network of in-situ soil moisture sensors was installed in the vicinity of the Irrigation Technology Center in Bago. This network not only provides soil moisture measurements, in addition soil temperature is measured. This means it is the first of its kinds in the tropics.

1.1. Research questions

The objective of this research was to install a reliable in-situ soil moisture network in Bago, Myanmar, which can be used for the validation of remotely sensed soil moisture products. Furthermore the objective was to validate satellite soil moisture products with a previously placed in-situ soil moisture network and to find possible sources for the errors that resulted from the validation.

The research questions that are formed to meet this objective are the following:
Main question:

- **How can the satellite retrieval of soil moisture in the tropics be improved, focusing on an in-situ network to validate and analyse satellite measurements?**

Sub questions:

- **What challenges are encountered when setting up an in-situ soil moisture network in tropic conditions, and how can they be dealt with?**
- **Do the in-situ soil moisture networks at 4 locations in Myanmar provide a reliable product?**
- **How do satellite soil moisture products perform in tropic conditions, compared to an in-situ soil moisture network?**
- **What could be possible sources for the errors that are found in the validation?**

1.2. Report outline

Part	Description	Chapter	Content
	Introduction	Chapter 1	Introduction Research questions
Part I	Background Information	Chapter 2	Myanmar and Bago
		Chapter 3	Soil Moisture Measurement Techniques
Part II	In-situ Soil Moisture Measurements	Chapter 4	Materials and Methods
		Chapter 5	Results In-Situ Soil Moisture Measurements
		Chapter 6	Discussion In-Situ Soil Moisture Set-Up and Measurements
Part III	Remote Sensing Analysis	Chapter 7	Data and Methods
		Chapter 8	Result Remote Sensing Analysis
		Chapter 9	Discussion Remote Sensing Analysis
Part IV	Conclusions	Chapter 10	Conclusion and Recommendations

Table 1.1: Outline of this thesis

In Chapter 1 *Introduction* the subject and importance of this research is introduced, and the research questions to be answered in this thesis are given. The outline for the report is shown.
Chapter 2 *Myanmar and Bago* describes the study area of this research, Bago, Myanmar. A focus lies on the tropical monsoon climate and various soil types and land cover.
In Chapter 3 *Soil Moisture Measurement Techniques* the theory behind the soil moisture measuring techniques is discussed. The International Soil Moisture Network is briefly explained. Microwave remote sensing is explained and the retrieval algorithm of the Land Parameter Retrieval Model is elaborated. Finally the downscaling technique of VanderSat is explained.
Chapter 4 *Materials and Methods* describes the network set-up of the fieldwork that was carried out in February and March 2020 in Bago, Myanmar. The the network that was placed in 2017 is discussed shortly. The methods to establish the reliability of the in-situ networks is described.

Chapter 5 *Results In-Situ Soil Moisture Measurements* shows the results of the measured soil moisture from the two networks. The timeseries of both networks are shown, basics statistic and notable pattern are described. The reliability of the 2017 network and 2020 network are discussed.
Chapter 6 *Discussion In-Situ Soil Moisture Network Set-Up and Measurements* describes the challenges that were encountered during the set-up and afterwards. The results and performance of the two networks and there reliability are discussed. It answers the first two sub questions.
In Chapter 7 *Data and Methods* the data and methods that are used for Part III, Remote sensing analysis, will be introduced. The satellite products are introduced and the parameters that are used in the Land Parameter Retrieval Model are described. The methods for validation and error analysis are described, including the parameterisation and preliminary comparison of the 2020 network and temperature bias.
Chapter 8 *Result Remote Sensing Analysis* shows the results of the validation and the error analysis, the optimal values found in the parameterisation are shown and the visual comparison of the new in-situ network versus the satellite products. Here possible sources of error for both the soil moisture and the temperature products are mentioned.
in Chapter 9 *Discussion Remote Sensing Analysis* discusses the results of the validation and error analysis. It answers the third and fourth sub questions.
In Chapter 9 *Conclusion and Recommendations* the conclusion of this research is given where the main research question and sub questions are answered and some recommendations for further research are given.

I

Part 1 Background Information

2

Myanmar and Bago

Myanmar, officially the Republic Union of Myanmar, is one of the largest countries in southeast Asia and it is located within the monsoon region of Asia. It is located between 9 deg and 38 deg N, and 92 deg and 101 deg E. The neighbouring countries are Bangladesh, India, China, Laos and Thailand (Figure 2.1). The south of Myanmar is bordered by the Andaman Sea and the Bay of Bengal. Myanmar can be divided into five major topographic and climatic zones: the mountainous region, the Shan Plateau, the (Central Dry Zone (CDZ)), the delta region and the coastal region, with a coastline of approximately 1930 kilometers long (FAO, 2016). The catchment and delta of the Irrawaddy river lie between two foothills of the Himalaya Mountains.The total population of Myanmar is 54,4 million people. About two thirds of the population of Myanmar lives in rural areas, of which around 80 percent is engaged in agricultural work. Agriculture includes crop production, livestock, fishery and forestry. Agriculture is the most important sector of the economy, generating 43 percent of the Gross Domestic Product (GDP), and the main source of livelihood for about 70 percent of the population of Myanmar (FAO, 2014, 2016, 2019).

The study area is located around Bago city, which is the capital of the Bago region and lies about 90 kilometers north-east of Yangon. The Bago region is indicated in yellow in the right image of Figure 2.1, Bago city is the black dot in this image. The Bago region is situated in the delta region of Myanmar. The fertile delta area has some of the most productive cropland in Myanmar. The cultivation of rice in flooded paddies predominates, 60 percent of the country's total rice crop is produced here. During the monsoon the rice production is rainfed, while in the dry season irrigation is used. (Frenken, 2012; JICA, 2013).

Figure 2.1: Geographical location of Myanmar in the world, Myanmar in yellow (Left), Bago region in Myanmar, Bago region in yellow (Right) with Bago city, black dot. Source: (Department of Population Ministry of Immigration and Population, 2015)

Climate

Myanmar has a typical tropical monsoon climate that consists of three seasons: the hot summer period, the southwest monsoon period and the cool and dry winter period. The hot period begins in March and lasts till mid May, with temperatures up to 40 °Celsius in Central Myanmar. The rainy monsoon season starts around mid May and ends in October, 90% of the annual rainfall is received in this period. The cool and dry period runs from November till February, with temperatures down to 16 °Celsius (Aung et al., 2017).

Bago city lies within the tropical zone, with monsoonal precipiation, Am according to the climate classification of the Koppen-Geiger climate zones (Figure 2.2a). Figure 5.9 shows the distribution of rainfall in Myanmar. The coastal region receives the most precipitation up to 5500 mm per year. The Mountainous area and the Shan plateau receive about 1250-3000mm, while in the CDZ less then 700mm precipitation falls per year. In the delta area between 2000-3500 mm falls each year (Naing, 2007). With 90% of the annual rainfall in the monsoon period, there is scarcity of water in the dry season all over the country, leading to severe droughts (FAO, 2019).

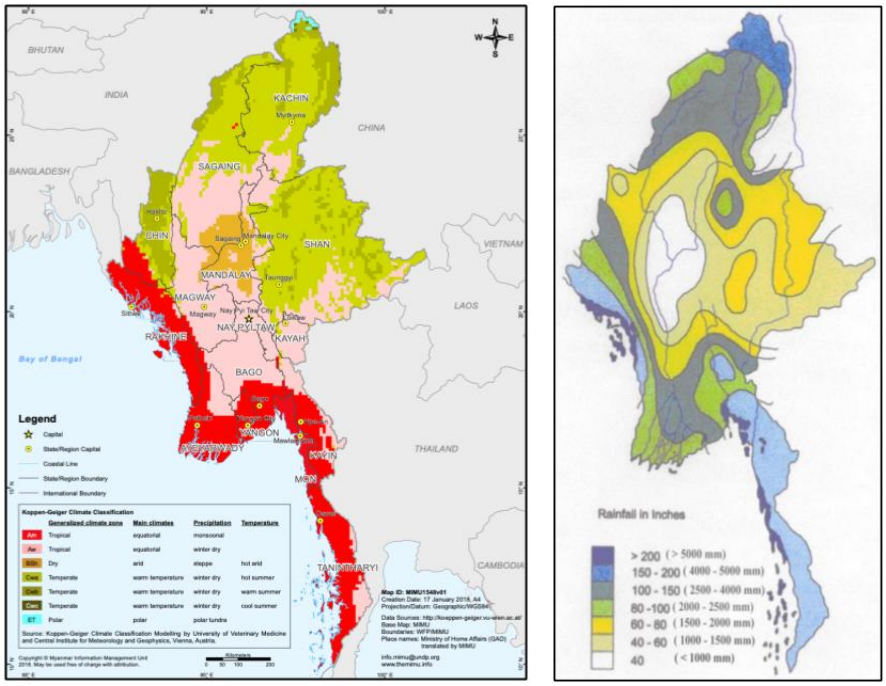

(a) Koppen-Geiger climate zones of Myanmar (1968-2010), source:http://koeppen-geiger.vu-wien.ac.at/ (b) Distribution of rainfall in Myanmar (FAO, 2016)

Figure 2.2: Figures on climate zones and rainfall distribution in Myanmar

The monsoon arrives in the southernmost part of the Andaman Sea about third week of May, then it gradually extends in northern direction and has covered the whole country by the first week of June. The Department of Meteorology and Hydrology (DMH) in Myanmar defines the onset of the monsoon at various places in Myanmar as the date of the first day of three consecutive rainy days with daily rainfall amount of 2.54mm or more (Htway & Matsumoto, 2011). Figure 2.3 indicates the normal monsoon on-set and off-set dates over Myanmar between 1981-2010, according to Aung et al. (2017). The Bago delta region is not sheltered by mountains and receives the full southwest monsoon. The annual rainfall in the delta region ranges from 2000-3500 mm (Naing, 2007). In Bago the monsoon on-set is expected around the 23^{rd} of May and the off-set around the 29^{th} of September (Aung et al., 2017).

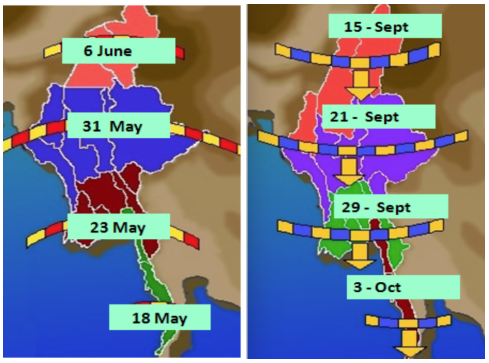

(a) On-set (b) Off-set

Figure 2.3: Normal monsoon on-set and off-set dates over Myanmar, between 1981-2010. Source:(Aung et al., 2017)

Soil types and land cover

While various soil types can be found in the regions of Myanmar, the surroundings of Bago City have two dominant soil types: Gleysols and Nitisols (Figure 2.4a), which can be retrieved from the (Harmonised World Soil Database (HWSD)) (`http://www.fao.org/soils-portal/data-hub/soil-maps-and-databases/harmonized-world-soil-database-v12/en/`). Gleysols are soils with permanent or temporary wetness near the surface. Nitisols are deep, dark red, brown or yellow clayey soils having a pronounced shiny, nut-shaped structure (Nachtergaele et al., n.d.).

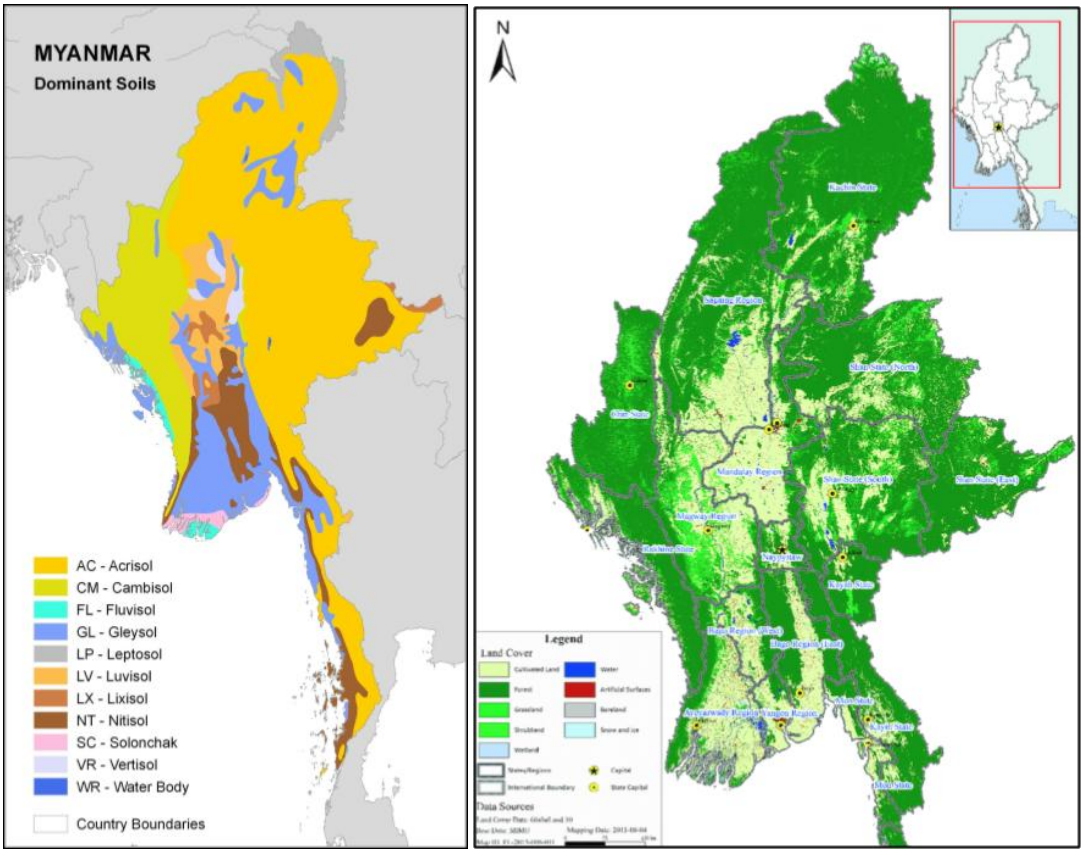

(a) Dominant soil types in Myanmar, source: (FAO, 2016) (b) Land cover in Myanmar, source: (FAO, 2014)

Figure 2.4: Geographical distribution of the dominant soil types and the land cover in Myanmar

In Myanmar the land cover mainly consists of cultivated land, forest and grassland (Figure 2.4b). In the mountainous areas and large parts of the coast, forest and grassland are predominant, while in the low areas in the CDZ and the delta area cultivated land is the most common land cover. The cultivated land around Bago city is divided in rainfed cropland and irrigated/post-flooding cropland (Figure 2.5).

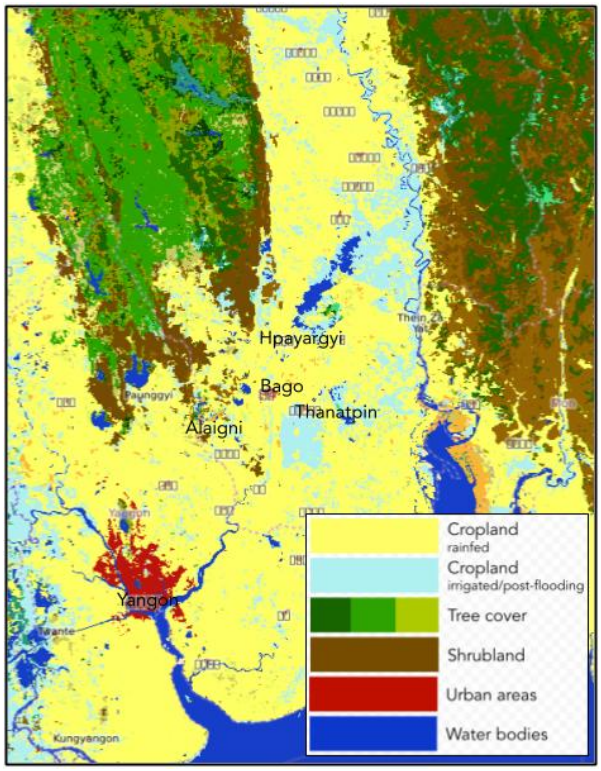

Figure 2.5: Landcover around Bago city, according to the ESA CCI (https://maps.elie.ucl.ac.be/CCI/viewer/)

3

Soil Moisture Measurement Techniques

3.1. In-situ soil moisture

In-situ measurements of soil moisture means the measurements are taking place at the exact location of choice. To measure the in-situ soil water content direct and indirect methods can be used. In situ-soil moisture is expressed in volumetric water content (θ), the ratio of water volume (V_{water}) to total soil volume(V_{soil})

$$\theta = \frac{V_{water}}{V_{soil}} \tag{3.1}$$

To directly measure soil water content, the percentage of water is calculated based on mass, gravimetric water content. This is done by comparing the amount of water, as a mass, to the total mass of the sample. The gravimetric water content (w) is multiplied by the bulk density (ρ_b) to get the volumetric water content(θ).

$$\theta = w * \rho_b \tag{3.2}$$

To measure volumetric water content indirectly, a parameter related to VWC is measured and a calibration is used to convert that amount to VWC. For this research sensors are used that an indirect method that is called capacitance technology.
Capacitance sensors use two probes, one with positive and one with negative charge, to form an electromagnetic field. The charge-strong capacity of the material between the probes is measured this way (Iksal, 2020).

International Soil Moisture Network

The International Soil Moisture Network (ISMN) `http://http//www.geo.tuwien.ac.at/en` is an international cooperation to establish and maintain a global in-situ soil moisture database. This database is an essential means for validating and improving global satellite products, and land surface, climate, and hydrological models (Dorigo et al., 2011). Taking part in the ISMN means being involved in cutting-edge research. Unfortunately the amount of soil moisture sensors in Asia and especially the tropical areas is low. To date, only a few Asian networks are involved, mostly in China, see Figure 3.1. This results in the fact that the understanding of the soil moisture dynamics in these tropical area's is substandard. The network that was placed during this research and the previous network were added to the ISMN and is thereby one of the first of its kind, in Figure 3.1 the network, named VDS, can be seen. In the Appendix B information can be found that was needed to participate in the ISMN and to continue the collaboration with the ISMN.

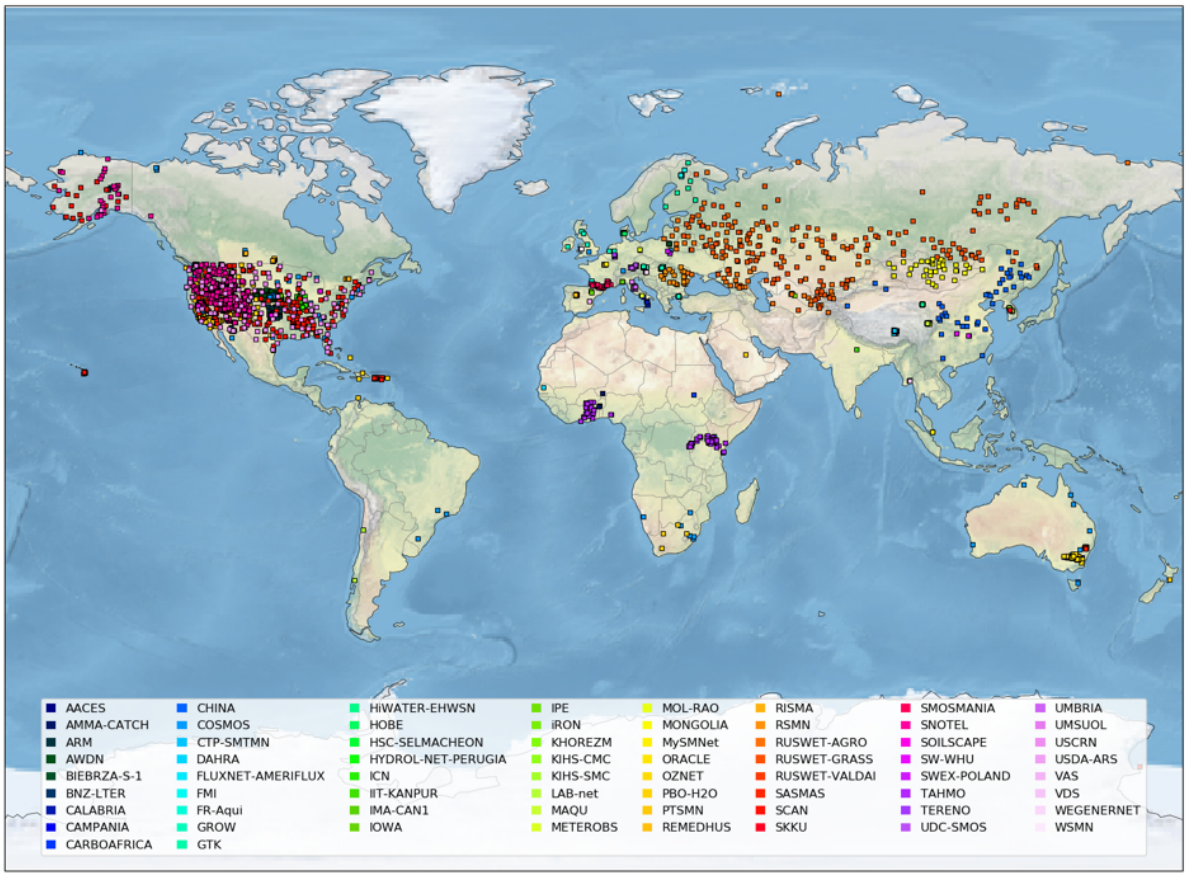

Figure 3.1: Locations of ISMN networks and sites, including the VDS network installed for this research. Source: (Dorigo et al., 2021)

3.2. Microwave Remote Sensing

Remote sensing is a technology to acquire observations and measurements without direct contact with the object. These measurements and observations are often done using satellites. Remote sensing can be applied along different wavelengths in the electromagnetic spectrum. Electromagnetic energy travels in waves through the atmosphere and space. These waves have different wavelengths and frequencies, where shorter wavelength indicates higher frequency. Longer wavelengths include radio, microwave and infrared, while ultraviolet, x-ray and gamma rays have a much shorter wavelength. The visible light, the light that the human eye is able to detect, sits in between these wavelengths. In Figure 3.2 an overview of the electromagnetic spectrum is shown. In this research the focus lies on microwave remote sensing. Microwaves have wavelengths of 0.1-100 cm. The big advantage of microwave wavelength is that it can penetrate through clouds. Furthermore no illumination from the sun is needed, so observations can be done day and night. In certain parts of the world the cloud coverage is very high, for example in Myanmar (Figure 3.3b). This type of remote sensing is therefore very useful in these areas to measure soil moisture.

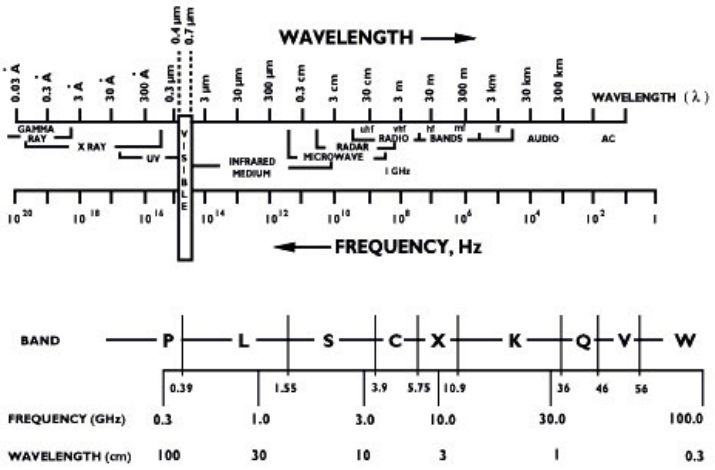

Figure 3.2: Electromagnetic spectrum and frequencies with bands, source: (ESA, n.d.)

The bottom part of Figure 3.2 shows the bands that are used in the microwave part of the electromagnetic spectrum, in this study the L-band, C-band and X-band were used. Figure 3.3a shows that L-band and C-band are not affected at all by the atmosphere and can therefore sense the surface. X and K band, 10-16 GHz, are often used for monitoring precipitation, because it can measure H_2O in the atmosphere. The sensing depths into the soil differs per band. The penetration depth is generally 1/3 of the wavelength. However, the penetration depth also depends on surface characteristics, where a wet soil has a smaller sensing depth than a dry soil.

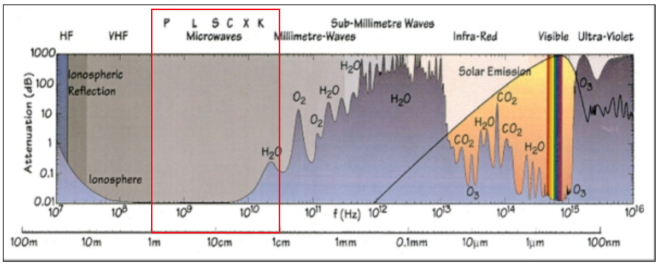

(a) Attenuation distribution of waves in the atmosphere

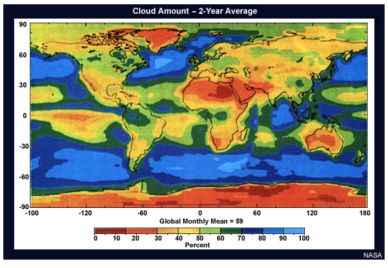

(b) Global average amount of cloud coverage

Figure 3.3: Attenuation distribution and cloud coverage.

A distinction is made between passive and active remote sensing. Passive remote sensing employs natural sources energy, for example the sun, the earth itself or a combination. Active remote sensing provides its own source of energy and measures the energy that is reflected back. The disadvantage of passive microwave remote sensing is that the low frequency of the microwaves leads to less energy, and a larger 'field of view' is needed compared to other measurement techniques. A larger 'field of view' results in lower resolutions. VanderSat uses passive microwave remote sensing therefore this research focuses on passive microwave remote sensing.

Since the 1970's several satellites have retrieved brightness temperatures with passive microwave remote sensing. Brightness temperature can be translated to multiple parameters such as soil moisture, surface temperature and vegetation optical depth. The products in this research are from VanderSat (C-band, L-band and X-band) and National Aeronautics and Space Administration (NASA)(L3) and are obtained from the Advanced Microwave Scanning Radiometer (for Earth Observation system) (AMSR), AMSR2 and Soil Moisture Active Passive (SMAP) satellites. Brightness temperatures were retrieved from satellite microwave measurements and translated to soil moisture and vegetation optical depth by using the Land Parameter Retrieval Model (LPRM) (Owe, de Jeu, & Holmes, 2008). VanderSat developed a downscaling technique that results in a higher resolution (de Jeu et al., 2017).

Brightness temperature

The brightness temperature that is retrieved from the microwave remote sensing is proportional to temperature, when considering the Rayleigh Jeans approximation of Planck's law, shown in formula (3.3). Planck's law is an expression for the amount of energy that a body radiates at different frequencies.

$$\text{Planck's law:} B_f = \frac{2hf^3}{c^2} \frac{1}{e^{\frac{hf}{kT}} - 1} \tag{3.3}$$

Where:

B_f	=	Spectral radiance of a body
h	=	Planck constant
c	=	Speed of light
f	=	Frequency
k	=	Boltzmann constant
T	=	Absolute temperature

Due to the low frequencies in microwave remote sensing the term (hf/kT) can be assumed to be much less then 1, which leads to a relatively simple expression. The approximation is a description of how the radiance depends on the temperature. The exponent term of the expression is much smaller than one therefore, the brightness temperature is proportional to the actual temperature(Equation 3.4. This proportion can be explained by the emissivity. The brightness temperature can be explained as the apparent temperature of a surface, assuming that it had a surface emissivity of 1 at a given frequency. Defining the brightness temperature (T_B), at a given frequency (f), wavelength(λ) and polarization(p) as the product of the physical temperature (T) and the surface emissivity(e_S):

$$T_B = e_S * T \tag{3.4}$$

Emissivity is the ratio of the thermal radiation from a surface compared to an ideal black surface. This results in the fact that in reality all objects have emissivities lower than 1. This means that the brightness temperature is measured by microwave remote sensing is lower than the actual air temperature.
The brightness temperature of the soil is highly dependent on the soil moisture content. With soil moisture, the amount of water that is present in the capillary layer of the soil, the emissivity rises. Since there is a relation between emissivity and dielectric constant the brightness temperature can be used to determine the soil moisture content. Besides soil moisture content there are other influences on the brightness temperature such as roughness of the soil surface, emission by vegetation cover, variability of soil texture and temperature. These influences can be distinguished by the fact that it is possible to polarize the brightness temperature in horizontal and vertical direction. The horizontal polarization results in higher sensitivity for soil moisture and

vegetation while the vertical polarization results in higher resolution temperature estimations. To eliminate the influence of the vegetation it is possible to use longer wavelengths, these penetrate vegetation and soil better. Longer wave lengths occur with lower frequency spectra such as C-band and L- band.
As mentioned above the brightness temperature is affected by a large variety of factors. Since it is possible to measure the brightness temperature by the microwave remote sensing, these factors of influence can be determined. Since vegetation absorbs and scatters the emitted soil radiation and has its own emissivity it is needed to identify these effects. With the omega tau model, see Formula 3.5, it is possible to take into account the influence of the vegetation.

$$T_B = T_{eff} e_r \Gamma_v + T_c(1-\omega)(1-\Gamma_v) + T_c(1-e_r)(1-\omega)(1-\Gamma_v)\Gamma_v \tag{3.5}$$

Where:

T_{eff}	=	Effective surface temperature
$e_{r(P)}$	=	Rough surface emissivity for H- or V-polarized radiation
Γ_v	=	Vegetation transmissivity
T_c	=	Canopy temperature
ω	=	single scattering albedo

The value of Γ_v is defined as:

$$\Gamma_v = exp(\frac{-\tau_v}{cosu}) \tag{3.6}$$

Where:

τ_v	=	vegetational optical depth
u	=	incidence angle

The τ-ω model can be used to distinguish the effects on the microwave emission of the soil and the vegetation. Important to note is the fact that the soil emits radiation and the vegetation itself emits radiation as well. If there is a higher canopy density, the soil radiation drops and the radiation of the vegetation increases. In this model the first term describes the radiation coming from the soil, that is attenuated by the canopy. The second term describes the radiation that is coming from the vegetation and the third term describes the downward radiation from the vegetation that is reflected by the soil, which depends on soil dielectric properties. This is shown in figure 3.4.

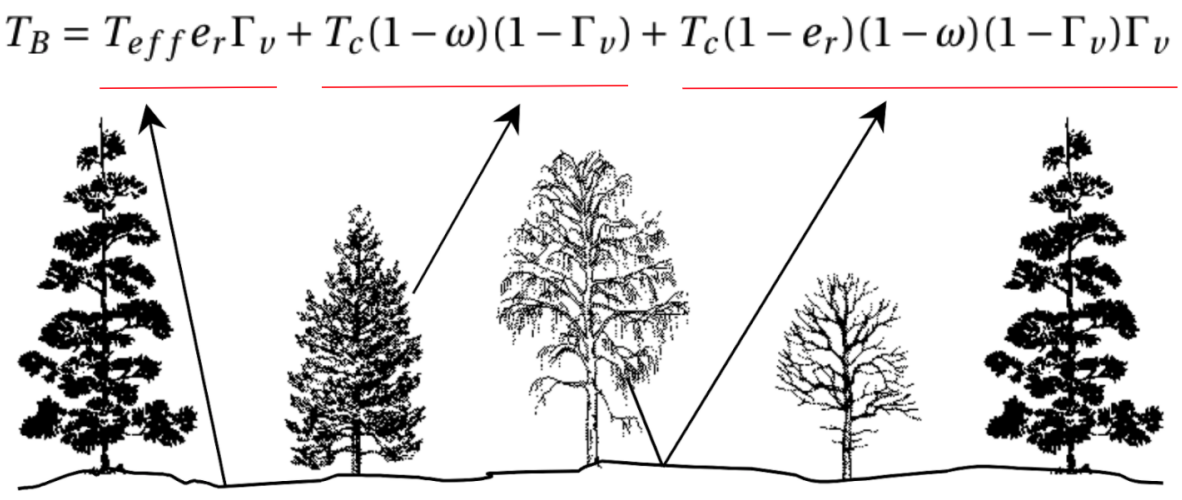

Figure 3.4: τ-ω model, source de Jeu (2003)

In each of the three terms, vegetation optical depth (τ) is of influence. This optical depth is dependent of the canopy density. The temperatures of the soil and the canopy often differ, but at 6 in the morning the temperatures are approximately even, so they can be related. To determine the rough surface emissivity first the dielectric constant has to be calculated. This constant can be computed by the dielectric mixing model. Then the smooth surface emissivity is determined by combining both the horizontally and the vertically polarized waves with the Fresnel equations. Finally the model of Wang and Choudhury (1980) was used to calculate the rough surface emissivity. This is embedded in the following formula:

$$e_{r(P1)} = 1 - ((1-Q)R_{(P1)} + QR_{(P2)}) * e^{-h*cosu} \tag{3.7}$$

Where:

Q	=	Polarisation mixing factor
$R(P_2)$ & $R(P_1)$	=	Polarisations
h	=	dimensionless roughness

Land Parameter Retrieval Model

The Land Parameter Retrieval Model (LPRM) is developed to retrieve land surface parameters from passive microwave observations. It is based on a forward modelling approach that uses horizontally and vertically polarized microwave brightness temperature. This means that it first separates the soil and the vegetation emission. When the emission is split, the soil emission is used to optimise for soil moisture and the vegetation emission is used to optimise for vegetation optical depth. The Vegetation Optical Depth (VOD) is computed by combining the analytical formula of Meesters, Jeu, and Owe (2005) and the (Microwave Polarisation Difference Index (MPDI)). The combination of the different polarisation results in a sensitivity for both the vegetation emission and the soil emission. The separate optimisation for soil moisture and the vegetation optical depth is executed for a large variety of soil moisture conditions with LPRM determining the brightness temperature values.

VanderSat downscaling technique

The VanderSat products that were used in this research, soil moisture, soil temperature and vegetation optical depth, are based on the downscaling technique that has been developed by VanderSat (de Jeu et al., 2017). This technique can be applied to passive microwave observations, with a spatial resolution of 25x25km. The obtained brightness temperature is downscaled to a product with a resolution of 100x100m.

The satellite observed brightness temperature is measured per footprint. Each of the different bands had a different footprint. The spacial resolution of the footprint can be found. The footprints have an oval shape, with a Gaussian distribution of the contribution of the signal. This means that the highest density of the signal is concentrated in the centre of the footprint and decreases towards the edges. The gaussian distribution results is characteristic and means that the intensity will decrease by 50% with 2.355σ from the centre of the footprint. When creating multiple oval footprints for 25% or 75% a large amount of footprints can be obtained. These different footprints have different resolution and different signal densities. When multiple footprints overlap it is possible to combine the footprints into a 100m x 100m map by the weighted sum of all overlaying footprints of the brightness temperature, see Figure 3.5

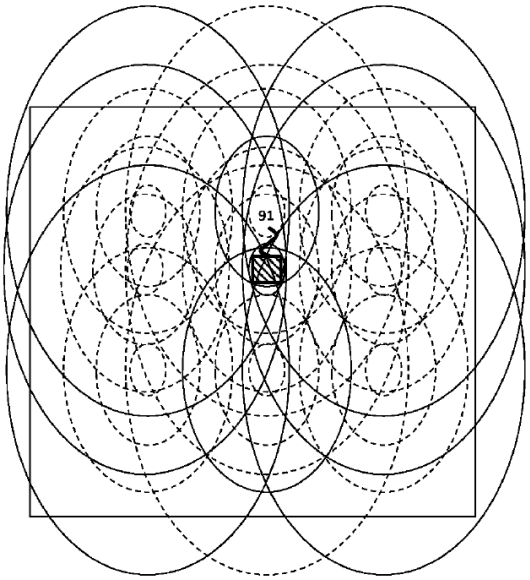

Figure 3.5: Overlapping footprints result is combination of measured brightness temperatures. Source: de Jeu et al. (2017)

To mask out water surfaces a high resolution a land water map is created. The ESA Sentinel satellite is combined with static land cover maps. This map is used to adjust the brightness temperature by masking values of water only pixels. This is a static water mask, which raises a possible drawback in the downscaling technique in the tropics. Since the tropical area is prone to monsoon flooding the water surface is a dynamic area. This might result in either smaller or larger water surface areas than anticipated. This will influence the masked area and therefore the measured brightness temperature signal density.

II

Part 2 In-situ Soil Moisture

4

Materials and Methods

4.1. In-situ soil moisture network set up

In-situ soil moisture networks are networks of sensors locally installed. These sensors measure the soil moisture content at a specific location. For this research two networks in Bago, Myanmar are described: A previous network that has run from June 2017 up to July 2018 and a newly installed network from 2020. Both in-situ networks were installed within a radius of approximately 20km from Bago City. The networks were installed at the same four locations, however the exact position of the sensors is optimised in the 2020 network. These four locations were selected to represent the different types of soil and land use in the Bago region.

Irrigation Technology Centre 17.3143° N, 96.4520° E
This location is situated within the main compound of the (Irrigation Technology Centre (ITC)), in the town Bago. It is protected by a concrete fence and surrounded by other measurement equipment.The location lies in an open landscape, no canopy at the site. The area around the location is not irrigated. The top layer of the soil consist of sand, the next layer is silty-clay. Dominant soil group HWSD: Nitisols. CCI ESA: Cropland, rainfed and in the surrounding area urban area and cropland, irrigated.

Hpa Yar Gyi 17.4661° N, 96.5303° E
This location is situated within a compound of the ITC near the town Hpa Yar Gyi. Within the compound there is an artificial pond surrounded by a small dike. The previous sensors where located on top of this dike, which could give incorrect results. The new sensors were placed in the grass area, which will be flooded during the monsoon season. The area around the compound consists of rice paddies which are irrigated throughout the dry season. The soil is covered with grass, consist mainly of silty-clay and some trash was found during digging, up to 20cm depth. Dominant soil group HWSD : Gleysols. Climate Change Initiative (CCI) ESA : Cropland, rainfed and in area around it grassland, urban area and cropland, irrigated.

Alaigni 17.2630° N, 96.3465° E
This location lies at the border of the Alaigni reservoir, within a compound of the ITC. The area in and around the compound is a forested area. The sensors and datalogger are placed within a small square, containing other measurement equipment and protected by a small wooden fence. The area does not flood during the monsoon. Soil consist of sand and further down silty-clay. Dominant soil group HWSD : Nitisols. CCI ESA : Cropland, rainfed and surrounded by grassland, waterbodies and natural vegetation.

Tha Nat Pin 17.2912° N, 96.5731° E
This location is situated within the town Tha Nat Pin. There is a weather station of the ITC, where the sensors and logger are placed as well. The soil consist of silty-clay, some bricks and a lot of trash was found while digging, up to 20 cm depth, which indicates an artificial ground. Dominant soil group HWSD : Gleysols. CCI ESA : Cropland, rainfed and next to urban area and cropland, irrigated.

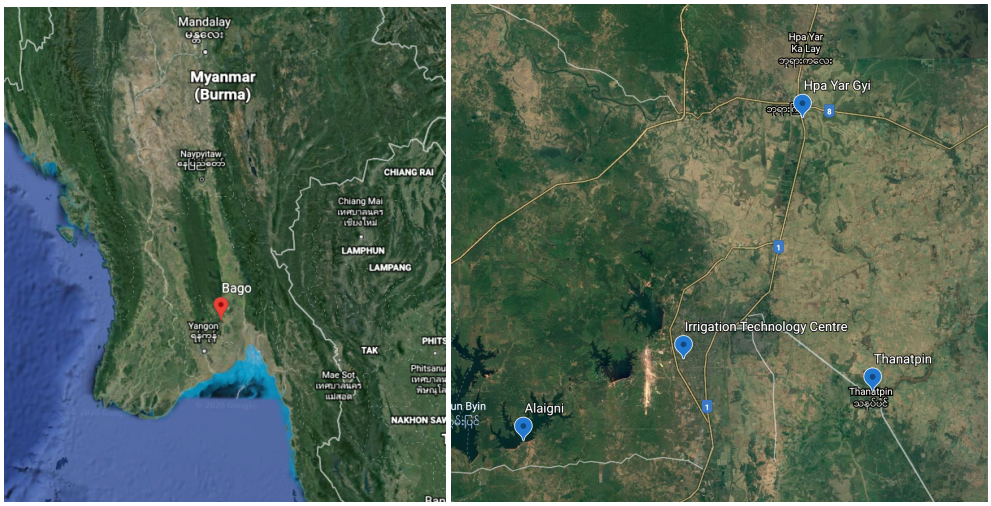

Figure 4.1: The four sensor locations of the in-situ soil moisture network installed at Bago, source: `https://www.google.nl/maps`

4.1.1. In-situ soil moisture network 2017

This network was installed in June 2017 and provided data up to July 2018. Five Decagon EM50 Analog Data loggers were used for this network, each data logger had five Decagon GS1 soil moisture sensors, of which one was placed vertically from the surface level to approximately 5cm , two horizontally at 10cm depth and two horizontally at 20cm depth, similar to the set up in Figure 4.3. The measurement interval was 30 minutes and the Irrigation Technology Centre team visited the network each month to extract the data and check the battery live. During two time periods ground truth sampling was carried out to calibrate the sensors. Due to the severe weather condition of the tropical monsoon climate the data loggers were damaged and no longer in use.

4.1.2. In-situ soil moisture network 2020

This network was installed as a part of this research. The fieldwork in Bago was carried out from the 17^{th} of February 2020 to the 19^{th} of March 2020. The goal of the fieldwork was to install an in-situ network that measures soil moisture and soil temperature at the four different locations.

Materials

For the network set-up and field work several materials were installed and used to collect data: 4 dataloggers and 24 sensors were installed and a manual Theta Probe was used for additional in-situ soil moisture measurements. Below the specifications of these materials can be found.The most important factor for the selection of the dataloggers was that they had to be robust. The previous data-loggers were damaged beyond repair, due to severe rainfall conditions and insects. Of the previously installed sensors most could be reused. Furthermore one soil moisture sensor per datalogger was added that can additionally measure soil temperature. The desired lifetime of the network is multiple years. The manual Theta Probe was used during the fieldwork, but will not continue to deliver data after.

ZL6 datalogger

This datalogger is engineered to be an ultra-rugged and durable construction, with low maintenance.The enclosure is made of weather-, impact-, and UV-resistant polymer. The integrated solar panel means that the NiMH batteries can be recharged, and so there is hardly any power maintenance needed. With unobstructed view of sun the lifetime of the batteries can be 3+ years. The logger has 6 sensor input ports, with secure cable handling. The operating environment ranges from -40 to 60 degrees Celsius and 0-100 percent relative humidity (METER GROUP, 2017). The collected data of the ZL6 is sent to the Zentracloud via a cellular network.

Soil moisture sensors: GS1 and TEROS12

Each datalogger has 6 sensor input ports, for 5 of these ports the sensors of previous research were reused. These are GS1 sensors,measuring soil moisture content. The sensor has a resolution of 0.001 m^3/m^3 volumetric soil moisture content. The maximum measuring capability is 0.57 m^3/m^3 volumetric soil moisture

content. The operating environment ranges from -40 to 50 degrees Celsius (Decagon Devices, 2015). In the last port of each datalogger a new sensor, the TEROS12, was added. This sensor measures temperature as well as soil moisture content, with also a resolution 0.001 m^3/m^3 volumetric soil moisture content. The maximum measuring capability is 0.70 m^3/m^3 volumteric soil moisture content. The temperature sensor has a resolution of 0.1 degrees Celsius. The operating environment ranges from -40 to 60 degrees Celsius (METER GROUP, 2019). Metergroup, the producer of the sensors ensures that during production the sensors are calibrated with a general mineral soil calibration.

Manual Theta probe ML3

The ML3 Theta probe (Delta-T Devices, 2017) soil moisture sensor is a manual logger and is highly accurate yet easy to use. The manual Theta Probe is inserted into the soil and a simple datalogger is connected which reads out the sensor directly. The manual Theta Probe ranges from 0 to 1.0 m^3/m^3.

(a) ZL6 logger (b) GS1 Sensors (c) Manual Theta Probe

Figure 4.2: The Zl6 logger(METER GROUP, 2017) and GS1 sensors (Decagon Devices, 2015) that were installed and the manual Theta Probe (Delta-T Devices, 2017) was used during the fieldwork.

Zentracloud

The measurements of the sensors in the 2020 network are uploaded once a day to the Zentra cloud, at 6am UTC. The Zentracloud is a data management software platform that works together with the ZL6 datalogger. The Zentracloud is accessible at any time and has a user friendly interface. More details can be found in the manual in appendix A. Information about the devices, calibrations, the upload and measurement times and more can be found and reconfigured at any time. The soil moisture measurements are given in volumetric water content (VWC), in m^3/m^3. Volumetric water content represents the ratio of water volume to soil volume in a given soil. The temperature is given in degrees Celsius. The battery power percentage can be seen, so that the replacement can be organised in time.

Installation of the loggers and soil moisture sensors

The dataloggers and sensors were installed at the four locations mentioned in section 4.1, see Figure 4.3 for the placement of the 6 sensors per datalogger. For the installation a hole was dug to insert the sensors at the desired depths. In February it is still dry season, which meant that the ground was very dry and hard. To let the ground settle faster when closing the hole, water was added. See appendix A for a visualisation of the installation. Care was taken to place the solar panel for maximum sun exposure. To ensure the new set-up was fully weather and insect proof, the dataloggers are protected with a layer of bitumen tape and bitumen paint, see manual x. The loggers were not opened during the wet season.

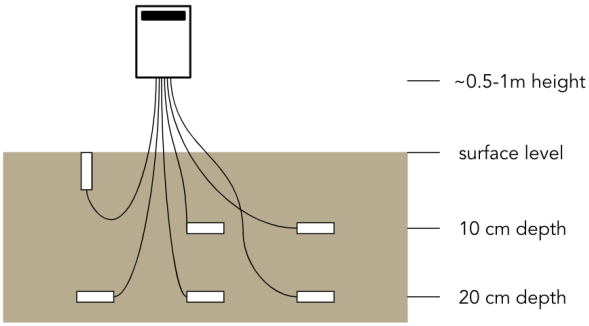

Figure 4.3: Schematic overview of soil moisture sensor set up

Infiltration test above the soil moisture sensors
An infiltration test was done at the surface above the sensors at the ITC soil moisture plot. The purpose of this test was to validate the installed soil moisture sensors with the manual Theta Probe soil moisture measurements at the surface and to check whether infiltration was visible over depth. Infiltration was performed using a single bucket set up with a constant 5 cm of ponding water, for at least an hour. When all the water had infiltrated, measurements were taken during the drying phase with the manual Theta Probe, every few hours for two days.

4.2. Reliability Analysis of the two networks

The products of both in-situ soil moisture networks are important to determine whether they can be used as reference for the validation of satellite soil moisture products. The second sub question states:

Do the data records of two soil moisture networks at 4 locations in Bago provide a reliable product?

A definition of reliability is required to answer the question. For this research the reliability of an in-situ soil moisture content network, is defined by two factors: availability and quality. The two factors are elaborated below and the analysis can be found in the result section.

Availability of soil moisture information

Availability of soil moisture information determines reliability of the network to produce data when needed. When looking at the availability the length and continuity of the sensor record is an important aspect. Cosh et al. (2016) state that the value of an in situ network is proportional to the length of the data record available. The data record of previous validation studies varies from 11 months to several years (Colliander et al., 2017; Cosh et al., 2016; Parrens et al., 2012). The international Soil Moisture Network (ISMN) usually requires that the length of data record should at least be 1 year. Discontinuity due to logger/sensor failure could lead to incomplete information. A second critical factor in the availability of soil moisture content data is the way that the data sets are retrieved from the datalogger. For most in-situ soil moisture networks manual extraction of the data is needed. The difficulty of manual extraction is to reach the remote locations of the in-situ network. In case of automatically uploading through the Zentracloud each day, the only limiting factor is the connection. Afterwards, when the data is extracted from the in-situ network locations, or downloaded from the Zentracloud, it should be accessible for use in research or other purposes. This could be done by sharing with those who request it, by uploading to online (private) platforms or through the ISMN, with an open access policy.

For this research an in-situ soil moisture network can be considered reliable, in the sense of availability, when the length of the available data record is sufficient for the purpose of the research, and when the data is easily accessible at all time. In this small scale validation a length of 1 year would be considered reliable to give representative validation results, but more years would greatly improve the reliability.

The quality of soil moisture content sensors and network

This is reliability in the sense of the possibility to consider the sensor and network data as reference measurements for validation of satellite soil moisture products. This includes quality of the sensors as well as the representativeness of the network.

Gruber et al.(2013) describe that in-situ data sets are often seen and used as ground-truth and state this is an inappropriate term to use, since in-situ sensors contain inherent errors. Besides, systematic differences between the represented extent of the observations ass well as the actual represented physical quantity are introduced by differences in spatial scale, the represented depth and the underlying physical measurement principles of the sensors. They mention the necessity of a comprehensive quality control process for in-situ measurements.

Sensor quality The ISMN collects and harmonizes soil moisture data sets. This is done from a large variety of networks that operate individually and thus have a highly variable quality. The ISMN performs quality control procedures on each network that participates. These quality control procedures include among others flagging values that exceed certain thresholds, checking the soil moisture variation in relation to changes in precipitation, detecting unresponsive sensors and identifying outliers, within the thresholds (Dorigo et al., 2013). Common errors that are mentioned for in-situ soil moisture measurements are random noise and spikes, breaks, constant low and high values.
Dorigo et al. (2011) introduce plausible ranges for the measurements, see table 4.4. Values that exceed these ranges are flagged. The quality flagging of the data is based on the CEOP-Data Flag Definitions, see table x in the appendix. C01-C03 flags detect values that are outside of reasonable geophysical range. D01-D05 show questionable result with geophysical basis, where it looks at the the plausibility of the observations in connection with additional environmental variables, such as temperature and precipitation. The last category, D06-D10, show suspicious measurements that are identified based on the spectrum of the soil moisture time series (Xaver et al., 2020). In the appendix the description of each flag can be found.

Variable name	Variable range
Soil moisture	0–0.6 $m^3\ m^{-3}$
Soil temperature	−60–60°C
Air temperature	−60–60°C
Precipitation	0–100 $mm\ h^{-1}$
Soil suction*	0–2500 kPa

Figure 4.4: Plausible variable ranges for the meteorological data stored in the ISMN.(Dorigo et al., 2011)

Next to the automated quality control of the ISMN, various other quality analyses are mentioned for in-situ sensors, such as: sensor calibration, sensor-to-sensor comparison, and soil moisture memory. (Cosh et al., 2016; Gruber, Dorigo, Zwieback, Xaver, & Wagner, 2013; Heathman et al., 2012; Xaver et al., 2020). Calibration of the in-situ sensors is an important component to check the performance of the sensors. Cosh et al. (2016) mentioned factory and soil specific calibration can differ a lot. Studies showed that the sensors did not meet the accuracy of the manufacturer calibration, and it was concluded that soil specific calibration is preferable. They state that sensors should be calibrated using volumetric soil moisture samples at the sensor sensing depth. Sensor-to-sensor comparison is done by collecting measurements in the field with a sensor that is known to give good results, and then comparing them with the measurements of the placed sensors. Soil moisture memory looks at the capability of the soil to store information of an atypical event (e.g, rain, drought) long after its occurrence (Gruber et al., 2020).

Network quality For the representativeness of the network overall, the network quality is evaluated. Temporal dynamics, agreement and stability, show the networks ability to capture the drying and wetting events. Precipitation data is often used to compare trends. Triple collocation is a method for estimating the random errors of three collocated data sets, these data sets are assumed to represent the same physical parameter

while simultaneously solving systematic differences. Spatial representativeness of a single station for a certain area looks at the stations surroundings and its ability to capture this.The reliability of both soil moisture content networks in the Bago region have been checked differently, as different information and test are available.

- In the overview, the timeseries of the measurements so far have been analysed and threshold values were inspected,according to the ISMN quality flags and the temporal stability was looked at a minimum amount missing data minimum surpassed threshold values and a trend that would be expected over these months would indicate a reliable network. Basics statistics were calculated to evaluate the variability of the measurements. This was executed for both networks.
- For both networks the precipitation data at the ITC location was compared to the soil moisture content data, showing the temporal dynamics.
- The 2017 network was evaluated by the calibration with ground truth measurements that were done at the time.

The 2020 soil moisture content network was additionally analysed with the following methods:

- The temporal agreement and spatial representativeness was analysed by focusing on the daily fluctuations. The measurements were considered reliable if the six sensors at each location were within range of each other and showed a similar pattern.
- The first rain event showed the soil moisture memory trough the behaviour of the different sensors over depth. A clear course over depth of rain entering and drying out indicated reliability.
- Sensor-to-sensor comparison was done, by looking at measurement with the manual Theta Probe and by comparing with the previous network. Here a visual agreement/correlation of the measurements would indicate reliability.

5

Results In-Situ Soil Moisture Measurements

In this chapter both in-situ soil moisture networks was evaluated based on the earlier described methods. First the previous placed in-situ soil moisture network, the 2017 network, were evaluated by looking at the overview, basics statistics, precipitation data and calibration results. Next the newly placed in-situ soil moisture network, the 2020 network, was evaluated. The overview, basics statistics, daily fluctuations, precipitation data and event and sensor-to-sensor comparisons were looked into.

5.1. 2017 network

Overview of the soil moisture timeseries

Figure 5.1 shows the timeseries of the soil moisture measurements between 2017 and 2018. The trend is similar at each location. Each location starts with a high soil moisture content, because the measurements started in June, which is during the monsoon period. Around November the values of the soil moisture content decrease as the monsoon ends and the ground dries up. At the end of May the soil moisture content starts to increase again, this is when the monsoon season starts.

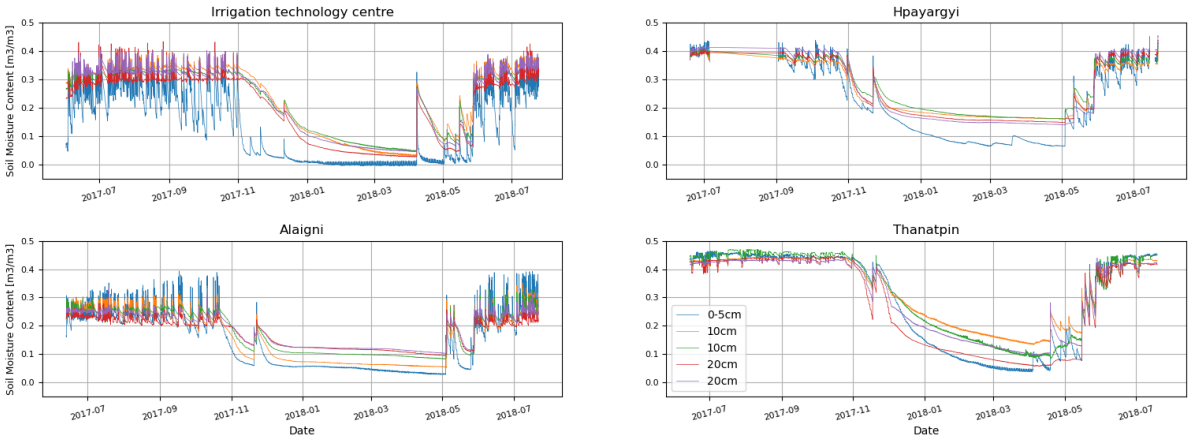

Figure 5.1: Timeseries of the soil moisture content resulting from the in-situ sensor measurements of the 2017 network at various depths for each location.

There are some data gaps during specific periods, especially at the location Hpayargyi between July and August 2017. This was due to severe damage to the datalogger, which was replaced afterwards. The timeseries of the soil moisture records at ITC and Alaigni show a lot of variability in their data record, particularly in the first few months of the measurements at ITC. This could be due to the surface sensor being to close to the surface cracks. Cracks in the surface means that the sensor could be exposed to air, which could lead to errors in measurement. The measurements of the locations do not surpass the range verification threshold of 0.6 m^3/m^3 for the soil moisture content, that the ISMN has set. At the ITC the measurements of the surface sensor do have values below 0.0 m^3/m^3, the bottom boundary value.

The timeseries are further evaluated with an statistical analysis to support the conclusion of large variability. In Table 5.1 values of this analysis are shown. The statistical characteristics that are shown determine the variability. The mean value is the average value of that is measured over time during at a certain depth at one location. The variance is the expectation of the squared deviation of the soil moisture content from the mean that is determined before. Finally the coefficient of variation shows the relative standard deviation. This is a measure that shows the dispersion of a probability distribution. As can be seen in Table 5.1 the values of the soil moisture content that are measured at the surface of the ITC location have a coefficient of variation 0.945. This means that the variability is large, which confirms the visual assumptions. The surface sensor at Alaigni shows similar behaviour, though less strong. The top soil layer of both ITC and Alaigni consist of sand, the large variability could relate to this. In the boxplots it can be seen that the location Hpayargyi and Thanatpin generally show higher soil moisture content than ITC and Alaigni. This is probably due to the differences in soil tecture, where both Hpayargyi and Thanatpin consist of silty-clay layers, while the others have a top layer of sand. These soil textures have different water retention capacities. The lowest mean value is found for the ITC surface sensor measurements, which is in agreement with the plots of the timeseries, where extremely low values are found for a long period between January and March.

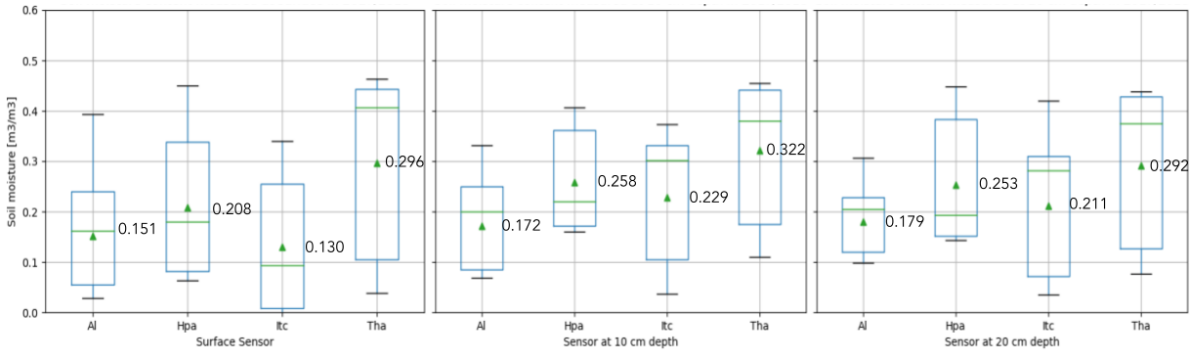

Figure 5.2: Boxplots of mean soil moisture at surface, 10cm and 20c depth for all the locations of the 2017 network. In the box the first and third quartile are shown en the green line shows the median. The green triangles represent the mean and the value is shown next to the box.

Table 5.1: Mean, variance and coefficient of variation for soil moisture measurements at different depth, for each location of the 2017 network

Location	**Depth**	**Mean value** $\mu[m^3/m^3]$	**Variance** $[m^3/m^3]$	**Coefficient of Variation**$[-]$
ITC	Surface	0.130	0.015	0.945
	10 cm	0.229	0.013	0.502
	20 cm	0.211	0.014	0.553
Hpayargyi	Surface	0.208	0.015	0.598
	10 cm	0.258	0.008	0.347
	20 cm	0.253	0.011	0.422
Alaigni	Surface	0.151	0.010	0656
	10 cm	0.172	0.006	0.465
	20 cm	0.179	0.003	0.303
Thanatpin	Surface	0.296	0.028	0.560
	10 cm	0.322	0.017	0.401
	20 cm	0.292	0.021	0.495

Calibration of soil moisture sensors

The 2017 soil moisture monitoring network was validated with ground truth sampling at the time it was installed and a year after. The measurements were acquired using soil sample rings, with a fixed volume of 100 cm^3. The samples were taken adjacent to the sensor nests, at depths corresponding to that of the sensors. The first experiments resulted in (Root Mean Squared Error (RMSE)) ranging from 0.023 to 0.051 m^3/m^3, which was a result verified with previous studies (Kattler, 2017). The second experiment showed a result for RMSE in the range from 0.011 to 0.059 m^3/m^3 for most sensors, except for three outliers at the location Thanatpin. The critical RMSE threshold of 0.05 m^3/m^3, mentioned in the report as an acceptable value, was exceeded by 6/20 measurements (Zonneveld, 2018).

Comparison of precipitation data and soil moisture content

In Figure 5.3 the precipitation measured at the ITC during 2017 and 2018 is shown. As this is the only location with rain measurements all the locations were compared to these measurements.
At each location the surface sensors show a clear response to the precipitation. The dry period, starting early November, is visible in the soil moisture measurements that dry down from this moment. The first spike of rain after the dry period, around the start of April 2018, shows a strong response of the soil moisture content at the same time at the ITC. At the other locations the timing of this event differs.

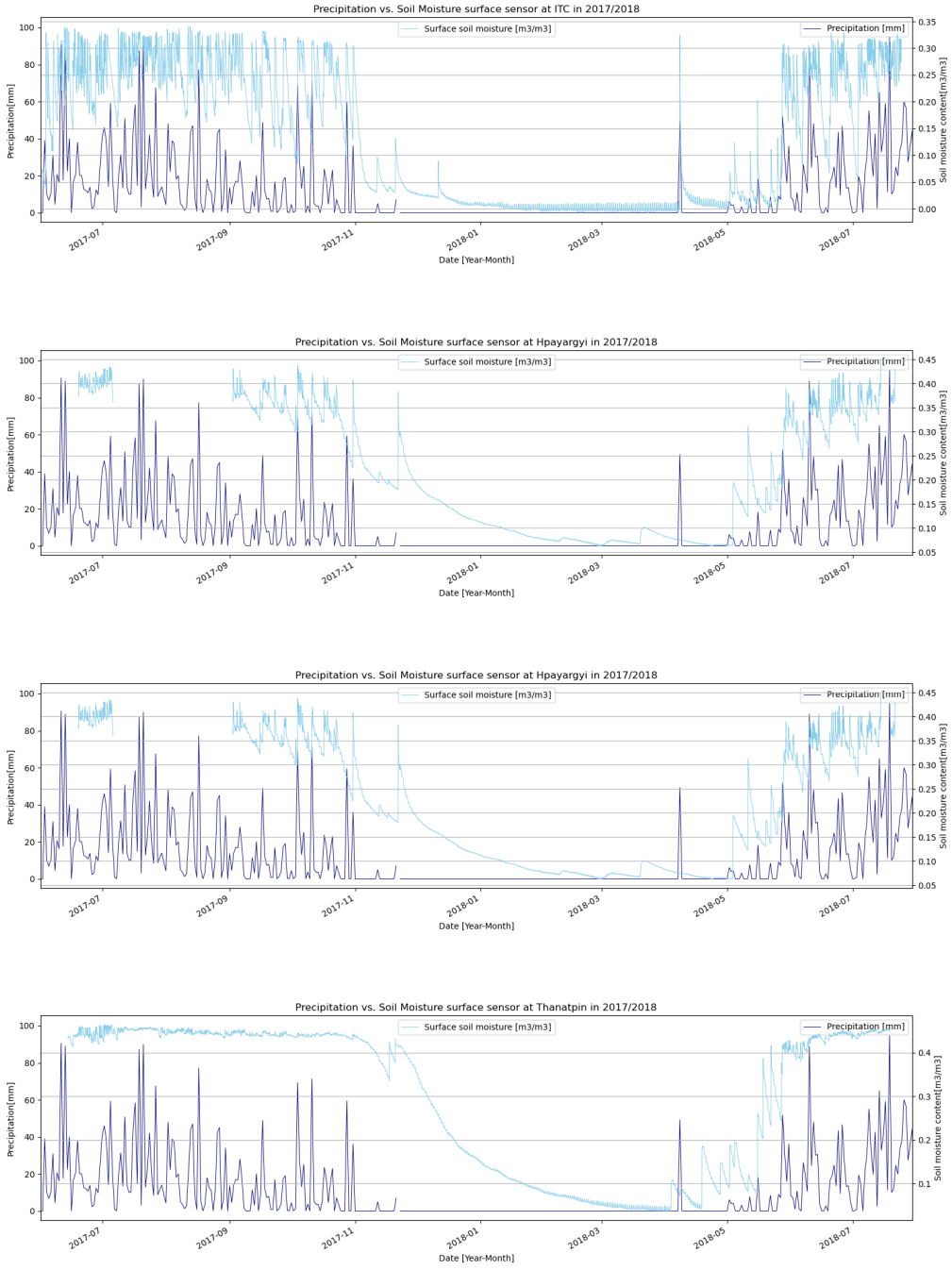

Figure 5.3: Precipitation measurements at the ITC vs. Surface soil moisture at four locations in 2017/2018

5.2. 2020 Network

Overview of the soil moisture timeseries

The 2020 network was set up in February 2020 in Bago, during this research. Below the timeseries of the measurements of the new soil moisture monitoring network can be seen for the four locations. These overviews show the development of the soil moisture content from the date that the sensors were placed in February, the first few weeks the high soil moisture results are due to tests and water settling.

In Figure 5.4 the performance of the sensors at ITC can be seen in the top left corner. The overall trend seems to represent the transition from the dry period into the wet period and back to the dry period well. What stands out is the surface sensor. In the dry period this sensor is near zero and in the wet period it shows a large variability. This could be due to the sensor being to close to the surface cracks, where cracks could lead to unreliable measurements. The values of measurement lie between 0.006 and 0.386 m^3/m^3. The soil temperature lies between 27.8 and 41 degrees Celsius.

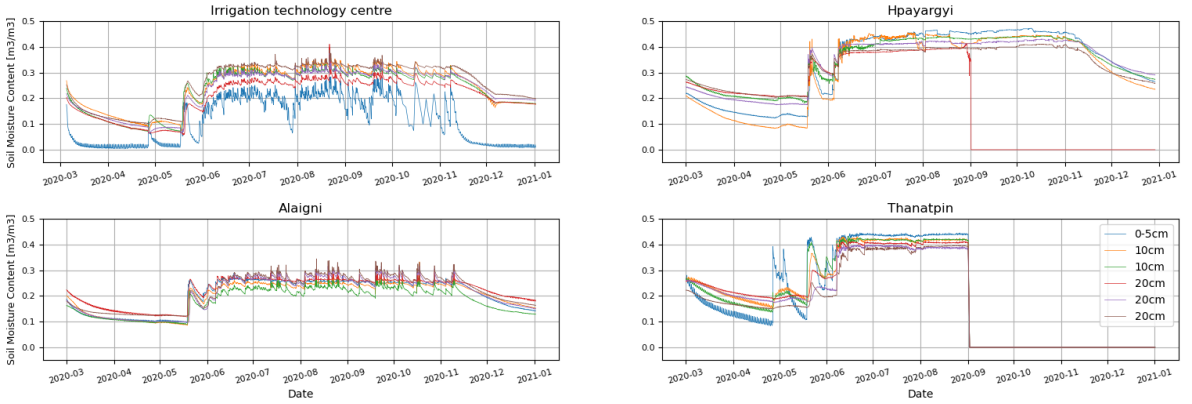

Figure 5.4: Timeseries of the soil moisture content resulting from the in-situ sensor measurements of the 2020 network at various depths for each location.

In Hpayargi, top right corner of Figure 5.4 the graphs suggests that the sensors react as expected. The values of measurement lie between 0.084 and 0.432 m^3/m^3. The soil temperature lies between 24.9 and 34.1 degrees Celsius. One sensor at 10 cm depth stopped working near the end of August. At the end of December 2020 the battery levels of the datalogger dropped to zero, after which no data was uploaded.
In Alaigni, bottom left, all the sensors show very similar trends, which implies a properly working station. Again the wet and dry period can be clearly distinguished. The values of measurement lie between 0.101 and 0.321 m^3/m^3. The soil temperature lies between 26.7 and 42.9 degrees Celsius.

At the station Thanatpin the surface sensor has a strong response in April, while the other sensor do not show much variation. Further in time the surface sensor does stabilize with the other sensors. The values of measurement lie between 0.087 and 0.435 m^3/m^3. The soil temperature lies between 24.4 and 37 degrees Celsius. The logger in Thanatpin stopped working at the end of August, so it does not provide data anymore. This means that for this research no data further then the 1st of September can be acquired.

The timeseries of the soil moisture content are further evaluated with an statistical analysis to support the conclusion of large variability. In Table 5.2 values of this analysis are shown. The statistical characteristics that are shown result in the variability. The mean value, the variance and the coefficient of variation. As can be seen in Table 5.2 the values of the soil moisture content that are measured at the surface of the ITC location have a large coefficient of variation, 0.747, which is in agreement with Figure 5.4. The surface sensor at ITC from the 2017 showed very similar behaviour, this could indicate that either the sensor itself has inherent errors or the sensor do not settle well into the top soil layer at the ITC. The boxplots (Figure 5.5) show that Hpayargyi and Thanatpin generally have higher soil moisture content than ITC and Alaigni. Next to that these two locations show a larger range of values, especially at the surface sensors.

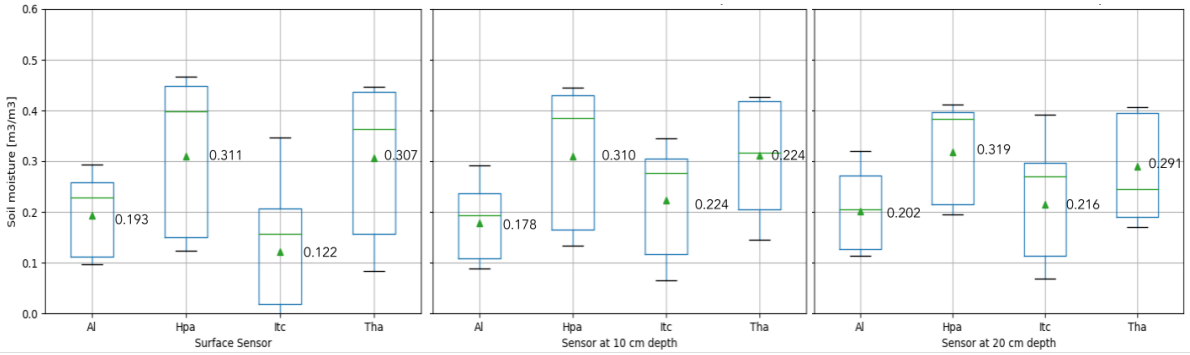

Figure 5.5: Boxplots of mean soil moisture at surface, 10cm and 20cm depth for all the locations of the 2020 network. In the box the first and third quartile are shown en the green line shows the median. The green triangles represent the mean and the value is shown next to the box.

Table 5.2: Mean, variance and coefficient of variation for soil moisture measurements at different depth, for each location of the 2020 network

Location	**Depth**	**Mean value** $\mu[m^3/m^3]$	**Variance** $[m^3/m^3]$	**Coefficient of Variation**$[-]$
ITC	Surface	0.122	0.008	0.747
	10 cm	0.224	0.009	0.414
	20 cm	0.216	0.008	0.418
Hpayargyi	Surface	0.311	0.020	0.455
	10 cm	0.310	0.016	0.403
	20 cm	0.319	0.008	0.274
Alaigni	Surface	0.193	0.005	0.364
	10 cm	0.178	0.004	0.343
	20 cm	0.202	0.005	0.333
Thanatpin	Surface	0.307	0.019	0.445
	10 cm	0.312	0.011	0.340
	20 cm	0.291	0.009	0.330

Close-up of daily fluctuations during the wet period

In the graphs in Figure 5.6 a period of three consecutive days during the wet season can be seen. In these days very little external factors influenced the soil moisture content. These days were evaluated to assess the mutual performance of the sensors, at each location it can be seen that the individual sensors react very similar, and are within range of each other. This again indicates a properly working network. As mentioned before the surface sensor at ITC shows deviating results which suggest that the sensor needs to be displaced.

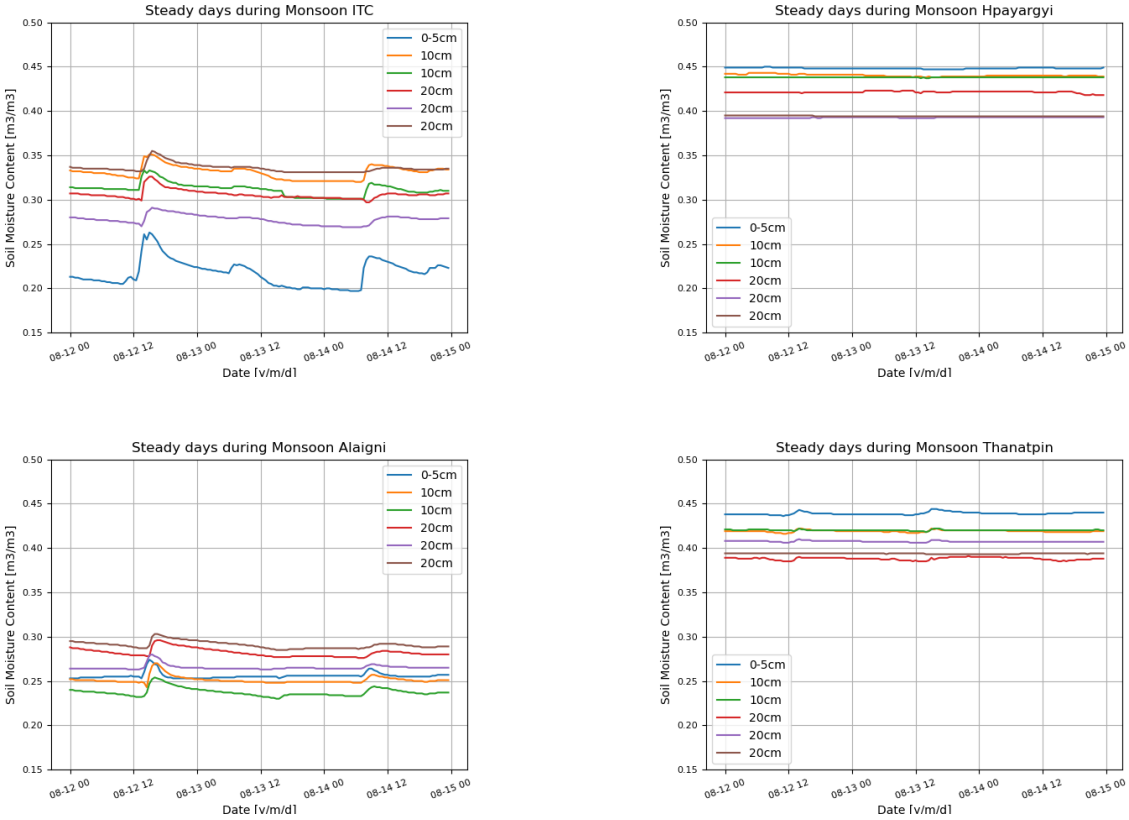

Figure 5.6: Soil moisture content on three consecutive days during the wet period, at each location of the 2020 network, shown over various depths

What stands out in the graphs is that at the locations Hpayargyi and Thanatpin the soil moisture content is higher, between 0.38-0.45 m^3/m^3, than at the other two locations, were the contents do not reach above 0.36 m^3/m^3. This is in line with the result of the statistical analysis. It can partially be explained by the composition of the soil. As mentioned in section 4.1, the soils of Hpayargyi and Thanatpin are silty-clay, while the first layers of the soil at ITC en Thanatpin consist of sand. Fine textured soils, like silty-clay, have a higher water retention capacity then coarser textured soil, like sand. This also explains the difference over the depth that can be seen, in Hpayargi and Thanatpin the soil moisture content decreases from the surface to the 20cm layers. In Alaigni it can be observed that the three sensors at 20cm depth have the highest soil moisture content, while the sensors 10 cm depth have lower soil moisture content.

The temperature fluctuation (Figure 5.7) show that ITC and Alaigni have a larger fluctuation than Hpayargyi and Thanatpin. The temperature sensors are at a depth of 20cm. The differences in soil temperature fluctuation between ITC/Alaigni and Hpayargyi/Thanatpin can be another effect of the soil textures.

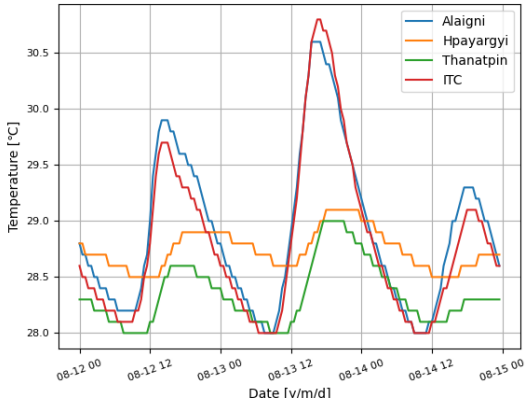

Figure 5.7: Soil temperature measurements during three consecutive days, at 20cm depth at the four locations

Comparison of precipitation data and soil moisture content

The graphs in Figure 5.8 show a good overview of the start of the monsoon season. The monsoon on-set is expected around the 23^{rd} of May in the Bago area and the off-set around the 29^{th} of September(Figure 2.3. In the precipitation data at the ITC in 2020 one can detect a similar pattern. There is a small rain event at the end of April, but the daily rainfall does not start until later, around mid-May. The large rain peaks have a sharp decrease near the end of September. However, some smaller rain events still occur up to the start of November. The soil moisture measurements of the surface layer show high values around March, while no rainfall was present during this time and the months before. This is due to the infiltration test and water that was poured over for settling of the soil.

At the ITC the response of the soil moisture sensor is similar to the rainfall pattern, where an increase in soil moisture follows directly from a precipitation event. Also a decrease in precipitation can be seen, for example in mid July a period of less rainy days results in a decrease in soil moisture, with a delay, due to the retention of the soil. At the other locations similar trends can be seen as at the ITC, however a strong comparison is not visible as the rainfall is not at the exact location of these measurements. In the graphs of the three location it can be seen that the sensor captures the monsoon well, with a increase of soil moisture content at the monsoon on-set and a fairly steady content during the monsoon season.

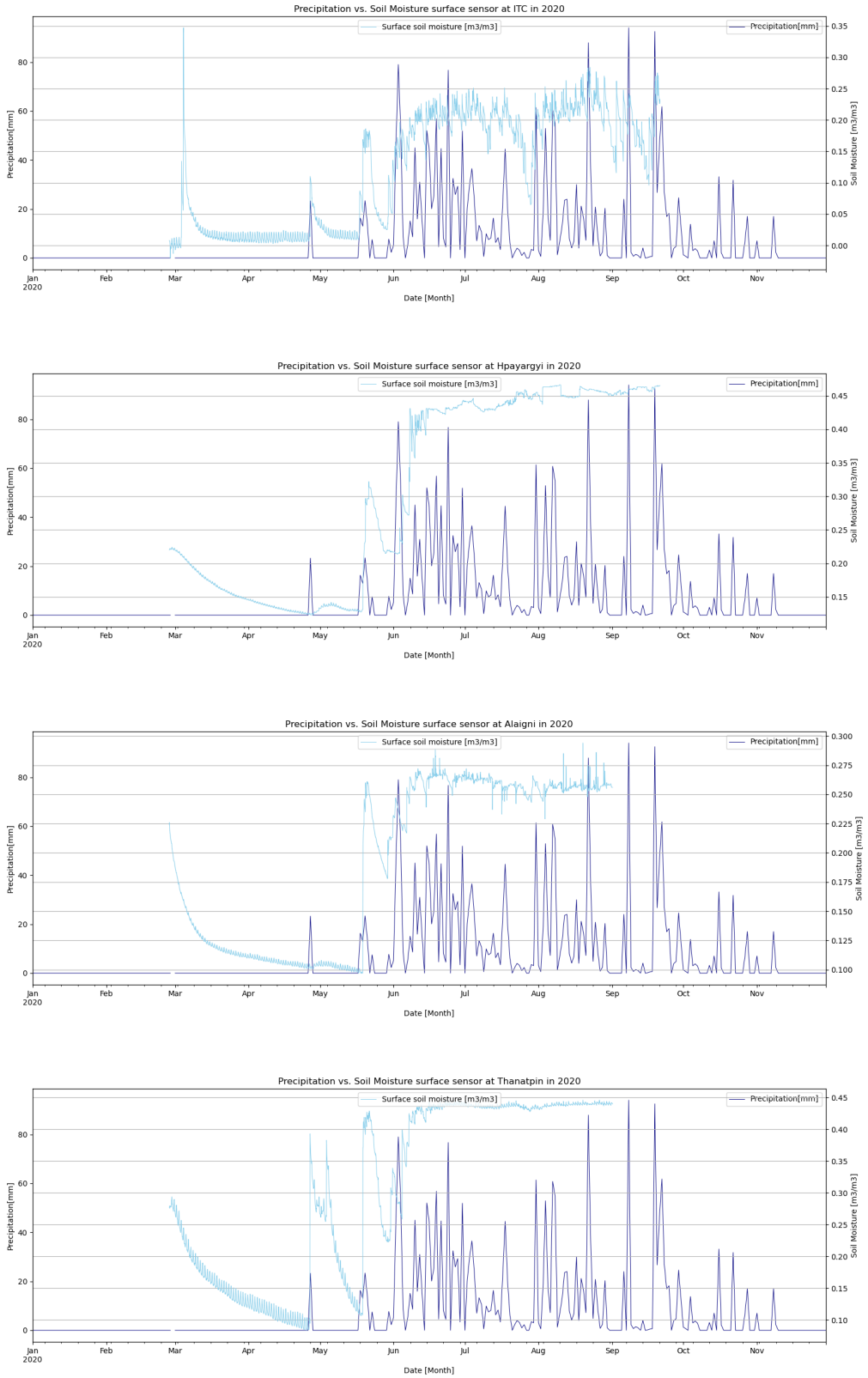

Figure 5.8: Visualisation of the precipitation and the surface soil moisture content that is measured at four location with the in-situ soil moisture sensor network of 2020

Close-up of the sensors during first rain event

Between the 17^{th} and 31^{st} of May the first large rain event occurred. This period can be seen as the start of the monsoon season. Below the responses of the sensors can be seen in this period. In Figure 5.10 the temperature plot can be seen. In each separate figure the individual responses over depth are visible. At ITC, the the surface sensor shows the first response to the rain event, which is then first followed by the sensors at 10 centimeter depth and then by the sensor at 20 centimeter depth. This is an expected response, as the water reaches the surface first and then travels percolates with depth. The surface sensors indicate that the soil at the surface dries down quickly after the event, while the soil moisture content decreases more gradually at 10cm and 20cm depth. As mentioned before this could be due to wrong placement of the surface sensor. In Hpayargyi the deeper sensors seem to react to the event before the surface sensor does. This could be due to various side effects, such as a leaf that covers the ground above the surface sensor, water that has been poured above the other sensors, or plastic in the ground near the surface sensor. At both Hpayargyi and Thanatpin plastic ploughed into the ground was observed up to 20cm depth. The sensors at Hpayargyi show have similar responses among each other to the rain event and indicate that the soil gradually dries down. At Alaigni the responses to the rain event show good behaviour, with steady dry down of the soil, and at the end a response to a new rain event. In Thanatpin the surface sensor and one of the sensors at 10 cm depth show a extreme and abrupt increase of soil moisture content, while the other sensors have a more moderate response where the soil moisture content increases gradually.

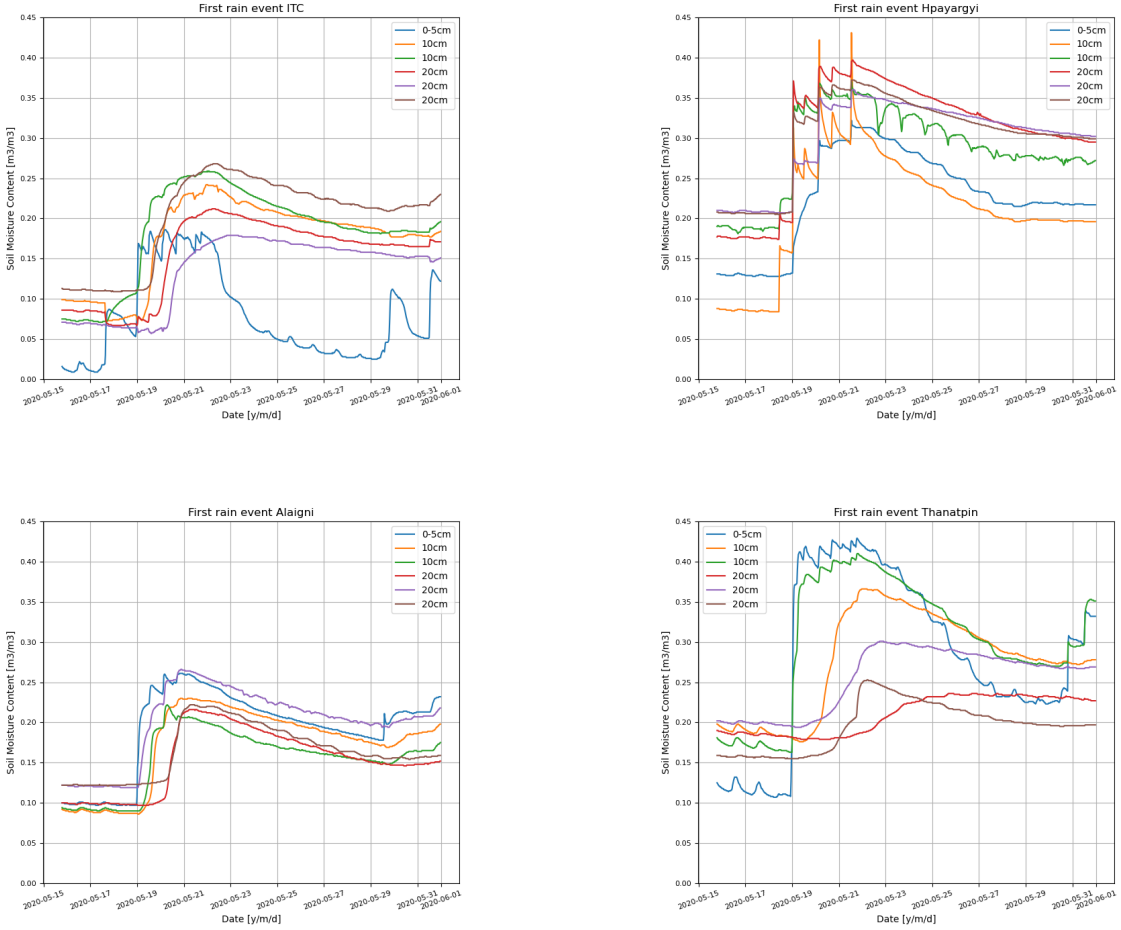

Figure 5.9: Measured soil moisture content between the 17^{th} and 31^{st} of May at each location of the 2020 network, shown over various depths

Overall the sensors show an accurate response to the rain event, and can therefore be considered reliable. In the soil temperature plot (Figure 5.10) a clear response to the rain event can be seen at each location. During the precipitation event the soil temperature decreases between 10-2 degrees, where it has a smaller effect at the locations where the temperature was already lower. After this the temperature starts to increase again until the next event. Again the most fluctuation can be seen at the locations ITC and Alaigni.

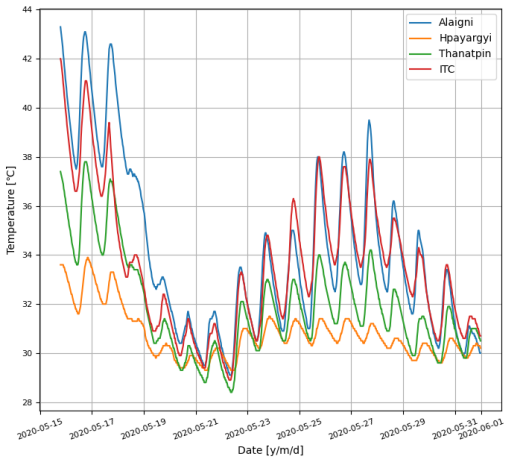

Figure 5.10: Measured soil temperature at 20cm depth between the 17^{th} and 31^{st} of May of 2020.

Sensor-to-sensor comparison

In-situ sensor vs. manual Theta Probe

Figure 5.11 shows the result of the infiltration test that was done at the ITC. In the first graph the measurement of the manual Theta Probe are plotted over time together with the measurements of three soil moisture in-situ sensors at different depths. It can be seen that the manual Theta Probe measurements follow the trend of the surface sensor. Furthermore the graph shows that the sensors respond to an infiltration, which indicates they work correctly. The surface sensor shows a steep increase and then gradually decreases, and returns to the initial value after two days. The sensors at 10 and 20 centimeter depth increase less then the surface sensor but remain longer at this increased level while very slowly decreasing. In the second graph the soil moisture content measured by the surface sensor and the manual theta probe are compared and show good correlation, with a slight underestimation of the soil moisture content measured by the in-situ surface sensor.

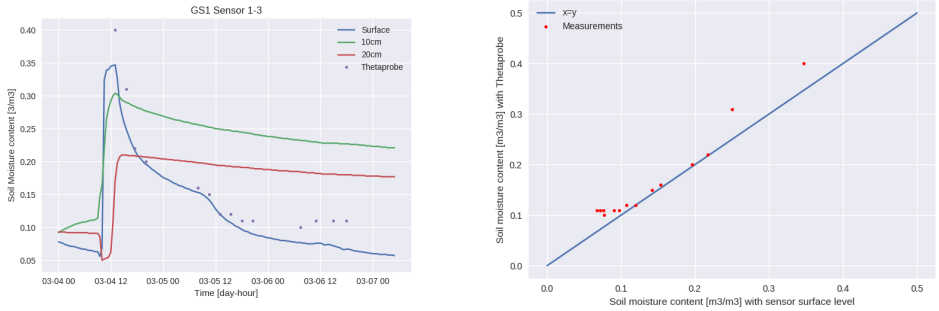

(a) Measured soil moisture content during infiltration test

(b) Visualisation of the measured soil moisture content of the manual Theta Probe versus the surface sensor

Figure 5.11: Measurement results of the infiltration test by the manual Theta Probe and in-situ sensors

In-situ sensor 2020 network vs in-situ sensor 2017 network In Figure C.2 the measurements from the surface sensors at each the stations can be seen for the 2017 network and the 2020 network. For each location a period of time was chosen where the measurements were minimally affected by external factors, which differs per station. This comparison is made to verify if the 2020 network is performing within the same ranges as the 2017 network. In the top y-axis the period in 2017 can be seen, and in the bottom axis the same period in 2020. In the appendix C the intercomparison between the 10cm and 20cm sensor can be found.

At each location the measurements of both periods lie very close to each other. The weather conditions were not exactly the same during these periods, so it is not expected for the measurements to be too similar, but these result show that the 2020 network behaves the same as the 2017 network. It is notable that the sensors of the 2017 network shows more variability than the 2020 network. In the precipitation plots it can be seen that there is heavier rain between the months June and August in the year 2017 than in these months in the year 2020, this could explain the difference partially. Additionally the sensor of the 2017 network were placed in June 2017, which means the sensors were still adjusting in the shown time period, while the 2020 was placed in March and could settle for 3 months before the shown time period. It is not known whether the exact same sensors where used at the the same depths, so inherent sensor errors could play a role too. At the location Hpayargyi the values of the surface sensor in 2017 are consistently lower than the measurements in 2020.As mentioned in the location description the newly placed sensor were installed at a slightly different location, that is flooded more during the monsoon than the previous location. This could indicate the higher values in 2020. In table 5.3 the min and max ranges at each location can be seen per depth. Here it is also visible that the soil moisture content falls within similar ranges at each depth.

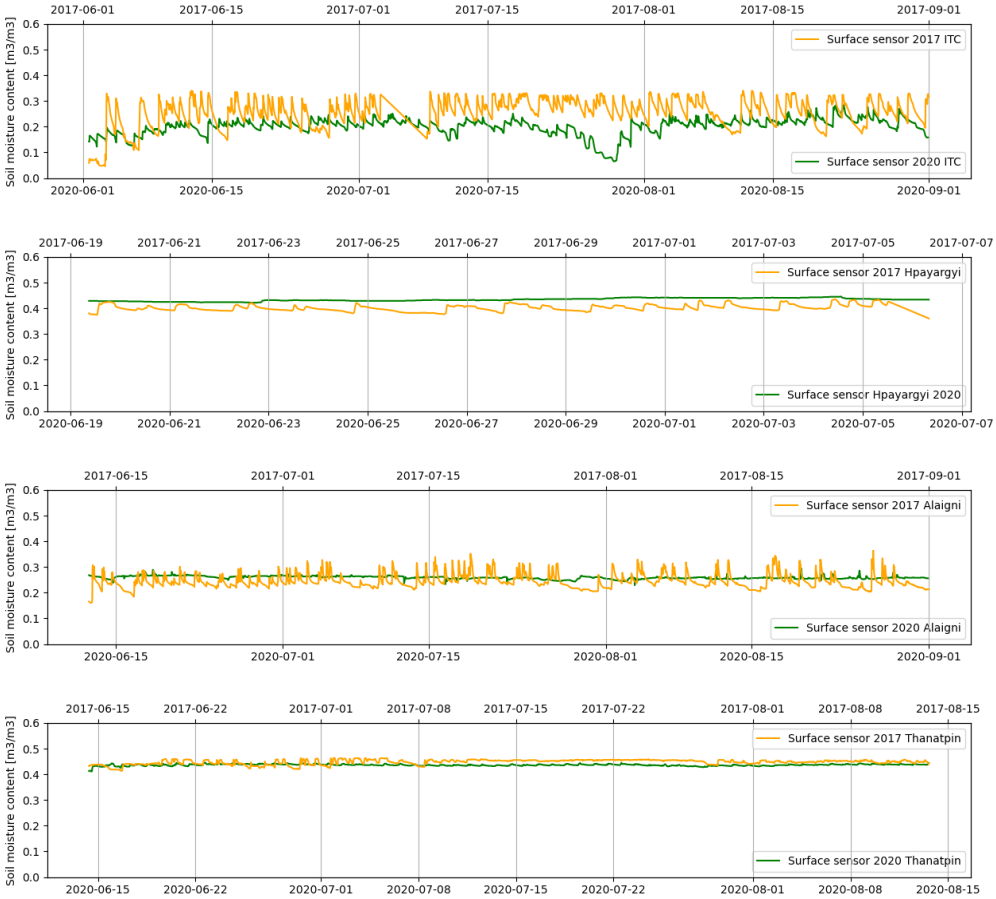

Figure 5.12: Visual comparison of the measured soil moisture content by the 2017 in-situ network and the 2020 in-situ network

Table 5.3: Ranges of the measured soil moisture content [m^3/m^3] from each location at all depths

Location	Depth	Range 2020	Range 2017
ITC	surface	0.065-0.284	0.045-0.341
	10cm	0.205-0.356	0.258-0.398
	20cm	0.149-0.411	0.232-0.433
Hpayargyi	surface	0.422-0.446	0.361-0.435
	10cm	0.390-0.453	0.367-0.406
	20cm	0.378-0.412	0.368-0.416
Alaigni	surface	0.229-0.294	0.160-0.364
	10cm	0.198-0.313	0.207-0.309
	20cm	0.237-0.324	0.203-0.336
Thanatpin	surface	0.411-0.446	0.414-0.464
	10cm	0.396-0.433	0.398-0.469
	20cm	0.337-0.412	0.284-0.440

6

Discussion In-Situ Soil Moisture Network Set-Up and Measurements

In this chapter the findings during the network set-up and measurement analyses will be discussed. In section 6.1 the challenges that were encountered during the preparation, fieldwork and the further use are discussed. By establishing these challenges future fieldwork and research can be well prepared for what to expect. In section 6.2 the reliability analyses of the installed networks of 2017 and 2020 was evaluated and a decision was made which network could be used for validation.

6.1. Exposed challenges during the set-up of an in-situ soil moisture network in Myanmar

Preparations

The locations of the network are in a quite remote area, which means preparation was needed. Once on the way , it is not easy to acquire extra equipment. An important factor for the selection of the materials was the weather condition. A heavy rain season from May till November, in combination with negligence of weather protection for the datalogger, has ruined a previous network. This means a robust logger that withstands the monsoon climate and that fits into the budget must be selected.

The weather also plays a role in the planning of the fieldwork. This fieldwork was preferred to be executed during the dry season, to get a good grasp of the transition of soil moisture from dry to wet season. This meant a quite quick departure, and little preparation time.

Fieldwork

For the installation of the network it was important that the exact locations were carefully selected. The four locations had to represent the neighborhood around it, to give a reliable result of the entire area. The possible places to install a network were limited because the property of land interferes, the network of this network could be installed at locations that were associated with the Irrigation Technology Centre. Additionally the exact position of the logger in the selected area had to be chosen: no canopy, to prevent alternative results due to less rain and to keep the solar panel activated. No trash in the ground, which could result in deviating results. Unfortunately this was not possible at each location.

In terms of logistics some difficulties arose. Three of the locations are not easy to reach on your own, this means that simple/fast checks and experiments could not easily be executed. Some preparation and funding were needed each time the locations must be visited.

During the installation it became clear that the digging and inserting the sensor was held back by the dry ground. Again the climate plays a role here, where a dry ground results in rough work and poorer attachment of the sensors, while wet ground could lead to messiness and less steady soil.

The staff of ITC always assisted in the fieldwork and were very eager to learn, but occasionally the communication was challenging. Explaining of the functions and maintenance of the devices was often not understood, this is why a manual is made to explain everything in detail, so that it can be read in their own time and pace. Likewise for the experiments it was confusing for both sides what to expect, but often it resulted in creative solutions. It became clear though that additional experiments without being there would not be possible to accomplish. Unfortunately, due to the corona virus situation, there was no time to do the calibration with ground truth samples, and explaining these methods to the staff at ITC would not have worked.

Further use
Although the early departure meant that a large part of the fieldwork and experiments could not be done, the network was installed and produced continuous data on the Zentracloud. Until, at the end of August 2020, two of the four devices stopped delivering data. After some research it was clear that a general reset by Metergroup of the ZL6 Logger, caused the sim-cards to be seen as forbidden, and thereby denying access to the cloud. A step-by-step performance should be performed to solve this problem. Here again the communication issue arose, where the given instruction was not sufficient. A new manual with a more comprehensive explanation has been sent. This situation showed that when one is at the location there are not too many obstructions, that being physically present can solve most problems, but from a distance this is a challenge.

Besides this particular problem, the maintenance of the network remains a challenge. Although the devices had been protected and haven't been opened during the entire monsoon season, at least two devices have been damaged by insects and/or water. This means the weather condition that occur in the tropics could not be completely avoided. The large variation in humidity will continue to be a challenge. The remote location makes it impossible to easily go into the field and solve the challenges, especially during a global pandemic, and the cultural differences and communication issues make it complicated to instruct from a distance.

6.2. Reliability of the in-situ soil moisture networks

2017 network

The 2017 network, the in-situ soil moisture network placed in 2017, was evaluated for its reliability, by looking at the availability and the quality of the soil moisture measurements. The network produced data from June 2017 to July 2018, which is 13 months of data. The data has some missing values, which means the continuity is not always guaranteed. The retrieval of the data was manual. The data records of the network were made available for this research and were uploaded to the ISMN during this research, which means it is now available with open access. Overall the availability of this network was considered reliable for the use of the small scale validation in this research.

The quality was evaluated by observing the time series. The timeseries showed plausible results, with trends that behaved according to the expected soil moisture trend following the monsoon climate in the tropics. There were values are missing, especially at Hpayargi a whole period is missing. Furthermore there were values below 0.0 m^3/m^3. The statistical analysis showed that the surface sensor at the ITC has a high coefficient of variation, 0.945, this lowers it reliability and therefore the measurements at 10cm depth was be considered as well. The box plots showed that the soil moisture content was generally higher at Hpayargi and Thanatpin, which is in agreement with the soil texture and its water retention capacity. Two experiments were done in order to calibrate the sensors. These resulted in acceptable errors, showing that the in-situ sensors correctly measure the soil moisture content. In the analysis with the precipitation data the sensors show responses that were expected after rainfall, and a good agreement could be seen between the precipitation data and the surface soil moisture. This indicates that the sensors are reliable.

Overall it was concluded that the 2017 in-situ soil moisture network provides an accurate estimate of the soil moisture content at the four locations and it can be used as reference for the validation of satellite soil moisture products in this research.

2020 network

The availability and quality of the in-situ soil moisture measurements of the 2020 network, the in-situ soil moisture network installed in 2020, were analysed. The 2020 network was installed in February 2020, which is still the dry period in the Bago region. This means that the sensor did not settle immediately. The network is considered to be usable after the first large rain event has passed. This was halfway through May. The data record at the time of the remote sensing analysis was 6 months. At the end of August one sensor in Hpayargyi had failed, and the entire station of Thanatpin had failed, this reduces the continuity of the network. The 2020 in situ-network automatically uploads the measurements to the Zentracloud. The Zentracloud allows the measurements to be accessed near real time, leading to excellent availability of the soil moisture data. Being able to watch and download the data every minute of the day, without going into the field, gives the opportunity to monitor and use the network without time consuming actions and without opening the loggers, which is a large asset in this remote tropical area. This creates a very reliable and easy to access data frame.

The quality of the sensors and the network were evaluated for the 2020 network. First the timeseries of the soil moisture content were given at each location. The result showed a strong trend in the transition from the dry period to wet period. Some spikes and jumps were detected, and the surface sensor at the ITC seemed to fall out of range. This was supported by the low mean value that was found, 0.122 m^3/m^3, for the surface sensor at the ITC compared to the means. The daily fluctuations showed that the 2020 network behaves according to expectations, where the different sensors at each locations agree with each other. Next to that the characteristics of the various locations can be detected. In the first rain event the four locations show the reaction to the rain. Each location shows good behaviour over the depth, and during the drying out. The sensor-to-sensor comparison showed promising results. The infiltration test showed that the manual ML3 Theta probe measured a soil moisture content very similar to the in-situ soil moisture sensors. The comparison with the 2017 network, assuming that the 2017 network was considered reliable, also showed good agreement. The 2017 network showed more variability than the 2020 network. Each location showed soil moisture content measurements that were within similar range to the measurements of the 2017 network in the same time periods. This means both networks represented the locations in the same way. When compared with precipitation data the surface sensors show responses that were expected after rainfall, especially at the ITC location, and a clear correlation could be seen between the precipitation data and the surface soil moisture, therefore the sensor can be considered reliable.

To conclude, the reliability of the 2020 in-situ soil moisture network is promising and showed similar behaviour to the 2017 network, however it could not yet be used for the validation of the satellite soil moisture products in this research. This is mainly due to the short data record of the measurements. A visual comparison of the in-situ measurements of the 2020 network with the satellite products was done in this research, were the first measurements have been visualized. Especially the temperature measurements, that are an addition to this network and thus one of the first in the tropics, were used for new insights.

III

Part 3 Remote Sensing Analysis

7

Data and Methods

In this chapter the in-situ and satellite data and the methods that were used for the validation and error analysis will be described.

7.1. Data

In-situ products

The in-situ products were extensively described in part 2 of this research and are each at the four exact coordinates and depths described in section 4.1, the following products will be used:

- Soil moisture content in m^3/m^3 from June 2017 - July 2018
- Soil moisture content in m^3/m^3 from February 2020 onward
- Soil temperature in ° Celsius from February 2020 onward

Satellite products

In this research several satellite products from VanderSat and NASA will are used: Soil moisture, temperature, vegetation optical depth(VOD) and Normalized Difference vegetation Index (NDVI).

Soil moisture(SM) products:

Name	Unit	Satellite	Band	Representative sensing depth	Pixel size	Overpass time
SM-AMSR-XN	m^3/m^3	AMSR	X-band	1cm	100x100m	01:30
SM-AMSR2-C1N	m^3/m^3	AMSR2	C-band	2cm	100x100m	01:30
SM-SMAP-LN	m^3/m^3	SMAP	L-band	5cm	100x100m	06:00
SM-D-SMAPL3LPRM	m^3/m^3	SMAP	L-band	5cm	9km	06:00

Land surface and soil temperature products:

Name	Unit	Pixel size	Day/Night
TEFF-AMSR2	K	100x100m	Night
MOD11-LST-Day	K	1km	Day
MOD11-LST-Night	K	1km	Night

Vegetation optical depth(VOD) products:

Name	Unit	Band	Representative sensing depth	
vod-AMSR-XN	AMSR	m^3/m^3	X-band	1cm
vod-AMSR2-C1N	AMSR2	m^3/m^3	C-band	2cm
vod-SMAP-LN	SMAP	m^3/m^3	L-band	5cm

Normalized difference vegetation index (NDVI) product: NDVI no unit, retrieved from Moderate Resolution Imaging Spectroradiometer (MODIS)-Terra MOD13c2, , accessed at Giovanni NASA EarthData.

The VanderSat products: soil moisture, temperature and VOD, were each down scaled and went through the Land Parameter Retrieval Model. Each signal has a pixel size of 100x100m. The fourth soil moisture product is from the SMAP satellite and gridded by NASA at 9km pixels and went trough the same LPRM as the VanderSat data. The level L3 indicates the level of data processing. Level 3 indicates geophysical parameters derived from level 1 or 2 data that have been spatially and/or temporally re-sampled to a global grid (Chung et al., 2017).

Vegetation optical depth (VOD) represents the canopy water content dynamics. The optical depth is a measure of how opaque a medium (the canopy) is to radiation passing through it. The optical depth is directly related to the vegetation water content and dielectric properties of water, and is also a function of the incidence angle and the radiometric frequency (Meesters et al., 2005). In this research the VOD data is calculated by the LPRM from brightness temperatures derived from X-,C- and L-band, like the soil moisture.

The Normalized Difference Vegetation Index (NDVI) measures the difference between the near-infrared radiation and the visible wavelength radiation. Near infrared is strongly reflected by vegetation, while visible light is absorbed by vegetation. With the difference the vegetation can be quantified.

Parameters Land Parameter Retrieval Model

In this section the parameters that are used in the LPRM will be described. The parameters that will be tested for sensitivity, are given a range. In table 7.1 the values that are used in the current LPRM can be seen.

Parameters	C-band	L-band	X-band
Q	0.115	0.0	0.127
w	0.056	0.12	0.048
opt_atm	0.01	0.0	0.01
u	55	40	55
h1	2.6	1.1	2.25
h2	4.9	2.2	3.0
f	6.9	1.4	10.7
vod_fm	0.45	0.3	0.45
vod_fh	0.6	0.4	0.6

Table 7.1: Parameters and values used in LPRM

Q: polarization mixing factor
Q is a mixing factor that takes the polarization mixing caused by rough surfaces into account. Q is often considered to be negligible, especially at L-band (Mialon et al., 2012) A rough surface would imply a value for Q that is higher than zero. Results of studies suggest that for a smooth surface the value of Q should be around 0.05 [-] and for rough surfaces 0.3[-]. For this research a range from 0-0.4 was used.

ω: single scattering albedo
ω is the single scattering albedo, which is defined as the the portion of total extinction that is due to scattering. The ω depends on the thickness of the canopy and generally varies between 0 and 0.15, however much higher values were reported as well. (van de Griend & Wigneron, 2004; van der Schalie et al., 2015). For this research a range from 0-0.3 was used.

opt_atm: optical depth of the atmosphere
The atmospheric opacity is often assumed to be near 0, due to the small atmospheric contribution. In this research a small range between 0.0 - 0.05 will be used.

u :incidence angle of the observation
The incidence angle of observation, u, is the angle between the satellite sensor and the angle normal to the surface. The incidence angle is a fixed value that is different for each satellite. In various studies angles be-

tween 40 degree and 60 are used (**??**), a range between 35 and 60 will be used in this research.

h1, h2: Roughness parameters
h1 as h2 are roughness parameters that relate to the height variation of the surface and the correlation length. In literature generally only the roughness parameter h is mentioned. Typical values for h have been mentioned, that range from 0 for a smooth surface to 0.4 for a rough ploughed field (de Jeu, 2003). The roughness factor h is considered as a dynamic variable that varies in time and space. In this research the parameters h1 and h2 are used to express h as a function of soil moisture (θ): h=h1-h2*θ. For these parameters the ranges 0.0-4.0 for h1 and 1-3*h1 for h2 are used.

f: frequency
The frequency, f, differs per wavelenght and band. For soil moisture studies the most important bands are: L-band (frequency f = 1 – 2 GHz, wavelength λ = 30 – 15 cm), C-band (f = 4 – 8 GHz, λ = 7.5 – 3.8 cm),and X-band (f = 8 – 12 GHz, λ = 3.8 – 2.5 cm) (Scanlon et al., 2020). The frequencies mentioned in Table 7.1 are set for these bands, and will not change.

Parameters	Ranges
Q	0.0-0.4
w	0.0-0.3
opt_atm	0.0-0.05
u	35-60
h1	0.0-4.0
h2	1-3*h1

Table 7.2: Ranges of the different input parameters of the model

7.2. Methods

Preprocessing

Spatial matching

The ground based measurements are based on in situ observations at a single location. Therefore the in-situ data has a spatial support that differs largely from the gridded soil moisture retrieval products. Consequently all metrics will be prone to representatives errors (Al-Yaari et al., 2019). This is a known problem in the validation studies of soil moisture. While VanderSat has managed to downscale the pixel size to 100 m x 100 m, the satellite product that is gridded by NASA still has a larger pixels size of 9 km. Therefore the SMAP-L3products was rescaled using linear regression to match the reference data set. The in-situ locations were selected based on representativeness of the surrounding area. In Figure 7.1 the pink dot/square represents one pixel of the VanderSat satellite products near Bago.

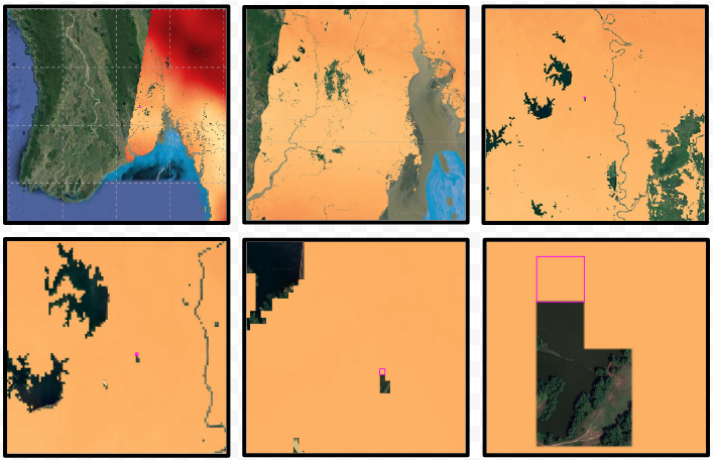

Figure 7.1: Pixel of satellite retrieved soil moisture on the map near Bago, source: maps.vandersat.com

Temporal matching

In order to correctly evaluate the measurements temporal matching is needed between the satellite and in-situ products. The satellite products have different overpass times. The overpass time of the X-band and C-band is at 1:30AM and the overpass time of both the L-bands is at 6:00AM. The in-situ sensors measure in half hour intervals. To match these products the in-situ measurements closest to the satellite observation time were considered. Given the high temporal resolution of in-situ measurements, the difference between satellite overpasses and in-situ observations was always a maximum of half an hour. Furthermore the satellite products have a measurement record of years and are still providing. The in-situ products have measured between June 2017 and July 2018, and from February 2020 onwards. These dates have been matched for comparison and validation. The days where no data was available for either the in-situ measurements or the satellite measurements were filtered out.

Validation satellite products with 2017 network

For the validation of the satellite products, the soil moisture data from the 2017 network, 2017/2018, will be used as reference. The surface sensors, that reach down to a depth of 5cm will be used. These sensors are chosen in relation to the representative sensing depths of the satellites. Because of the very noisy surface sensor at the ITC, the validation is also done with an average of the sensors at 10cm depth. The satellite products that are used in the validation are the soil moisture products mentioned in the data section.

The validation results are presented per location. First the timeseries of both the in-situ and satellite measurements are analysed and compared with the vegetation optical depth and normalized difference vegetation index products. The statistical analysis to evaluate the satellite products in reference to the in-situ network was done. This was done in python, using the package pytesmo, which provides a standard library that can be used for the comparison and validation of geospatial time series datasets with a focus on soil moisture. The following statistical scores will be used to validate the performance of the satellite soil moisture products: Pearson R, Root Mean Squared Difference (RMSD), unbiased RMSD and bias:

Pearson's R, a correlation coefficient. R is a measure of linear association between two variables, if the data sets from the two variables constitutes exactly a straight line when plotted, R equals plus or minus 1. The Pearson correlation coefficient is calculated as follows:

$$R = \frac{\sum(x - m_x)(y - m_y)}{\sqrt{\sum(x - m_x)^2(y - m_y)^2}} \tag{7.1}$$

where:
m_x = the mean of the vector x.
m_y = the mean of the vector y.

The root means square difference(**RMSD**) is used for estimating uncertainty and it shows the accuracy. RMSD is the square root of the variance, also known as the standard error. It is the standard deviation of the errors in the predication, therefore it is a measure of accuracy. The RMSD ranges from 0 to infinite, where the unit will be the same as the dependent variable, in this case m3/m3. Unbiased RMSD (**ubRMSD**), where the bias component is removed from RMSD shows the precision. The ubRMSD ranges from 0 to infinite as well, with unit m3/m3. Both for RMSD and unbiased Root Mean Squared Difference (ubRMSD) values approaching zero are optimal. Although satellite soil moisture validation studies often use a threshold of 0.04 m^3/m^3 for the ubrmsd, this is based on a rough estimate of what is currently achievable, rather than an indication of the product quality (Gruber et al., 2020). The value of 0.04 m^3/m^3 is therefore used as a target value, however values that do not meet this requirement are not depreciated.

$$RSS = \sum((o - p)^2) \tag{7.2a}$$

$$RMSD = \frac{\sqrt{RSS}}{n} \tag{7.2b}$$

$$ubRMSD = \sqrt{\frac{\sum(((x - m_x) - (y - m_y))^2)}{n}} \tag{7.2c}$$

where:
RSS = Residual Sum of Squares (RSS)
o = observations
p = predictions
m_x = mean of vector x
m_y = mean of vector y
n = number of observations

Bias, the temporal mean difference between the data sets, shows accuracy. The bias is used to measure dryness or wetness of the satellite-based retrievals on capturing soil moisture seasonal variations of the satellite-based retrievals compared to in-situ observations. Smaller values mean more accuracy.

$$bias = m_x - m_y \tag{7.3}$$

Figure 7.2: Explanation of the definition of accuracy and precision

Parameterisation Land Parameter Retrieval Model

For the sensitivity analysis of the satellite products, the soil moisture data from the 2017 network will be used as reference. The surface sensors, that reach down to a depth of 5cm will be used. These sensors are chosen in relation to the sensing depths of the satellites. A sensitivity analysis is done to determine how independent variable values will impact a particular dependent variable under a given set of assumptions. In this case the independent variables are 6 parameters that are used to calculate the soil moisture content with the Land Parameter Retrieval Model. The impact the parameters have on the soil moisture will be evaluated by calculating the unbiased root mean square errors, with in-situ soil moisture as reference. To evaluate the sensitivity of these 6 parameters that are used in the LPRM a part of the algorithm is tested. First a code was written to run the part of LPRM that is needed for this research. This code was calibrated until lead to the outcomes that are the standard product, which is necessary before alterations can be made.

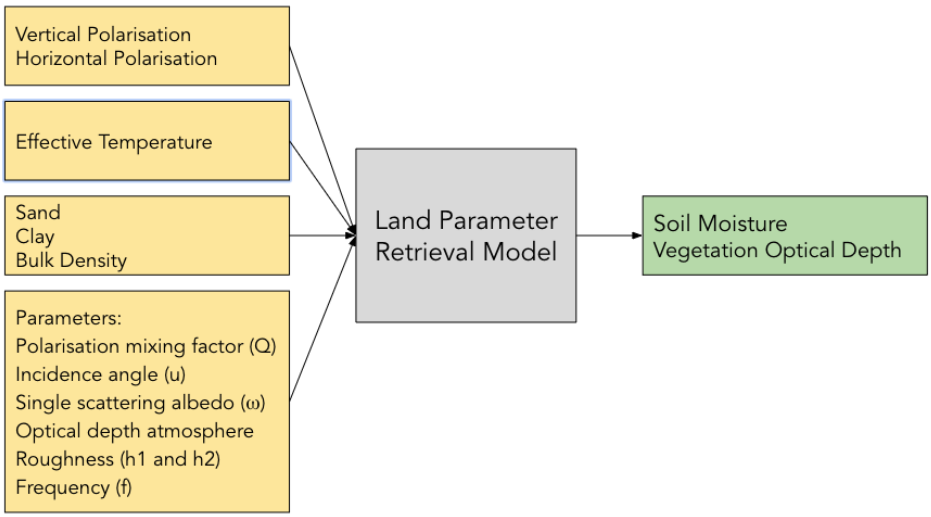

Figure 7.3: Schematic overview of the input and output of the Land Parameter Retrieval Model in this research

To run the model and get the soil moisture (SM) and vegetation optical depth (VOD) outcome there are several inputs needed (Figure 7.3). The vertical and horizontal polarisation timeseries, the sand, the clay and bulk density values and the Ka-band brightness temperature were downloaded from the vandersat maps (`https://maps.vandersat.com`), where the in-house products of VanderSat were made available for this research. T_{eff} the effective temperature (land surface temperature) is calculated from the brightness temperature retrieved by the Ka-band. These parameters were each downloaded at the specific locations of the in -situ sensors. The last input are the individual parameters that are filled in manually, more information on these parameters can be found in the previous section. During the parameterisation the ranges that were mentioned in the data section Table 7.2 will be used to investigate the sensitivity of the 6 parameters. The model parameters Q, ω, opt_atm, u, h1 and h2 were adapted in order to minimize the unbiased root mean square error of the satellite soil moisture products versus the in-situ soil moisture products, while keeping the Pearson R > 0.75. The sensitivity test is visualised in graphs to show the influence of the parameters and identify the optimal ranges. The combinations of parameters that lead to the 100 lowest ubRMSD were selected and plotted again to further narrow down the ranges. An overview of the ranges where the top 100 values of lowest ubRMSD fall within is given in boxplot per band and location.

Visual comparison 2020 network

For the visual comparison the in-situ soil moisture and temperature data from the newly placed network in 2020 were used. The 2020 network placed in Bago will eventually be used for further validation studies in this area. For now the period is not long enough to do these validations, but the first visual comparisons were done, where especially the temperature measurement were of interest. The soil moisture products were visually analysed and a closer look was taken at the on-set of the monsoon season in both the in-situ and satellite soil moisture products. The temperature measurements were analysed and compared to other temperature products and possible sources of errors were discussed.

8

Results Remote Sensing Analysis

In this chapter the in-situ products that were installed in Bago, Myanmar were used as reference to validate and analyse four satellite products. First the validation of the satellite products of VanderSat and NASA was done with the in-situ soil moisture network that operated between 2017 and 2018. Four metrics were computed for each location: Pearson correlation coefficient(R), RMSD, ubRMSD and the bias. The result were evaluated by looking at the VOD and NDVI. In the second section a part of the retrieval algorithm, the LPRM, that is used for the satellite products of VanderSat has been looked at. A sensitivity test was performed to analyse certain parameters, and ranges for the optimal values are given. In the last section the in-situ soil moisture network that was placed in 2020 was used to evaluate the temperature measurements. First the soil moisture and temperature satellite products of VanderSat were visually compared to the in-situ soil moisture and soil temperature data of the new network from 2020. Here a closer look was taken at the ability of the satellite products to capture the monsoon on-set and off-set. Next the temperature measurements of the satellite were compared to the measurements of the in-situ network. The deviant behaviour of the temperature measurements is compared with additional in-situ and satellite temperature data.

8.1. Validation of satellite products vs. the 2017 network

Below the timeseries of the soil moisture, vegetational optical depth (vod) and normalized difference vegetation index (NDVI), at the four locations, Irrigation Technology Centre (ITC), Hpayargyi, Alaigni and Thanatpin are shown and analysed. After this the results of the validation by statistical analysis can be found, summarized in table 8.1.

Irrigation Technology Centre

In Figure 8.1 the soil moisture measurements of the in-situ surface sensor and satellites at the ITC can be seen. As mentioned in the in-situ soil moisture chapter, the measurements of the surface sensor at the ITC show a lot of noise and values below 0.0 $m3/m3$, which is not expected behaviour. The sensor at 10cm depth (lightblue) is therefore also considered. The trends of the three VanderSat soil moisture products, C-band, L-band and X-band, are similar, with some outliers in the wet period of the L-band. The three bands overestimate the soil moisture content in the dry period compared to the in-situ soil moisture measurements, a result that is found in more validation studies (Dente et al., 2020). The L3 product seems to follow the trend of the in-situ measurements, although it starts drying down way earlier. Montzka et al. (2020) mentions soil surface roughness could lead to overestimation of the soil moisture, when the microwave emission that is caused by surface roughness is not corrected or isolated.

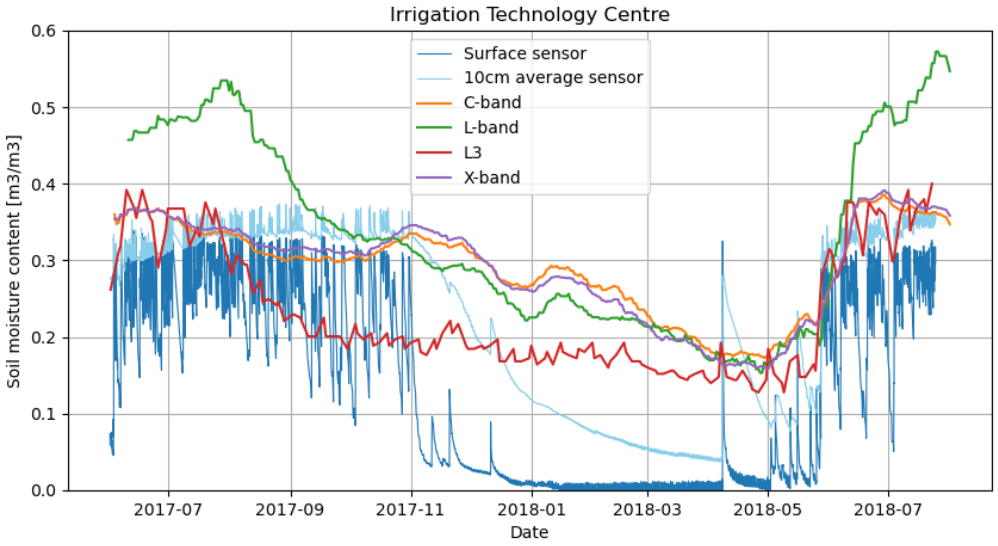

Figure 8.1: Timeseries the surface sensor and different satellite bands at ITC

The left graph in Figure 8.2 shows the vegetation optical depth (VOD) for the location ITC. The C-band and X-band show a very similar pattern with VOD values between 0.3 - 0.4 m^3/m^3 in the months November to May. The L-band has significantly higher values during the months June, July and August, both in 2017 and 2018, than the other bands. The VOD represents the canopy water content. The vegetation produces microwave emissions itself, and attenuates the emission from the soils underneath. If this is not accounted for, this would lead to underestimation of soil moisture (Montzka et al., 2020). The optical depth increases with higher vegetation densities. Higher vegetation densities means that more soil emissions are attenuated by the canopy and the signal contains emission from the vegetation as well. As a result, the increase of VOD means that the sensor sensitivity to soil moisture variations decreases. Fernandez-Moran et al. (2017) mentions that VOD values at L-band generally vary between 0 and 0.6 over croplands and grassland. Their study also showed temporal mean values of VOD between 2010 and 2015 from SMOS-IC and SMOSL3 which indicated values below 0.4 for Myanmar. The normalized difference vegetation index (NDVI) quantifies vegetation as well and is often used to study vegetation optical depth (Grant et al., 2016). Note that the axes of VOD and NDVI do not indicate the same range of values. The values of the NDVI range between 0 and 1, where higher values indicate a larger amount of greenness. In the right graph in Figure 8.2 the NDVI indicates a high amount of vegetation between August and November 2018, the C-band and X-band increase as well during this period, in contrast to the L-band, which decreases during these months.The L-band is much less sensitive to the effects of vegetation, due to the larger penetration depth following from the longer wavelength (Jackson et al., 2012).

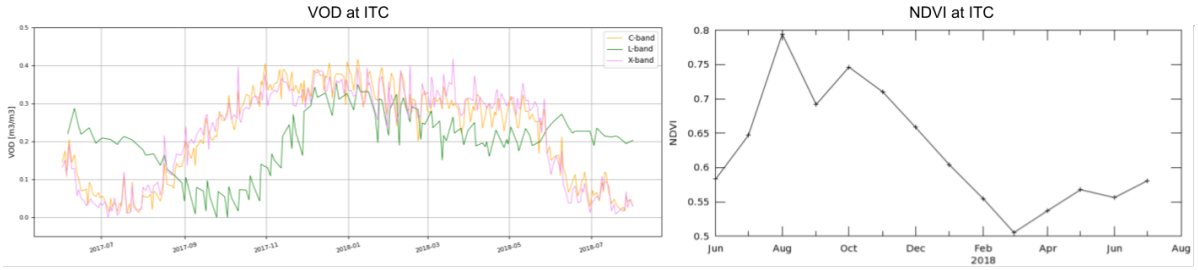

Figure 8.2: Timeseries of the vegetation optical depth of VanderSat C-band, L-band and X-band and Timeseries of area averaged Normalized Difference Vegetation Index obtained from NASA Earthdata from the MODIS-Terra satellite, both between June 2017 and July 2018 at ITC

Hpayargyi

In Figure 8.3 the timeseries of soil moisture measurements at Hpayargyi are shown. The C-band and X-band show similar results again. These bands show a underestimation in the first wet period, from June 2017 to September 2017. The L-band again shows some outliers in the wet periods, but follows the dry-down trend of the other bands. The L3 dries down sooner then the in-situ product, and the other satellite products. In the dry period from November 2017 to May 2018 an overestimation can be seen. The overestimation over soil moisture content by satellite retrieval in dry periods is seen more often in validation studies Colliander et al. (2017); Mascaro, Ko, and Vivoni (2019). All the satellite products overestimate the soil moisture content compared to the soil moisture content of the surface sensor, however the difference is smaller than at the ITC. The monsoon on-set, which started early May 2018, is captured well by all the satellite products.

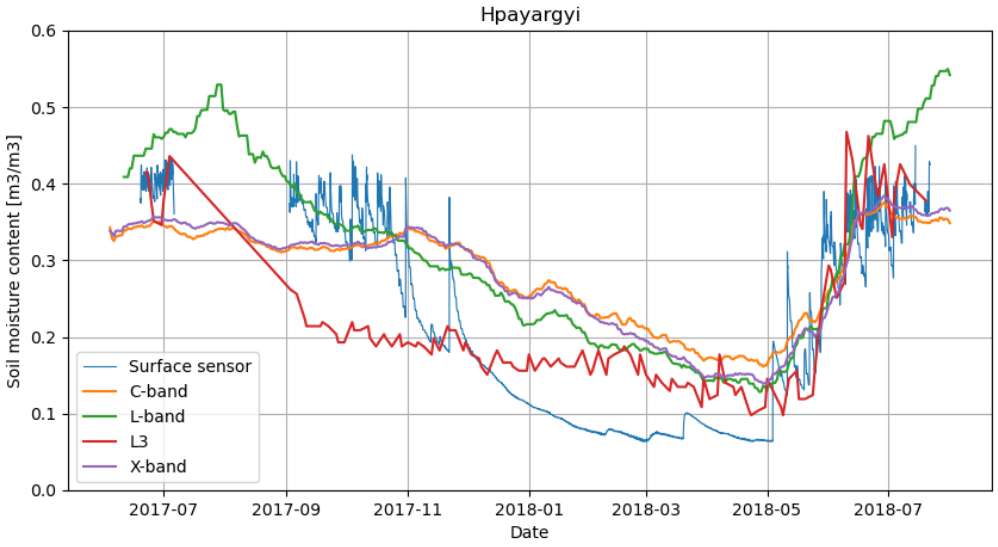

Figure 8.3: Timeseries of the surface sensor and different satellite bands at Hpayargyi

The VOD and NDVI at Hpayargi are shown in Figures 8.4. Again the L-band shows a different trend than the C-band and X-band, where the values lie high in the months June and August and decrease from September to November. These higher values of VOD could result in lower sensitivity to soil moisture variations, which could explain the high soil moisture values in these months that are measured with the L-band. The NDVI shows high values from July to October and then decreases fast and stays lower until the start of May. This follows the Monsoon season.

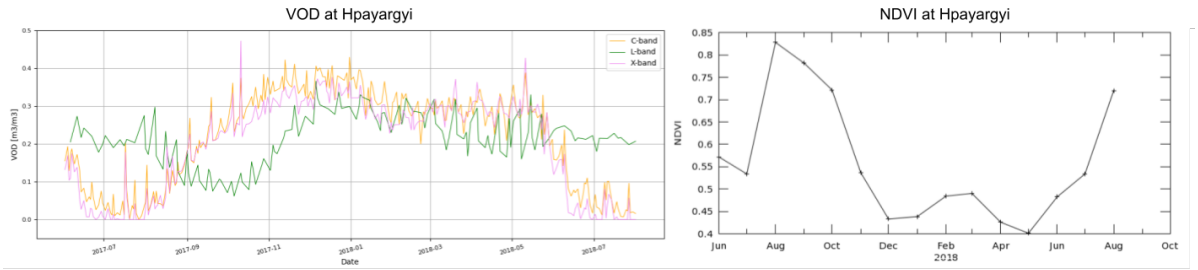

Figure 8.4: Timeseries of the vegetation optical depth of VanderSat C-band, L-band and X-band and Timeseries of area averaged Normalized Difference Vegetation Index obtained from NASA Earthdata from the MODIS-Terra satellite, both between June 2017 and July 2018 at Hpayargyi

Alaigni

The timeseries of the soil moisture measurement at Alaigni can be found in Figure 8.5. C-band and X-band show very similar result to each other, in relation to the in-situ soil moisture they show high values during the dry period. The L-band measurements values are very high, up to 0.58 m^3/m^3, during the wet season. The

L3 product shows a dry down from late July on wards, which cannot be seen in the in-situ soil moisture.

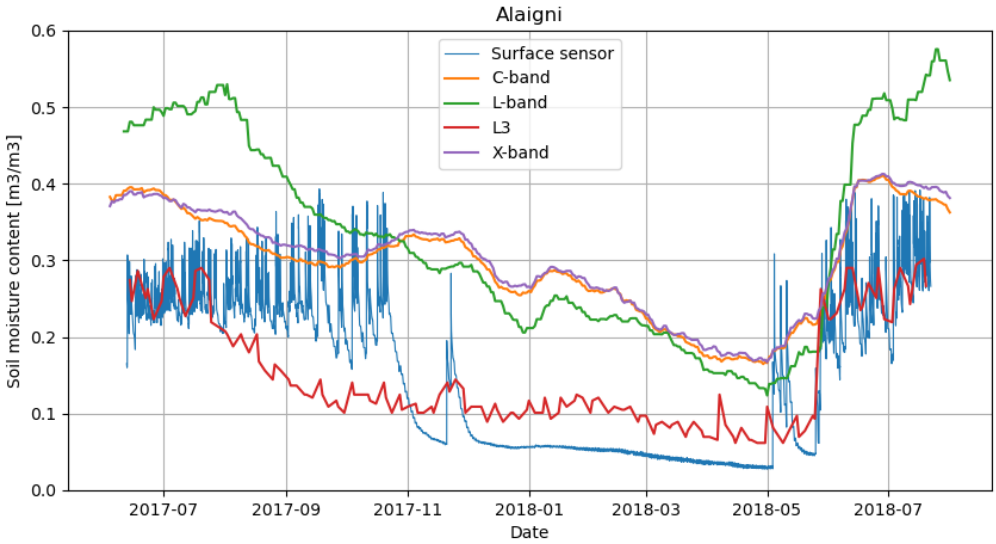

Figure 8.5: Timeseries the surface sensor and different satellite bands at Alaigni

In the VOD measurements in Figure 8.6 a strange behaviour can be seen at the L-band between September and October 2017, a behaviour that can not be seen back in the soil moisture measurements. The C-band and X-band show no particular deviating behaviour during these months, neither does the NDVI in the right graph of Figure 8.6. In the NDVI graph the steep increase in May 2018 stands out, this means the greenness is suddenly very high. This could have several reasons, for example sudden precipitation or irrigation. In the soil moisture graph it can be seen that the soil moisture content of the in-situ sensor increases sharply as well during this period.

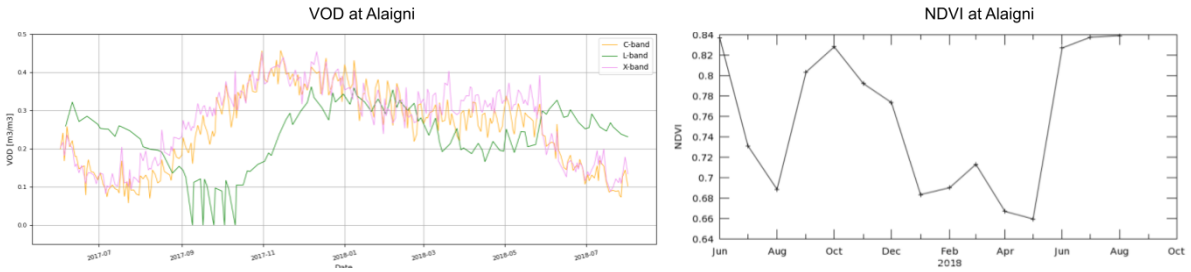

Figure 8.6: Timeseries of the vegetation optical depth of VanderSat C-band, L-band and X-band and Timeseries of area averaged Normalized Difference Vegetation Index obtained from NASA Earthdata from the MODIS-Terra satellite, both between June 2017 and July 2018 at Alaigni

Thanatpin

In Figure 8.7 the measurements of soil moisture at Thanatpin can be seen. The values of the soil moisture measured by the in-situ sensor in the period from July to November 2017 are relatively high, up to 0.47 m^3/m^3. The L-bands show values within range of this in the first month, but they dry down quickly from August on. The values of C-band and X-band start out with lower values, but the dry down sets in around the same time as the in-situ measurements, around December 2017. As mentioned at the other locations the in-situ sensors show significantly lower values during the dry season after the dry down, from around November till May. In Thanatpin these lower values in the in-situ measurements are visible from the end of December 2017.

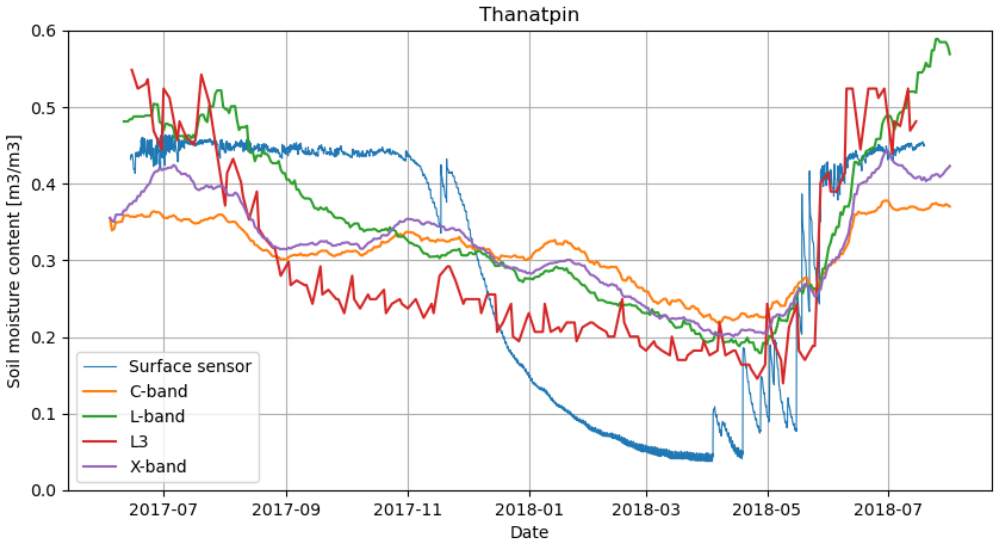

Figure 8.7: Timeseries of the surface sensor and different satellite bands at Thanatpin

In the VOD data in Figure 8.8 the values that approach values near 0.0 m^3/m^3 between June and August 2017 and June and August 2018 stand out. These low values are explained by a lack of vegetation. The values of the NDVI show low values as well, where at the other location no values below 0.4 were found, the values at Thanatpin do not pass 0.4 in these months. Thanatpin is located in a urban area, which could explain the lack of vegetation, that is removed due to hinder for example.

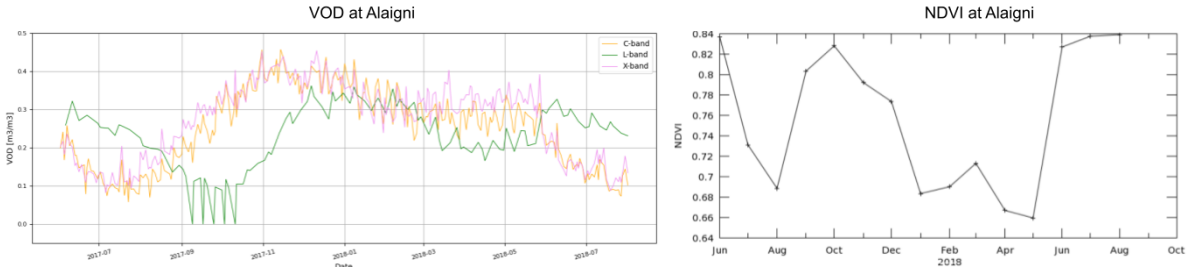

Figure 8.8: Timeseries of the vegetation optical depth of VanderSat C-band, L-band and X-band and Timeseries of area averaged Normalized Difference Vegetation Index obtained from NASA Earthdata from the MODIS-Terra satellite, both between June 2017 and July 2018 at Thanatpin

Figure 8.9 shows the comparison between the surface in-situ and satellite retrieved soil moisture products. For the in-situ soil moisture values between 0.0 and 0.2 m^3/m^3 there is a clear overestimation by the satellite products. This agrees with the dry period between November 2017 and May 2018 in the timeseries of Figures 8.1, 8.3, 8.5 and 8.7. For ITC and Hpayargyi the higher soil moisture values show good agreement between the in-situ and satellite soil moisture, with some outliers for the L-band. At Alaigni the overestimation trend seems to continue with the higher values as well, expect for the scaled L3 product. The higher values at Thanatpin show an underestimation of the satellite products.

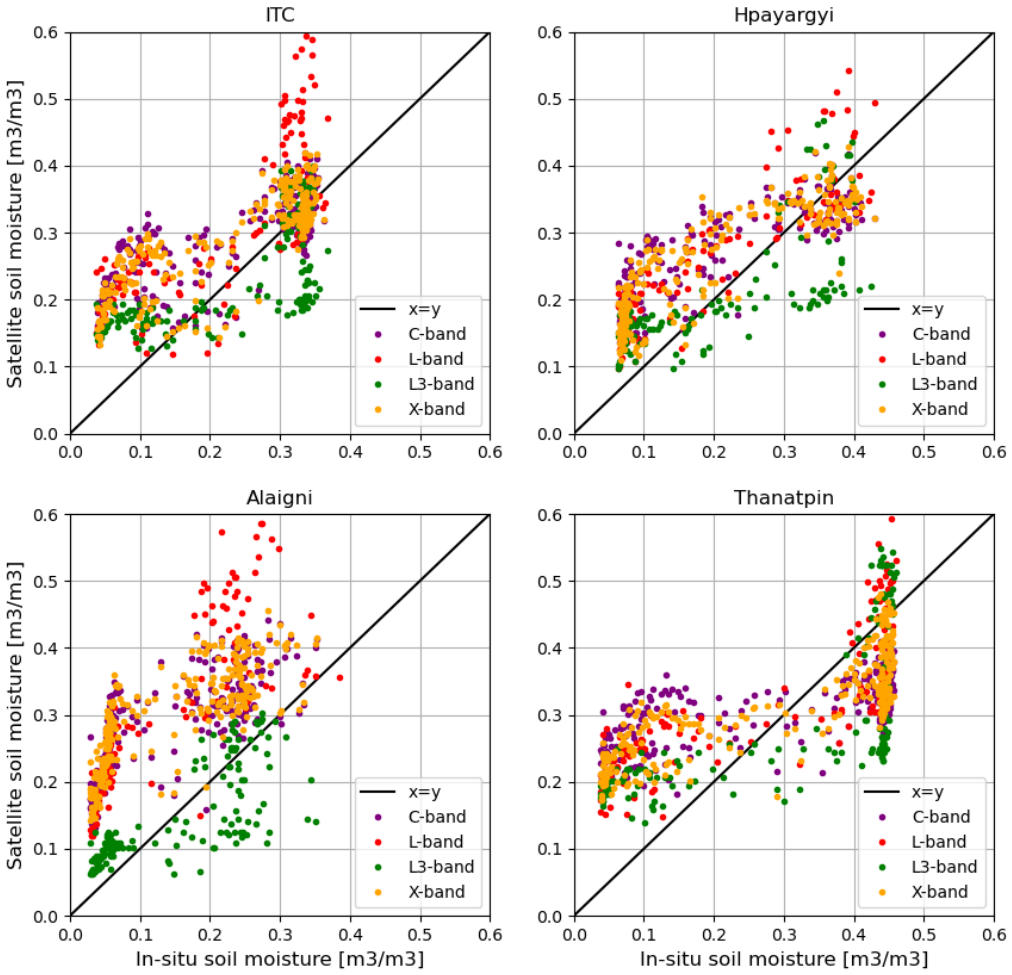

Figure 8.9: In-situ soil moisture measurements versus satellite retrieved soil moisture at ITC, Hpayargyi, Alaigni and Thanatpin.

Table 8.1 lists the performance metrics: Pearson's R, RMSD, ubRMSD and bias for each location and band combination. The colors in the cells indicate the relative performance of the score, where green indicates the best result, yellow a moderate, and red the least.

The **Pearson's R**, is above 0.7 for all the locations and bands, which is a good result. A study over a tropical region in Malaysia showed very weak to moderate results for the correlation, between 0.006 and 0.540 (Kang et al., 2016). In the United States a watershed network in a humid climate showed a correlation of 0.631 for AMSR-E X-band and 0.643 for SMOS L-band (Jackson et al., 2012). Colliander et al. (2017) showed validations studies of SMAP L-band that resulted in R-values between 0.489 - 0.969 for arid and semi-arid regions. In this research the correlation seems highest for the L-band, ranging from 0.78 to 0.89. L-band was expected to have the best performance, because it has the same representative sensing depth as the in-situ soil moisture sensors. Hpayargi is the location that produces the best results for correlation, in agreement with Figure 8.9. When looking at the differences between the two ITC depths, it can be observed that the R increases for the X-band and C-band, but decreases for both L-bands at 10cm depth.

Table 8.1: Performance metrics for validation of satellite retrieved soil moisture at ITC, Hpayargyi, Alaigni and Thanatpin. Surface in-situ soil moisture as reference

Location	Band	Pearson R	RMSD	ubRMSD	Bias
ITC	C-band	0.7339	0.1843	0.0897	-0.1622
	L-band	0.8081	0.2112	0.0740	-0.1975
	L3-band	0.7432	0.0819	NA	NA
	X-band	0.7803	0.1809	0.0815	-0.1618
Hpayargyi	C-band	0.8369	0.0991	0.0715	-0.0626
	L-band	0.8858	0.0870	0.0593	-0.0651
	L3-band	0.7292	0.0839	NA	NA
	X-band	0.8551	0.0904	0.0674	-0.0566
Alaigni	C-band	0.7542	0.1582	0.0676	-0.1449
	L-band	0.8115	0.1871	0.0614	-0.1704
	L3-band	0.7386	0.0651	NA	NA
	X-band	0.7773	0.1639	0.0644	-0.1523
Thanatpin	C-band	0.7008	0.1365	0.1287	-0.0103
	L-band	0.7793	0.1155	0.1114	-0.0425
	L3-band	0.7018	0.1195	NA	NA
	X-band	0.8086	0.1177	0.1029	-0.0183

Table 8.2: Performance metrics for validation of satellite retrieved soil moisture at ITC. In-situ soil moisture at 10cm depth as reference

Location	Band	Pearson R	RMSD	ubRMSD	Bias
ITC 10cm	C-band	0.7700	0.0986	0.0780	-0.0613
	L-band	0.7651	0.1223	0.0810	-0.0903
	L3-band	0.6787	0.0847	NA	NA
	X-band	0.8271	0.0920	0.0676	-0.0609

Satellite soil moisture validation studies often evaluate products against a target accuracy thresholds (Gruber et al., 2020). The SMOS mission set a target accuracy for 0.04 m^3/m^3 (Kerr et al., 2001; van der Schalie et al., 2015), while for SMAP products target accuracy thresholds of both 0.04 m^3/m^3 and 0.06 m^3/m^3 are mentioned (Colliander et al., 2017) (Entekhabi et al., 2010). These target threshold are mentioned for both **RMSD** and **ubRMSD**.

The **RMSD** values range between 0.08 and 0.21 m^3/m^3. The studies in a tropical region in Malaysia showed RMSE values between 0.09 and 0.16 m^3/m^3 (Kang et al.,2016a; Kang et al.,2016b) Liu, Yang, and Yue (2018) evaluated satellite based soil moisture in various regions. A humid temperate marine climate region in Spain showed a RMSE values between 0.12 and 0.18 m^3/m^3 for AMSR products and between 0.06 and 0.09 m^3/m^3 for Soil Moisture and Ocean Salinity (SMOS) products. At the Tibetan Plateau with cold dry winters and humid cool monsoon summers, values for RMSE between 0.09 and 0.14 m^3/m^3 for AMSR products and 0.1 and 0.2 m^3/m^3 for SMOS products were found. The RMSE values at the humid climate region in the U.S. were 0.049 m^3/m^3 for AMSR-E and 0.072 m^3/m^3 from SMOS. Colliander et al. (2017) showed RMSE values between 0.03 and 0.06 m^3/m^3 for SMAP products in arid and semi-arid regions. The values of the RMSD for this research in Myanmar are at the high end of the ranges in (somewhat) similar regions. The location Hpayargyi shows the lowest RMSD values. The L3 shows the lowest values but this is due to the scaling, which results in zero bias. The mentioned target thresholds are not reached by any location or band.
Looking at the **ubRMSD**, where the bias is removed from the RMSD, values between 0.06 and 0.13 m^3/m^3 are found. A humid temperate marine climate region in Spain showed ubRMSD values between 0.10 and 0.105 m^3/m^3 for AMSR products and between 0.06 and 0.08 m^3/m^3 for SMOS products (Liu et al., 2018). The validation of SMAP surface soil moisture resulted in values between 0.03 and 0.06 m^3/m^3 for semi arid and arid regions (Colliander et al., 2017). Especially at the locations ITC, Hpayargyi and Alaigni the ubRMSD values are very similar to other studies, and for the L-band at Hpayargyi the target threshold of 0.06 m^3/m^3 is met. At Thanatpin the values are considerably higher.

The **Bias** resulted in values between -0.02 and -0.2 m^3/m^3. The negative biases mean that the satellite products overestimate the soil moisture content, which confirms the observations at the start of the section. (Kang

et al.,2016b) found a wet bias ranging from -0.06 to -0.11 m^3/m^3. (Liu et al., 2018) showed bias between -0.09 -0.14 m^3/m^3 for AMSR and 0.03 and 0.04 m^3/m^3 for SMOS at the Tibetan Plateau and between -0.07 and -0.10 m^3/m^3 for AMSR and between 0.074 and 0.10 m^3/m^3 for SMOS in Spain. In the humid climate region in the U.S. a mean bias of -0.04 m^3/m^3 was found for AMSR-E and -0.045 m^3/m^3 for SMOS (Jackson et al., 2012). For the semi arid and arid regions evaluated by Colliander et al. (2017) result between -0.01 and 0.03 m^3/m^3 were indicated. With the large range found in this study, a part the biases can be found back in literature, but the bias values above 0.10 are not represented. These high values are found at the locations ITC and Alaigni, however when the measurements at 10cm depth are considered for ITC the bias improves. This could be due to the fact that the in-situ sensor at 10 cm depth show less variability. The in-situ surface sensor at Alaigni shows some variability to, which could be a source of larger bias. The low bias at Thanatpin could be an effect of cancelling out of over- and underestimations, as can be seen in Figure 8.9. For the L3-band all the biases were zero, as this band is scaled to the sensors, so these were not considered.

To summarize, the performance metrics indicate that the satellite retrieved soil moisture has a good correlation with the in-situ products, with values of R between 0.7 and 0.89. The RMSD and ubRMSD partially fall in the same range when compared to other validation studies, but there are values that are too large and thus can not be considered to provide an accurate product. The locations ITC and Alaigni have very strong biases. At ITC this is reduced when looking at the in-situ sensor at 10cm depth, which has less variability is soil moisture measurements. When evaluating the performance several sources of errors must be taken into account. First it must be considered that the reference data, the in-situ measurements, contain errors (Gruber et al., 2020), the small scale calibration that was done for this in-situ network indicated a RMSE ranging from 0.011 to 0.059 m^3/m^3 between the sensor measurements and the ground truth samples. Furthermore the spatial mismatch is often a source of error, where the point-scale observations of the in-situ measurement do not represent the same grid size as the satellite measurements. With the downscaling method of VanderSat the soil moisture can be obtained at a resolution of 100 x 100 m. which is a large improvement of resolution compared to the pixel sizes of other satellite products. With the downscaling method of VanderSat the pixel is calculated as a weighted sum of all overlaying ellipses of different footprints, see chapter 3.2, the amount of footprints contributing to a single value is approximately 4 to 6 in the tropics (Hemshorn de Sanchez, 2018). In the tropical areas there are two main drawbacks with the downscaling, the first being limited variety in brightness temperatures and the second is the dynamics of open water bodies. Water surfaces are masked out using a high resolution land water map from ESA. In the tropics the water bodies are often not mapped well and they can change in shape, next to that the temperature of their surface is not well known and has to be estimated. As a result possibly not all water bodies are masked out properly (Hemshorn de Sanchez, 2018). The sources of errors can also be related to the model. "In the modelling community representativeness errors mostly refer to a model's lacking ability to represent reality and, as such, to imperfections in the model structure and in parameterisation." (Gruber et al., 2020). In the next section a parameterisation was performed to evaluate the sensitivity of the algorithm of the Land Parameter Retrieval Model to certain parameters. In the last section the land surface temperature product of VanderSat was evaluated using the newly placed 2020 network, that measures soil temperature in addition to soil moisture. As the land surface temperature is an input in the algorithm to retrieve soil moisture, the uncertainty in the temperature estimates will result in soil moisture uncertainty (Saleh et al., 2007).

8.2. Parameterisation Land Parameter Retrieval Model

Following the results of the validation, a sensitivity test was executed to understand if certain parameters could be of influence on the errors. The sensitivity test was done for 6 parameters simultaneously, the following parameters were given a range: Q: polarisation mixing factor, ω: single scattering albedo, opt_atm: optical depth of the atmosphere, u: incidence angle, h1 and h2: roughness parameters. The 20.000 runs of the algorithm were done with the 6 parameters that take random values each run, these values are within the given range, see Table 7.2. The sensitivity test is expressed in scatter plots of each parameter versus the unbiased root mean square deviation (ubRMSD). Afterwards an optimisation was done to select the ranges that resulted in the lowest ubrmse, these are shown in the box plots in Figure 8.12. The test was done at each location, and for the C-band, L-band and X-band soil moisture products of VanderSat. The L-band at Alaigni will be discussed extensively as an example of analysis, the other graphs can be found in the appendix.

In Figure 8.10 an example can be seen of the graphs, showing the ranges of the 6 selected parameters versus the unbiased RMSD, at Alaigni with L-band, for the 20.000 runs.

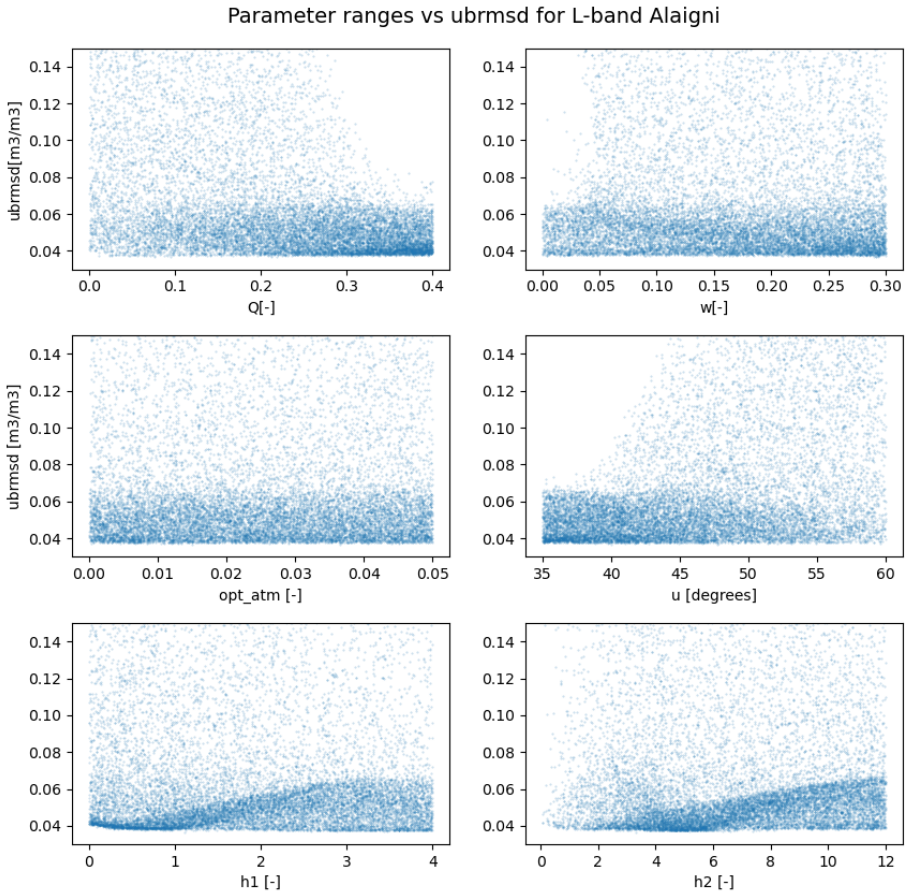

Figure 8.10: UbRMSD vs. Parameters after 20.000 runs at Alaigni with L-band

Here it is clearly visible that for some parameters certain values result in a lower ubRMSD, while other parameters have a lower sensitivity. In the top left graph, parameter Q, a pattern can be seen where it gets darker towards the bottom right corner, which means most runs have results with these values as optimum. An optimal range between 0.25-0.4 can be expected. The graph of parameter ω shows a clear path where most of the result are. For the optimal ubRMSD the values at the bottom are of interest, thus a range between 0.15-0.3 is expected. In the mid-left panel, the opt_atm is shown, where the 20.000 results are quite evenly distributed

in the lower regions of the ubRMSD. This means that this parameter has a low sensitivity in this range and does not have a lot of influence on the outcome. In the graph of the parameter u, the incidence angle, a clear pattern can be found again, the density of the values increases towards the left bottom corner. The optimal range for this parameter is likely between 35-45 degrees, leaning towards 40 degrees. For the parameters h1 and h2 some patters can be distinguished as well. For parameter h1 a thickening is visible between 0 and 1, but some values between 3 and 4 show lower values. To distinguish between these ranges, a more detailed plot is required. For parameter h2 an evident thickening lies between 4 and 6, this range seems to produce the lowest values as well.

The combinations of the 6 parameters leading to the 20.000 ubRMSD outcomes, were arranged in order to find the optimal ubRMSD. The 100 lowest ubRMSD and their corresponding parameters were selected. Figure 8.11 shows the result of the top 100 lowest ubRMSD at Alaigni with the L-band. Here scatter plots are zoomed in to the ranges and ubRMSD of the top 100 'dots'. For some of the parameters the ranges can be narrowed down again, while others show a more distributed pattern. For example the plot of parameter w shows a distribution that increases towards the higher values. The plots of parameters h1 and h2 shows a clear pattern. Where the range of h1 can be narrowed down to 2.5-4.0 and the range of h2 can indeed be optimised to 4-6. On the other hand, for the parameter opt_atm, the values are distributed within the same range as the 20.000 values and a clear pattern cannot be found, this parameter was therefore not considered during further research. The sensitivity of the parameter u, the incidence angle indicates that the parameter has influence on the algorithm, however this parameter is constant per satellite and thus a new optimal range is not considered.

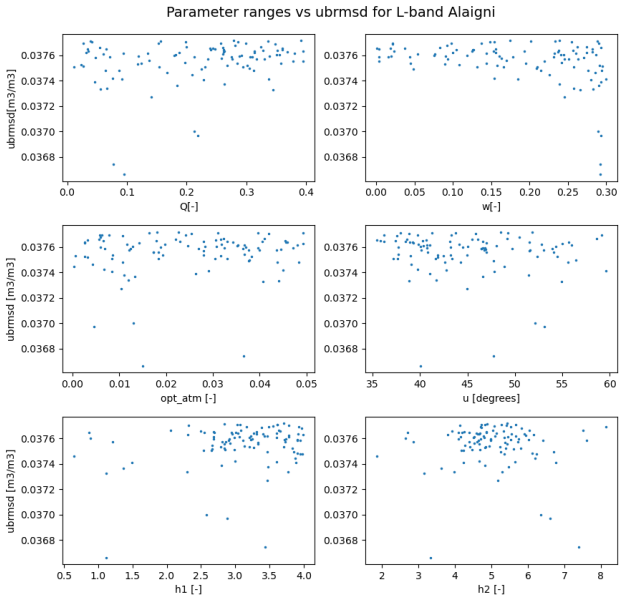

Figure 8.11: UbRMSD vs. Parameters of top 100 ubrmse results of 20.000 runs at Hpayargyi with L-band

The optimal ubRMSD that was composed with the combination of the optimal values of each parameter at each location and band is shown in Table 8.3. The runs of 20.000 parameters lead to a slightly different result each time the code was executed, so these parameters are not the same each time. This is why a range of the top 100 is given. For the selection of the optimal ubRMSD only parameter combinations that led to a correlation coefficient, R, higher than 0.75 were considered. The result of the top 100 lowest ubRMSD show that the R improves greatly as well, where no value below 0.85 is found for any band/location combination. In Figure 8.12 the 4 parameters Q, ω, h1 and h2 are shown with boxplots, which summarize the results of the optimal ranges of the top 100 values. The red points represent the original values of each parameter that are used in the Land Parameter Retrieval Model (LPRM).

For the parameter Q, the polarisation mixing factor, it is remarkable that for the L-band the optimal values according to this research lie between 0.15-0.4, while the original parameter value is 0. Q is often assumed to be very small for L-band, commonly below 0.1 but mostly zero. (van der Schalie et al., 2015). There is no support in literature and no physical explanation for the values of Q to be above 0.1 for L-band, so these optimal values were not considered as improvement of the error and could be compensating other errors. For C-band and X-band the original parameter values, respectively 0.115 and 0.127, fall within the optimal ranges for Q for the locations Alaigni, Hpayargyi and ITC. For Thanatpin the original value of the X-band is higher.Q is a mixing factor that takes the polarization mixing caused by rough surfaces into account. A rough surface would imply a value for Q that is higher than zero. For a smooth surface the value of Q should be around 0.05 [-] and for rough surfaces 0.3[-] . For Alaigni and ITC the values are slightly higher, ranging between 0.06 and 0.16, than for Hpayargyi and Thanatpin, ranging between 0.03 and 0.15.

The single scattering albedo, ω, is shown in the second boxplot. The first thing to notice here is that the L-band gives significantly larger ranges than the other bands. ω expresses the scattering of the emitted microwaves through vegetation. Theoretically it depends on the plant geometry, so it varies per plant species. Crops often have values of ω between 0.04-0.12 and for natural vegetation a value around 0.05 is mentioned (de Jeu, 2003). At the L-band locations Hpayargyi and Thanatpin the original values fall within the large ranges. van der Schalie et al. (2015) found optimal values for ω between 0.15-0.18 for L-band, depending on the incidence angle, Mo et al. (1982) reported values between 0.15-0.20 for L-band, depending on the canopy. In another study values up to 0.37 were found for particular types of vegetation (van de Griend & Wigneron, 2004). These studies support that the input value of ω for L-band should be higher. However, the vegetation covers at the 4 locations do not show a strong support for the different ranges, which could also be due to seasonal changes in vegetation. A study by Park et al. (2020) indicated that a time-varying single scattering albedo would result in better represented vegetation dynamics within croplands. For the C-band and the X-band the values of the original parameter, respectively 0.056 and 0.048 , are lower than the optimal ranges for each location. For most locations at C-band and X-band the ranges are quite small and would indicate that the optimal values for ω for these bands can be limited to a range between 0.05-0.15, depending on the location. For each band showing parameter ω a pattern can be seen for the values at each location, where Alaigni and ITC result in relatively higher values and Hpayargyi and Thanatpin in relatively lower values. The highest values, within this range, are at the location Alaigni. Alaigni is characterised in the surrounding area by the natural vegetation and forested area, a higher value of ω agrees with a denser canopy (van de Griend & Wigneron, 2004). The lower values within this range are found at the location Hpayargyi. The surroundings of this location are mostly grassland and cropland, which agree with a lower ω.

For the parameter h1 the first thing that stands out is the L-band, where three locations indicate a high value within the range, the location ITC shows completely deviating results in the lower ranges. In the other bands this pattern cannot be found, the location ITC shows the least deviating behaviour here. The original values of parameter h1 don't agree with the optimal ranges of the boxplot at most band/locations. For c-band the original input value of 2.6 seems to be on the high side of the range, which is also the case for the X-band with the original value 2.2. For the L-band the original input value of 1.1 is much lower than the optimal ranges according to this test, except for ITC. van der Schalie et al. (2015) found optimal values for h1 between 1.0 and 1.8, depending on the incidence angle. The high values that are found in this research are thus not supported. Parameter h2 again shows deviating behaviour for the L-band at the ITC locations, this would be expected as h1 and h2 are related. Other than the ITC location, the L-band shows very small optimal ranges, where Hpayargyi and Thanatpin agree the most. The original value of 2.2 is on the low side of the ranges, here values of 3.5-6.3 were found for L-band by van der Schalie et al. (2015), which agree with the results in this study. For C-band the original value of 4.9 falls within most ranges, except at ITC where it is higher. For X-band the original value of 3.0 is within/close to the ranges, but lies on the low end of the range. As parameter h1 and h2 together form the roughness factor h, it is difficult to evaluate individually. Typical values for h have been mentioned, that range from 0 for a smooth surface to 0.4 for a rough ploughed field de Jeu (2003). It can be argued that higher values of h1 lead to higher values of h. With this in mind the result of h1 were evaluated. The values of C-band and X-band show lower results than the original input parameters. This means that the original parameters indicate a rougher surface than is suggested in this study. For Alaigni the values are the highest, this location is mostly forested area and the furthest away from urban area, which could indicate that it has higher roughness.

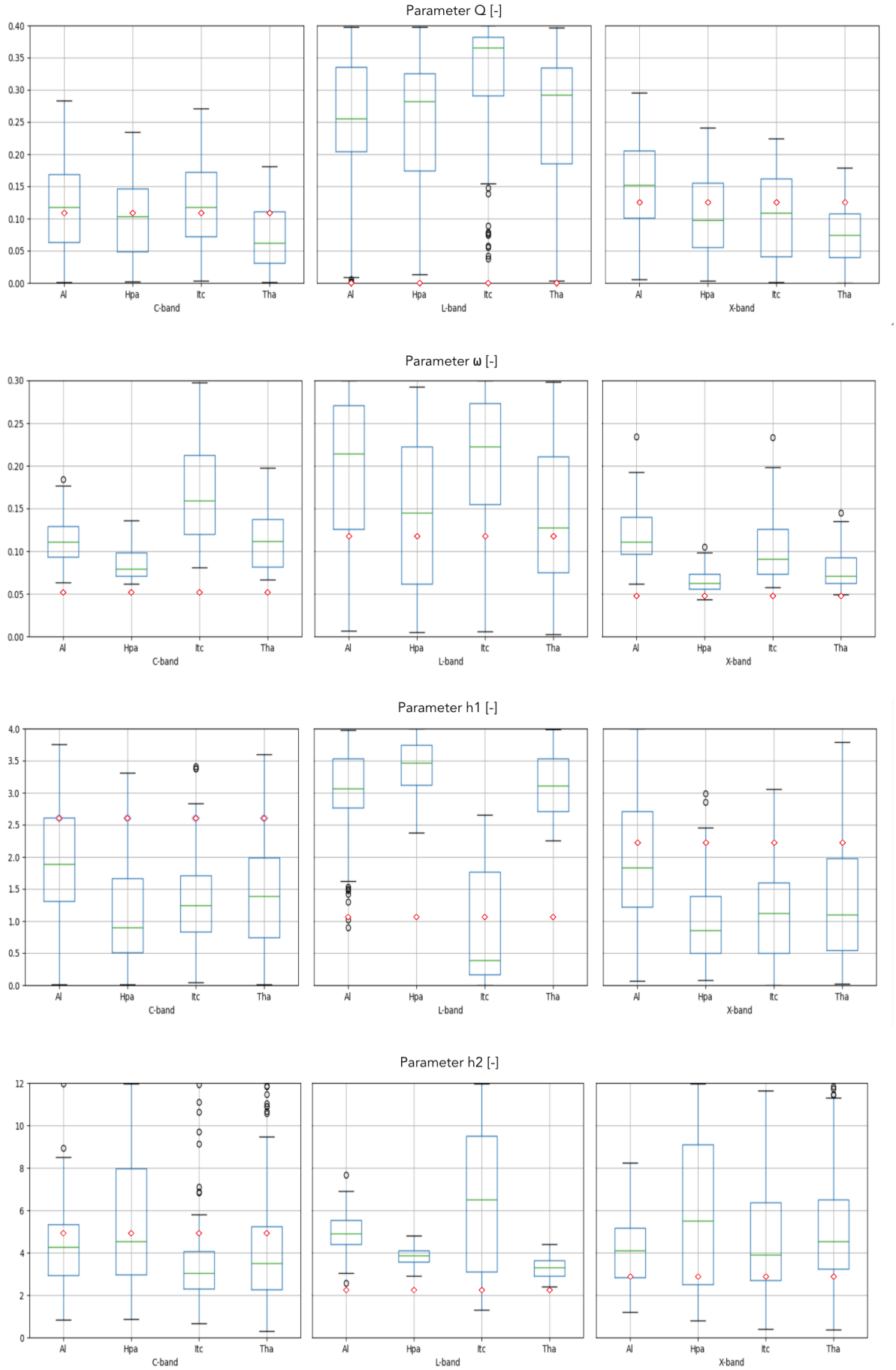

Figure 8.12: Boxplots showing the parameter ranges of the top 100 minimized ubRMSD and the original parameter value

Table 8.3 shows the previous ubRMSD and optimal ubRMSD after the optimised ranges for the parameters for each location and band. The percentage of improvement and the R value that correspond to the new ubRMSD are given as well.
The table shows that that the adjustment of the parameters could lead to an improved ubRMSD at each location. Compared to the validation the ubRMSD improved with differences from 0.014 to 0.049 $m^3/m3$. The R values indicate that the correlation is not badly affected with the adjustments, it has even increased. The results show that the L-band result in the lowest ubRMSD, as low as 0.037 m^3/m^3 and the highest percentage of improvement, up to 39.2%. However the literature and this research do not show enough support to verify that the optimised ranges of the four parameters are related to the source of the errors.

Table 8.3: Optimal ubRMSD at each location/band, with the corresponding R value

Location	Band	Previous ubRMSD	Optimal ubRMSD (m^3/m^3)	Improvement (%)	R (new)
	C-band	0.090	0.062	31.1	0.86
	L-band	0.074	0.045	39.2	0.93
ITC	X-band	0.082	0.060	26.8	0.87
	C-band	0.072	0.053	26.4	0.91
	L-band	0.060	0.037	38.3	0.95
Hpayargyi	X-band	0.067	0.053	20.9	0.90
	C-band	0.068	0.049	27.9	0.86
	L-band	0.061	0.037	39.3	0.93
Alaigni	X-band	0.064	0.049	23.4	0.86
	C-band	0.129	0.085	34.1	0.86
	L-band	0.111	0.074	33.3	0.90
Thanatpin	X-band	0.103	0.071	31.1	0.91

8.3. Visual comparison of satellite products vs in-situ products 2020

In this section the satellite products of VanderSat were evaluated by visual comparison with the 2020 in-situ network. First the soil moisture products were compared with the in-situ soil moisture measurements, to evaluate the performance so far. The added value of this network is the soil temperature measurements at 20cm depth, with this information the uncertainty of the temperature input in the soil moisture retrieval algorithm can be addressed. These in-situ soil temperature measurements were compared with the satellite retrieved land surface temperature. Figure 8.13 shows the timeseries, between March 2020 and January 2021, of the soil moisture measurements of the new in-situ network in Bago and of the soil moisture measurements from the satellite products with C-band, L-band and X-band.

In the first graph, top left, the timeseries at the ITC are shown. As was noticed in the analysis of the in-situ soil moisture products, in chapter 4, the in-situ soil moisture surface sensor at the ITC shows a lot of noise. Furthermore all the graphs show that the L-band shows a higher soil moisture content, up to 0.45 m^3/m^3 between July and September, at each location than the other two bands. For Hpayargyi and Thanatpin these higher values seem to agree with the in-situ measurements, while at the ITC and Alaigni the values remain at around 0.25 m^3/m^3.

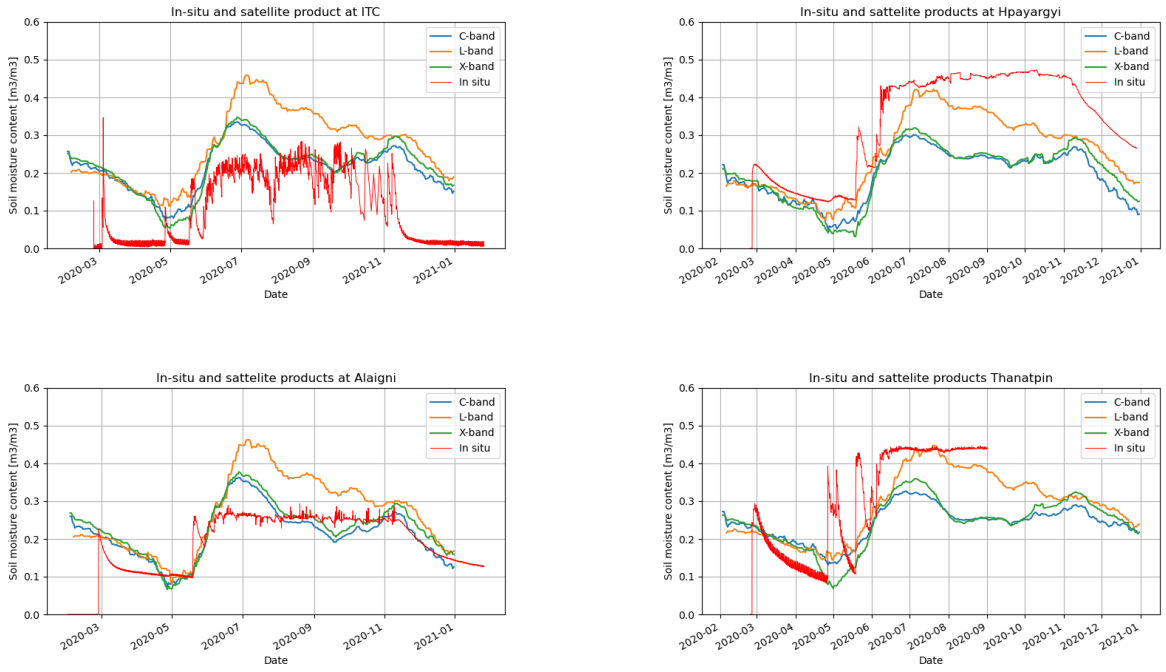

Figure 8.13: Surface soil moisture in-situ sensor versus Satellite soil moisture of bands C,L and X 2020

Close-up monsoon on- and off-set

The in-situ soil moisture measurement show the monsoon on-set from mid May with increased values and they stabilize around the start of June. In the first weeks of November the dry down as a result of the monsoon off-set is visible in the in-situ soil moisture measurements. In Figures 8.14 and 8.15 the in-situ soil moisture measurements during the on and off-set of the monsoon are compared with the satellite products to evaluate their performance of capturing the on and off-set of the monsoon.

In Figure 8.15 the three satellite bands are shown with the surface sensors at each location during the on-set period of the monsoon. At ITC the sensor at 10cm depth is used. At ITC the satellite measurements follow the same trend as the in-situ sensor, especially the X- and C-band. The L-band seems to overestimate the increase of water content. In Hpayargyi a slightly similar trend can be found between the satellite and in-situ products, except for two rapidly increasing events in the in-situ measurements. Here the L-band shows the best correlation, while the X- and C-band underestimate the entire period. At Alaigni the first rain event shows a rapid increase in the in-situ sensor, after which the measurements are steady. This is a different reaction than can be seen in the satellite products, where the water content slowly increases, and eventually reaches higher values then the in-situ measurements. In Thanatpin the in-situ sensor again shows extreme reactions compared to the satellite products. The L-band shows the best result after the increase.

Figure 8.15 shows the period between the 1st of October 2020 and the 1st of January 2021, the period where the monsoon off-set is visible in the soil moisture content. In the top left corner, at the ITC, the sensor at 10cm is used again. The soil moisture of the three satellite bands show a good match with the in-situ soil moisture. In the first period, up to mid November, the L-band shows the best result, while in the second period the C and X band show better results. In Hpayargyi the overall trend of the dry down seems to be captured well, but there is a bias between all three satellite products and the in-situ product. In the last graph the result at Alaigni can be seen, again the trend is good, and the C-band shows the result that is closest to the in-situ measurements. The location Thanatpin could not be evaluated, as there are no in-situ measurement after September 2020.

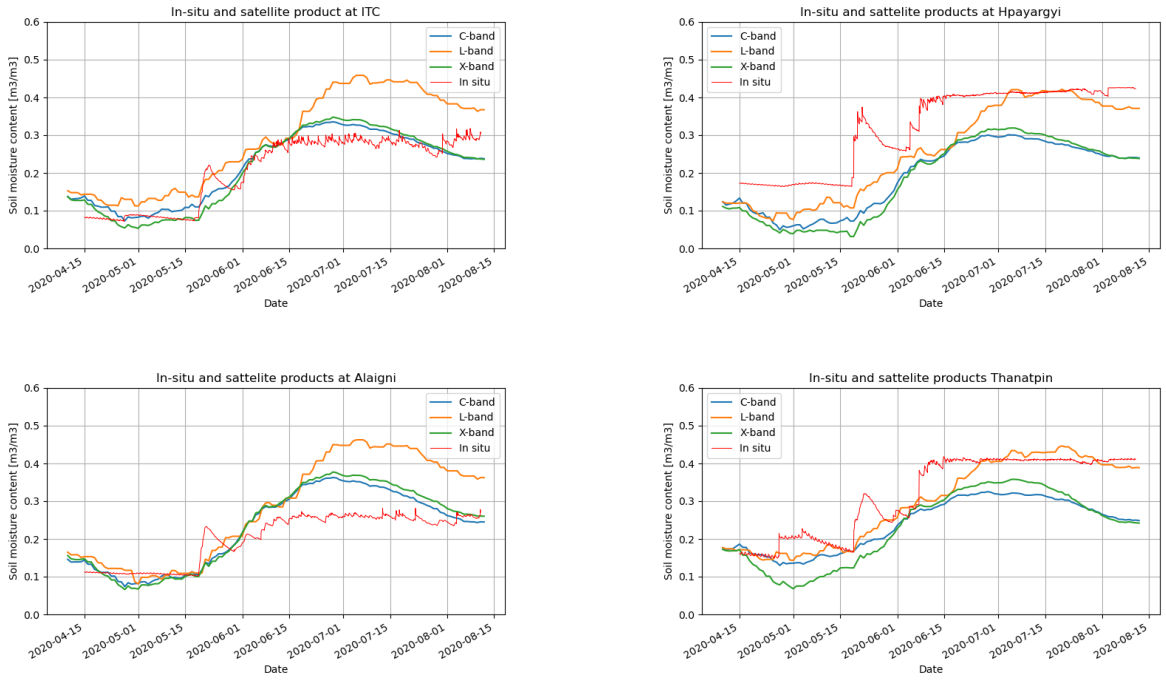

Figure 8.14: Timeseries of soil moisture measurements during the monsoon on-set in 2020

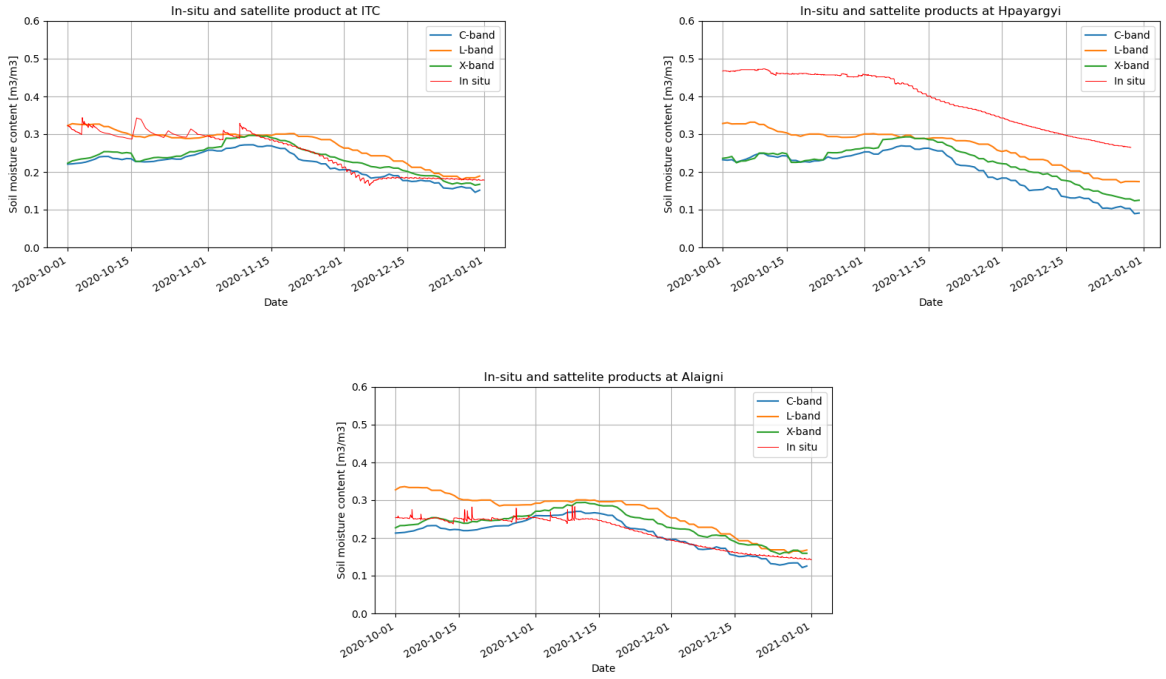

Figure 8.15: Timeseries of soil moisture measurements during the monsoon off-set in 2020

In-situ temperature versus satellite temperature

The in-situ temperature measurements that are shown below are the first temperature measurements done in this and similar areas. This means that the satellite measurements that are derived to effective temperatures have not been verified before. The in-situ measurements show daily fluctuations, while the satellite measurements have one measurement per day. The first thing that is noticed, is the bias of approximately 15 ° Celsius between the products, with the satellite underestimating. Furthermore it can be seen that at each location the temperature increase from March to mid May is quite steady and similar in both products. After this the satellite products at all the location show a dip between June and August, which cannot be found in the in-situ measurements.

Figure 8.16: Timeseries of the in-situ and satellite retrieved soil temperature measurements in degrees Celsius at each of the four locations.

The large bias in the temperature could be a source of error for the soil moisture retrieval. The land surface temperature is a direct input to run the model. The bias that was found was added to this product and the model was rerun. The result of the rerun with the corrected temperature can be seen in Figure 8.17. It is clear that the temperature input has a significant impact on the soil moisture product, however the result with the corrected land surface temperature creates a very large bias compared to the in-situ measured soil moisture content. This could indicate either that the in-situ temperature measurements are not correct or that the algorithm adjusted several other input parameters for the wrong reasons. To verify both the in-situ and the satellite measurements additional temperature products were used. In Figure 8.18 the in-situ soil moisture temperature is compared with with air temperature that was measured at the ITC weather station. In the months June to September a strong correlation can be seen. In the months March to June the minimum and maximum air temperature differ around 20 degrees. This large difference can be seen back in the daily fluctuations of the soil moisture temperature which show larger variations than in the months from June on wards. This comparison indicates that the soil temperature that is measured by the 2020 network is in the correct range and that the bias is probably due to the satellite temperature.

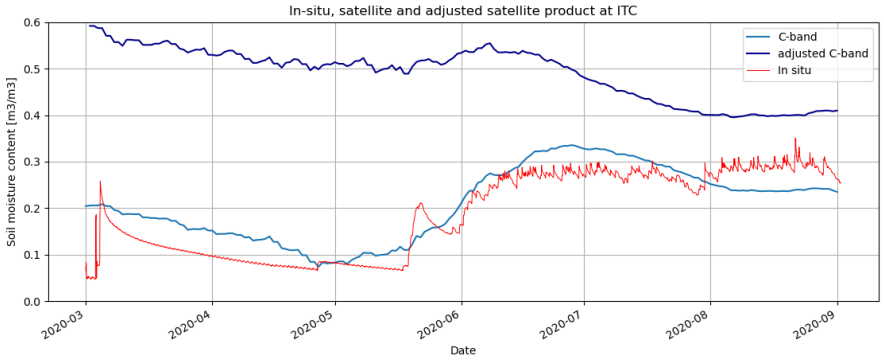

Figure 8.17: In-situ surface soil moisture measurements at ITC versus Satellite retrieved soil moisture and Satellite retrieved soil moisture with corrected temperature, at ITC with C-band.

Figure 8.19 shows the land surface temperature that is currently used in the algorithm (orange), next to that the land surface temperatures of the MODIS terra satellite, both day and nighttime, the Famine Early Warning Systems Network Land Data Assimilation System (FLDAS) soil temperature and the Modern-Era Retrospective analysis for Research and Applications (MERRA) surface temperature are shown. It is clear that the VanderSat land surface temperature is has the lowest values. The MODIS nighttime land surface temperature is comparable, which is because both are measured at night. However between the two nighttime land surface temperatures there is still a bias around 9 degrees. The FLDAS soil temperature and the MERRA surface temperature of the unsaturated zone show very similar behaviour and lie between the day and night time land surface measurements of the MODIS satellite. The various satellite products indicate that indeed the land surface temperature product of VanderSat show values that are too low to represent the land surface temperature near Bago.

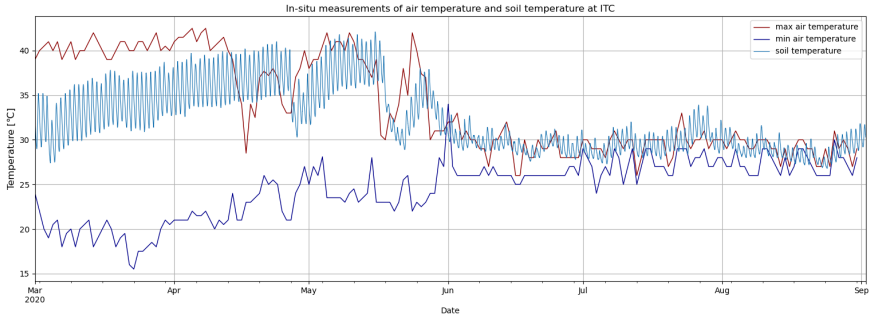

Figure 8.18: In-situ surface soil moisture compared with in-situ minimum and maximum air temperature measurements at ITC.

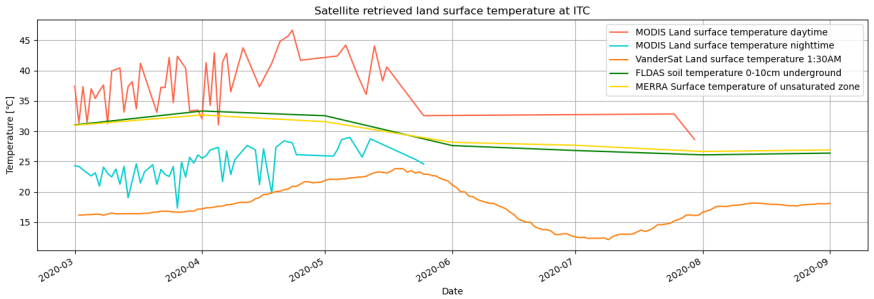

Figure 8.19: Land surface temperature and soil temperature products of various satellites.

One of the possible sources of the bias of temperature lies within the water masking technique. In the tropics the water bodies are dynamic, while the water mask is static. Figure 8.20 shows the area around the Bago city, where the four in-situ networks were placed. In the land cover map the water bodies are indicated by the dark blue areas. In the worldview maps , although the images are not very sharp, the water bodies can be detected as well. Two days days were selected, one in March before the monsoon and one in November, after the monsoon. The image during/after the monsoon was difficult to find as the cloud cover during the monsoon period is extremely high in the tropics. In the images it can be detected that the water bodies indeed change in size depending on the season. After multiple months of monsoon season the water bodies could have grown, this is of influence on the measured values but is not taken into account on the water body area that is masked. That could explain a decline in estimated land surface temperature in this period, since the measured values are averages of a 100 x 100 pixel. This explains the seasonal effect that is seen in Figure 8.16, but it does not account for the large bias that is present throughout the year. Furthermore, the land cover maps clearly shows two water bodies near the urban area, which can be found back in the worldview images, however the water bodies that is in the top left of the worldview images cannot be fully seen in the land cover map. This indicates that land cover maps are not always accurate, the mapping over land cover can be difficult, especially in the tropic where cloud cover often disturb the images.

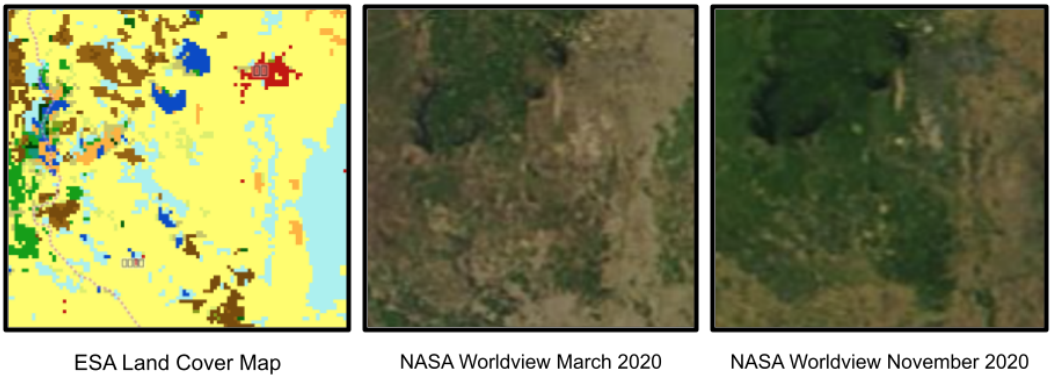

Figure 8.20: ESA land cover map and NASA world view, showing the land cover and water bodies near Bago. Sources: https://maps.elie.ucl.ac.be/CCI/viewer/ and https://worldview.earthdata.nasa.gov/

Another possible source of error could be that the in-situ measured temperature is determined for each site separately while the satellite estimated temperature is based on a large area. Heterogeneity within the satellite footprint can cause a bias between two measurements. Another source of error could lie within the retrieval of the land surface temperature. According to (Parinussa, Holmes, & Jeu, 2012) the land surface temperature retrieval is based on a simple linear relation between the vertical-polarised Ka-band observations and land surface temperature. The Land Parameter Retrieval Model takes the weighted average mean temperature between the soil temperature and canopy temperature. This weighted average is because for bare surfaces T_s represents soil temperature and for vegetated areas it represents the canopy surface temperature. According to Holmes et al. (2009) there is a relation between outgoing longwave radiation and longwave surface temperature. The emissivity and the sensible heatflux determine that relation. The sensible heat flux can be described by $H = C * \Delta T$ where C represents the vegetation dependent parameters and ΔT represents temperature difference between air and soil temperature. The emissivity is determined by optimising ΔT since H=0 when ΔT approaches 0. When the variation in H can't be explained by ΔT, because the roughness length of vegetation is high and only a minimal difference between air and vegetation temperature is found, it is assumed that $T_s = T_a$. The canopy temperature is then determined by the integrated temperature T_s. In tropical areas the difference between these optimisations may cause imperfections in the prediction of the temperature.

9

Discussion Remote Sensing Analysis

In this chapter the results of the validation of the satellite products versus the in-situ products and the analysis of the sources of the errors are discussed.

9.1. Validation of the satellite products with 2017 in-situ network

In the validation section of chapter 8.1, the satellite products of VanderSat and NASA were compared and validated by the in-situ network that was placed in 2017. In the timeseries the patterns of the in-situ soil moisture measurements and the satellite retrieved soil moisture were generally in good agreement. The in-situ soil moisture measurements in the dry period, from November to May, were significantly lower than the satellite retrieved measurements in this period. This was especially the case at ITC and Alaigni, these two location seemed to have similar responses in the in-situ analyses as well. In these months the vegetation optical depth(VOD) had higher values than in the wet-period. The increased values of VOD means that soil emissions are attenuated and the sensor sensitivity to soil moisture variation decrease. This can be a limitation for the soil moisture prediction, and might explain the large differences in these periods.

The results of the statistical analysis of the validation were high for the correlation coefficient, Pearson's R, however the other scores showed less good results. The R values ranged between 0.70 and 0.89. Results of R above 0.7 are generally considered to have a strong correlation. The highest correlations are found for the L-band, between 0.78 and 0.89, and per location Hpayargyi shows the best results ranging between 0.73-0.89. The root mean square deviation (RMSD) and unbiased RMSD (ubRMSD) show varying results. The best result of ubRMSD is 0.059 m^3/m^3, for L-band at Hpayargyi and the worst 0.1295 m^3/m^3, for the L3-band at Thanatpin. The results of the RMSD and ubRMSD are the highest, thus least good, at Thanatpin. The target values of either 0.04 m^3/m^3 or 0.06 m^3/m^3 are is only met at Hpayargyi with the L-band satellite product. The other products range between 0.07 and 0.13 m^3/m^3, this means that the the LPRM does not yet provide the optimal result for the soil moisture measurements in the Bago area and improvement is needed for better accuracy and precision. This improvement can only be executed when the sources of the errors are discovered.

9.2. Analysis of possible error sources

When the performance of the satellite products is evaluated several sources of error must be taken into account. The errors that arise from the in-situ soil moisture sensors itself, which are not ground truth measurement, must be considered. The sensors that were used for the validation resulted in RMSE between 0.01 and 0.059 m^3/m^3, while an resolution of 0.001 m^3/m^3 is promised by the production company. This indicates that the sensors need re-calibration, here the challenges of the tropics arise, where the remote locations make it difficult to perform such experiments. The next error is related to the in-situ measurements as well, by looking at the spatial mismatch. The in-situ measurement are point scale, while the satellite measurements have large grid sizes. The networks in this study are very sparse networks, containing only 4 stations were soil moisture is measured. Gruber et al. (2020) indicates a network as sparse when footprint-scale areas contain only a single or very few soil moisture stations. This is another consequence of the remote tropical

area, where maintaining an in-situ network is challenging and scaling it up would only increase these challenges. When the sources of the error do not lie within the in-situ networks, a closer look must be taken at the retrieval algorithm. This is done by looking at the the input parameters of the LRPM, which are elaborated below.

9.2.1. Parameterisation of the Land Parameter Retrieval Model

In the parameterisation the parameters Q, ω, opt_atm, u, h1 and h2 were given a wide ranges of values. The LPRM was run using these parameter ranges to create sensitivity plots and find optimal values to obtain low ubRMSD. It was concluded that opt_atm, the optical depth of the atmosphere, had no influence on the outcome and this parameter was not further included. The u, the incidence angle, is a fixed parameter for each satellite and it was concluded that these do indeed have optimal values around the original input. Both these parameter are not further discussed in the optimisation process. The sensitivity study showed that the parameters Q, ω, h1 and h2 have a certain pattern, depending on the band that is used and the location of the measurements. In the scatter plots of 20.000 and 100 points the ranges of these parameters were indicated. The box plots summarized the results, showing the optimal ranges to result in lower ubRMSD. The combination of the optimised parameters led to improvement of the ubRMSD between 20 and 40 % at each location/band. This result is significant and indicates that the LPRM is sensitive to its input. Below the individual parameters are elaborated en after a conclusion is given whether the optimisation has enough support linked to the tropics.

Optimisation Q

Q is a mixing factor that takes the polarization mixing caused by rough surfaces into account. For parameter Q it can be concluded that for C-band and X-band the original values represent the optimal values for the locations well. A rough surface would imply a value for Q that is higher than zero. For a smooth surface the value of Q should be around 0.05 [-] and for rough surfaces 0.3[-]. For Alaigni and ITC the values are slightly higher, ranging between 0.06 and 0.16, than for Hpayargyi and Thanatpin, ranging between 0.03 and 0.15. For the L-band a very deviating result is found. In literature there is a general agreement that at low frequencies, thus L-band, the polarisation mixing factor, Q, is negligible (Escorihuela et al., 2007; van de Griend & Wigneron, 2004). Although this assumption could work on global scale, it can have different results on local scale, however there is no support that the optimal values found in this research, ranging between 0.18-0.37, are representative for the tropics.

Optimisation ω

The parameter ω, the single scattering albedo, expresses the the scattering of the emitted microwaves through vegetation. Theoretically it depends on the plant geometry, so it varies per plant species. Crops often have values of ω between 0.04-0.12 and for natural vegetation a value around 0.05 is mentioned (de Jeu, 2003). The optimal ranges of C-band and X-band were found to be between 0.05 and 0.15, with an exception at ITC that goes up to 0.21. For both C-band and X-band these values are higher than the original values of respectively 0.056 and 0.048. The highest values, within this range, are at the location Alaigni. Alaigni is characterised in the surrounding area by the natural vegetation and forested area, a higher value of ω agrees with a denser canopy (van de Griend & Wigneron, 2004). The lower values within this range are found at the location Hpayargyi. The surroundings of this location are mostly grassland and cropland, which agree with a lower ω. For the L-band the range of optimal values is considerably larger than for C-band and X-band. The original input value of 0.12 is represented in the ranges of Hpayargyi and Thanatpin, but is low for Alaigni and ITC. Again the higher range of values is found in Alaigni and ITC.

Optimisation parameters h1 and h2

The result of the parameters h1 and h2 showed that the LPRM is sensitive to these parameters and the ubRMSD can be improved by adjusting the parameters within the given optimal ranges. However, h1 and h2 are difficult to evaluate individually, as they form the roughness factor h together. The roughness factor h is considered as a dynamic variable that varies in time and space. In this research the parameters h1 and h2 are used to express h as a function of soil moisture (θ): h=h1-h2*θ. Typical values for h have been mentioned, that range from 0 for a smooth surface to 0.4 for a rough ploughed field. It can be argued that higher values of h1 lead to higher values of h. With this in mind the result of h1 were evaluated. The values of C-band and X-band show lower results than the original parameters. This means that the original parameters indicate a rougher surface than is suggested in this study. For Alaigni the values are the highest, this location is mostly

forested area and the furthest away from urban area, which could indicate that it has higher roughness.

These optimisations result in better correlation and smaller ubRMSD. Which indicates that based on the data a better performing estimation is executed. However, in the results chapter it is determined that the algorithm has a fairly good estimate for the soil moisture content while the estimated land surface temperature has a large bias. This could be explained by the fact that the algorithm is optimised on data and masks the offset of the land surface temperature. Since the algorithm has a multidimensional aspects with lots of degrees of freedom, parameters can always be adjusted to optimal ranges, but this can be for the wrong reason. In this case there is not enough evidence to adjust the parameters to optimal ranges that link to the tropics. In short, the soil moisture estimates could be (near to) right for the wrong reasons. With this optimisation it is proven that this could even be further optimised, potentially for the wrong reason. It should be kept in mind that the temperature should be corrected to acquire the right results for the right reason.

9.2.2. Visual comparison of the 2020 in-situ network and the satellite products

In chapter 8 the satellite products of VanderSat were compared with the network that was placed in 2020. The additional soil temperature measurements are a first for a network in the tropics, and therefore the uncertainty of the temperature as input for the retrieval algorithm could be evaluated. First the soil moisture measurements will be compared to evaluate their performance. The comparison is visual only, as it was decided that the data record was not long enough to do a full validation. For the timeseries during the entire measurements period it can be concluded that the main trends are followed, but some bias can be detected as well. The L-band shows high soil moisture content during the wet season, which relates to the soil moisture content at Hpayargyi and Thanatpin during this season. C-band and X-band show very similar results to each other, and remain at a lower soil moisture content level during the wet season, which is more in line with the in-situ soil moisture content at ITC and Alaigni. When looking at a close-up of the monsoon on-set, it can be concluded that the transition from dry to wet is predicted well by the satellite products. However, at each location the first large precipitation event caused a large increase in soil moisture content for the in-situ sensors, which then slightly decrease again till the next precipitation event. The satellite products have a more gradual increase of the soil moisture content during these events. The monsoon off-set graphs show very good predictions of the satellite products. At the three shown locations the trends of the dry down are very similar to each other. At the location Hpayargyi the soil moisture content is much higher than the satellite products. The satellite products show similar soil moisture content at each location, while the in-situ soil moisture content differs per location. This can be due to differences in the soil texture, that could be lost with the differences in resolution.

The second satellite product that was compared was the temperature, in situ soil temperature was compared with the land surface estimation of the LPRM. A temperature difference of approximately 15 ° Celsius was observed, which is very large. Furthermore the temperature drop in the satellite measurements during the months June and July is not found in the in-situ measurements. This large bias in the temperature can be a source of the errors that were found in the validation of the soil moisture products. The possible underlying reasons for this large bias were briefly evaluated. First both the in-situ and the satellite measurements were compared with similar products to determine which measurements were the source of the bias. Here it could be concluded that the satellite product underestimation of the soil moisture is incorrect. The land surface temperature estimates of the LPRM show good result on global scale, but in this particular case the local scale is not represented. One of the reasons for this could be the static water mask that is used. In the tropics the water bodies are dynamic due to the long wet period that alternate with dry periods. This is not accounted for in the masking, and could therefore lead to wrong measurements. This effect mainly explains the seasonal differences that were detected in the satellite temperature measurements and not in the in-situ temperature measurement. Another source for the bias could lie within the retrieval of the land surface temperature. The emissivity that is determined by optimising the ΔT can cause imperfections in the prediction of the temperature.

IV

Part 4 Conclusion and Recommandations

10

Conclusion and recommendations

The objective of this research was to install a reliable in-situ soil moisture network in Bago, Myanmar, which can be used for the validation of remotely sensed soil moisture products in the tropics. Furthermore the objective was to validate satellite soil moisture products with a previously placed in-situ soil moisture network and to find possible sources for the errors that resulted from the validation. A parameterisation was done for a part of the algorithm that is used to derive the satellite soil moisture product. Several temperature products were compared and analysed. This objective was executed by answering the main research question that is composed of the answers of the four sub questions. The conclusions and answers to these question are elaborated below.

How can the satellite soil moisture retrieval in the tropics be improved, focusing on a in-situ network to validate and analyse satellite measurements?

To answer this question the question was divided into four sub-questions, the more extensive answers to these question can be found below. The first two question addressed the in-situ soil moisture network. Here it was concluded that a properly working in-situ network is difficult to set-up in tropical conditions, which is why there is limited amount of in-situ soil moisture networks in the tropics that can be used for the validation of satellite soil moisture retrieval. The two networks that were used in this research were evaluated on their performance to represent the soil moisture content at each location. Both networks showed good results and the 2017 network was indicated as reliable to use for validation in this research. The 2020 network was not yet indicated as reliable to use for validation, mainly due to the limited data record.

The performance of the satellite retrieved soil moisture products was analysed in part 3 of this research. The validation of the satellite retrieved soil moisture with the in-situ soil moisture measurements during 2017 and 2018 resulted in high correlation coefficients, R, ranging between 0.70 and 0.89. This indicates that the satellite products are in good agreement with the in-situ measurements. However, the RMSD, ubRMSD and bias showed that the accuracy and the precision of the satellite products needs improvement in this area. The visual comparison of the satellite and in-situ measurements of the soil moisture content in 2020 showed promising results, indicating a good performance so far. However, the satellite retrieved surface temperatures were compared to the in-situ soil temperature measurement, and a large bias, around 15 degrees, was found. This indicates that the temperature product needs improvement and the approach used on a global scale, does not work on this local scale.

The possible sources for the errors found in the validation were analysed to answer the last sub question. Here it was concluded that the errors can partially be appointed to the in-situ network. Here the ability of the sensors to represent the ground truth can be improved. This raised the challenge of maintenance and experimenting at a remote tropical location. Furthermore the spatial mismatch is considered as a source of error related to the in-situ network. The sparse network of four station is not representative enough for the grid size of the satellite products, even with the downscaling technique that is applied to the satellite measurements. Secondly the source of error was sought in the retrieval algorithm. A parameterisation was performed to asses the sensitivity of certain parameters. The parameterisation of the parameters Q, ω, h1 and h2 lead

to improved results for the ubRMSD up to 40 %. This result indicated that the algorithm is sensitive to these parameters, however there was no evidence to link the optimised parameters to the tropical conditions. Here it is concluded that the optimising could be done for the wrong reasons, where it only covers the large bias of temperature. The temperature bias that was found was appointed as a source of error for the retrieval of soil moisture, as it is a direct input into the LPRM. The masking of water bodies and the determination of the emissivity can be of influence in the temperature bias.

To conclude the satellite soil moisture retrieval in the tropics showed promising results when compared to an in-situ soil moisture network, with high correlation. However there are still relatively large errors that can be improved by updating the in-situ soil moisture network, correcting the masking of water bodies in the down-scaling technique, solve the retrieval algorithm for the temperature bias and then optimising tropical specific location parameters.

What challenges are encountered when setting up an in-situ soil moisture network in tropic conditions

The purpose of this question was to show the reason behind the limited amount of networks in the tropics. This limited amount of in-situ soil moisture networks leads to minimal possibilities to validate satellite soil moisture retrieval. The validation of satellite soil moisture retrieval is necessary to verify the performance of the satellite products, and assess whether improvement is needed. The challenges that were encountered during preparation were mainly addressed to the material selection. For the tropics the selection of material is important, as it has to withstand severe weather conditions, such as heavy rainfall during the monsoon. During the fieldwork the main challenge was to find the ideal location to install the sensors, where pollution in the ground played a role, as well as the ability to dig and install in dry ground and the representation of the surroundings. After the field work, during the further use of the network, the remote location of the network formed the largest challenge. Broken down loggers, lost cellular connection and low batteries could not be fixed easily because the site could not be visited. The fieldwork showed the difficulties and limitations of setting up and maintaining a network in a remote tropical area. It would be recommended for further fieldwork campaigns in the tropics to find even robuster loggers that require almost zero maintenance and are fully weather and insect proof. Next to that a calibration study for the sensor and a study of the surrounding area is recommended. Furthermore a scale up of the network would be recommended to get a better representation of the area.

To conclude the challenges that were encountered in the tropics consist of location, climate and communication challenges and these can be dealt with by good preparation, robust materials and time.

Do the in-situ soil moisture networks at 4 locations in Myanmar provide a reliable product?

Two in-situ soil moisture networks were analysed. The 2017 network, an in-situ soil moisture network that was active from June 2017 to July 2018, was considered to provide a reliable product that could be used for the validation on satellite retrieved soil moisture measurements in this research. The 2017 network was evaluated on 4 aspects: The availability of the data, the ISMN quality checks, the correlation with precipitation and the calibration. The directly available data record of 13 months has a few missing values and values below 0.0 m^3/m^3 , but is otherwise considered reliable. The timeseries showed an expected pattern for the dry and monsoon periods that occur in Myanmar. The surface sensor at the ITC showed large variability, which was supported by the large coefficient of variation of 0.945. The correlation with the precipitation data was good and the calibration with ground truth samples resulted in acceptable errors, which indicated that the in-situ sensors could represent the the soil moisture content for this research. The 2020 network, an in-situ soil moisture network that was placed as a part of this research, was considered promising to provide a reliable product in the future. The network was evaluated on aspects: The availability of the data, the ISMN quality check, the daily fluctuations, precipitation data and sensor-to-sensor comparison. The availability evaluation showed that the data is constantly available, but the length of usable the data records is about 6 months, which is not enough to use as validation network. Furthermore data was missing and there were values below 0 m^3/m^3. The daily fluctuations shows expected behaviour and characteristics of the locations could be detected. The precipitation data compared with the soil moisture data indicated an accurate response, over time as well as over depth. The sensor-to sensor comparison with the manual theta probe showed very good results, indicating a reliable response. The comparison of the 2017 and 2020 network demonstrated that the

locations have similar behaviour in both years, and are within the same ranges.

To conclude, the 2017 network provides a reliable product that can be used for the validation in this research. The 2020 network cannot be used for validation, but has promising results that indicate that the network will be reliable in the future, when a longer data record is available.

How do satellite soil moisture products perform in tropic conditions, compared to an in-situ soil moisture network?

The satellite soil moisture products between 2017-2018 and from 2020 were be evaluated on their performance. With the in-situ soil moisture network that was deemed reliable, the 2017 network, the satellite products were validated. The Pearson correlation coefficient, R, showed results between 0.70 and 0.89, which is very good. The highest correlations were found for the L-band and for the location Hpayargyi. The root means squared deviation (RMSD) resulted in values between 0.065 and 0.21 m^3/m^3, which is high. The highest RMSD were found at the ITC and Alaigni. The unbiased RMSD had values between 0.0593 and 0.1295 m^3/m^3, where only the L-band at Hpayargyi had an acceptable value. The bias was the highest at the ITC, with values up to 0.2 m^3/m^3. Thanatpin shows good results for the bias, with values as low as 0.0103 m^3/m^3.

The 2020 network was visually compared, as the in-situ network was not indicated as reliable yet. This visual comparison showed promising results, especially at the close-up of the monsoon on-set and off-set. The C-band and X-band showed the best agreement with the in-situ sensors at the locations ITC and Alaigni, while the L-band seemed to agree better at Hpayargyi and Thanatpin. The first comparison of the satellite temperature product with the in-situ soil temperature measurements revealed that there is a large bias of approximately 15 degrees. Additionaly a seasonal variation was found, that did not show in the in-situ measurements. This indicates that the temperature product needs improvement and the approach that is used on a global scale, does not work on this local scale.

Overall it can be concluded that the satellite soil moisture products already perform well in the tropic conditions, with high correlation. However the RMSD, unbiased RMSD and bias showed high values compared to other validation studies. Therefore it can be concluded that the products need improvement in accuracy and precision.

What could be possible sources for the errors that are found in the validation?
To improve the accuracy and precision of the satellite soil moisture retrieval the sources of the errors were evaluated. The in-situ network is responsible for a part of the error. The sensor that were installed to measure the soil moisture contain errors when compared to ground samples, these errors are larger than the accuracy that is promised by the manufacturer. Furthermore the spatial mismatch between the in-situ and satellite retrieved soil moisture measurements is considered as a source of error. The sparse network of four station is not representative enough for the grid size of the satellite products, even with the downscaling technique that is applied to the satellite measurements. The other part of the error sources is found in the retrieval algorithm. A parameterisation was performed to asses the sensitivity of certain parameters. The parameterisation of the parameters Q, ω, h1 and h2 were optimised and led to improved results for the ubRMSD between 20 % and 40 %. The values of the location ITC, Hpayargyi and Alaigni show promising values for the ubRMSD between 0.037 and 0.062 m^3/m^3. Thanatpin shows higher values, up to 0.085 m^3/m^3, however there is still an improvement of >30% with the original outcome. The corresponding Pearson R values were found between 0.86 and 0.93, which is an very good result. By optimising the parameters Q, ω, h1 and h2 the tropics conditions could be represented in the model. This result indicated that the algorithm is sensitive to these parameters, however there was no evidence to link the optimised parameters to the tropical conditions. Here it is concluded that the optimising could be done for the wrong reasons, where it only covers the large bias of temperature. It can be concluded that the temperature bias that was found can be a large source of error for the retrieval of soil moisture, as it is a direct input into the LPRM. The masking of water bodies, where the dynamic effect of the tropical monsoon on the water bodies is not taken into account can explain the seasonal bias. The land cover map showed that the mapping of water bodies, independent of the season, are not always correct. This could have influence on the temperature retrieval as well. A possible source of error could be within the retrieval of the emissivity of crop land and higher canopy areas. The soil surface temperature and canopy surface temperature are of influence in these areas and could be different in the tropics.

Recommandations
For further research in the field of this report a few recommendations are given. For the in-situ part it is clear that an update of the network is necessary. A part of the newly installed loggers and sensors has failed and should be repaired as soon as possible, to ensure the continuity of the data. If the loggers are damaged beyond prepare it is recommended to look at even robuster logger, that could be put into the ground and require even less maintenance. Another recommendation would be to up-scale the network, this would greatly improve the reliability of the in-situ measurements, and would thereby be an important step towards improvement of the satellite retrieved measurements in the tropics. Here it would be good to look into the possibilities to collaborate with other researchers or companies, as the interest in the field is very high and the lack of the in-situ measurements in the tropics is often mentioned. A recommendation for the fieldwork would be to have a critical look at the the surface sensors, especially at the Irrigation Technology Centre and Alaigni. Further more the calibration of the sensor is of importance. A great addition to the fieldwork would be to map the surroundings of the sensors, this can contribute to the represenativeness of the network and the understating of the area.

For further research into the improvements of the retrieval algorithm a critical first step is to analyse the large temperature bias that was found. Here it is advised to look at the water masking technique, mostly to get rid of the seasonal bias. Furthermore it is recommended to take a critical look at the retrieval of the emissivity in the tropical areas, as this could make a difference in the calculations of the land surface temperature. When a solution is found for the temperature bias, it would be good to dive into the specific parameters that are used in the LPRM, and research if a strong link could be made to the tropics. The suggestion of dynamic in stead of static parameters could be of influence, since tropical areas are very dynamic. It is therefore strongly recommended to look in to this.

References

Al-Yaari, A., Wigneron, J. P., Dorigo, W., Colliander, A., Pellarin, T., Hahn, S., … De Lannoy, G. (2019). Assessment and inter-comparison of recently developed/reprocessed microwave satellite soil moisture products using ISMN ground-based measurements. *Remote Sensing of Environment*, *224*(February), 289–303. Retrieved from https://doi.org/10.1016/j.rse.2019.02.008 doi: 10.1016/j.rse.2019.02.008

Aung, L. L., Zin, E. E., Theingi, P., Elvera, N., Aung, P. P., Han, T. T., … Skaland, R. G. (2017). Myanmar Climate Report. *Norwgian Meterological Institute*(9), 105.

Chung, D., Dorigo, W., Reimer, C., Hahn, S., Melzer, T., Paulik, C., … Kidd, R. (2017). ESA Climate Change Initiative Phase II - Soil Moisture: Algorithm Theoretical Baseline Document (ATBD). (Version 03.2), 1–25.

Colliander, A., Jackson, T. J., Bindlish, R., Chan, S., Das, N., Kim, S. B., … Yueh, S. (2017). Validation of SMAP surface soil moisture products with core validation sites. *Remote Sensing of Environment*, *191*, 215–231. doi: 10.1016/j.rse.2017.01.021

Cosh, M. H., Ochsner, T. E., McKee, L., Dong, J., Basara, J. B., Evett, S. R., … Sayde, C. (2016). The Soil Moisture Active Passive Marena, Oklahoma, In Situ Sensor Testbed (SMAP-MOISST): Testbed Design and Evaluation of In Situ Sensors. *Vadose Zone Journal*, *15*(4), vzj2015.09.0122. doi: 10.2136/vzj2015.09.0122

Decagon Devices. (2015). GS1: Soil moisture sensor. , *November*, 1–18. Retrieved from http://publications.decagon.com/Manuals/14640_GS1_Web.pdf

de Jeu, R. A. (2003). Retrieval of Land Surface Parameters Using Passive Microwave Remote Sensing. *Ph.D Thesis Vrije Universiteit Amsterdam*, 144.

de Jeu, R. A., de Nijs, A. H., & van Klink, M. H. (2017). Patent Method and system for improving the resolution of sensor data. (12).

Delta-T Devices. (2017). Delta-T Devices, User Manual for the ML3 ThetaProbe Design. User Manual Version. , 1–47. Retrieved from www.delta-t.co.uk

Dente, L., Vekerdy, Z., Wen, J., & Su, Z. (2012). International Journal of Applied Earth Observation and Geoinformation Maqu network for validation of satellite-derived soil moisture products. , *17*, 55–65. doi: 10.1016/j.jag.2011.11.004

Department of Population Ministry of Immigration and Population. (2015). The 2014 Myanmar Population and Housing Census Sagaing Region. *The Republic of the Union of Myanmar*, *3-E*(May). Retrieved from https://asiapacific.anu.edu.au/mapsonline/base-maps/myanmar-statesregions

Dorigo, W., Himmelbauer, I., Aberer, D., Schremmer, L., Petrakovic, I., Zappa, L., … De, N. V. (2021). The International Soil Moisture Network : serving Earth system science for over a decade. (January).

Dorigo, W., Wagner, W., Hohensinn, R., Hahn, S., Paulik, C., Xaver, A., … Jackson, T. (2011). The International Soil Moisture Network: A data hosting facility for global in situ soil moisture measurements. *Hydrology and Earth System Sciences*, *15*(5), 1675–1698. doi: 10.5194/hess-15-1675-2011

Dorigo, W., Xaver, A., Vreugdenhil, M., Gruber, A., Hegyiová, A., Sanchis-Dufau, A., … Drusch, M. (2013). Global Automated Quality Control of In Situ Soil Moisture Data from the International Soil Moisture Network. *Vadose Zone Journal*, *12*(3), vzj2012.0097. doi: 10.2136/vzj2012.0097

Entekhabi, D., Reichle, R. H., Koster, R. D., & Crow, W. T. (2010). Performance metrics for soil moisture

retrievals and application requirements. *Journal of Hydrometeorology*, *11*(3), 832–840. doi: 10.1175/2010JHM1223.1

ESA. (n.d.). *radar-course-3-electromagnetic-spectrum @ earth.esa.int*. Retrieved from https://earth.esa.int/web/guest/missions/esa-operational-eo-missions/ers/instruments/sar/applications/radar-courses/content-3/-/asset_publisher/mQ9R7ZVkKg5P/content/radar-course-3-electromagnetic-spectrum

Escorihuela, M. J., Kerr, Y. H., De Rosnay, P., Wigneron, J. P., Calvet, J. C., & Lemaître, F. (2007). A simple model of the bare soil microwave emission at L-band. *IEEE Transactions on Geoscience and Remote Sensing*, *45*(7), 1978–1987. doi: 10.1109/TGRS.2007.894935

FAO. (2014). FAO Country Programming Framework for Nigeria - 2013-2017. , 1–24. Retrieved from http://www.fao.org/nigeria/programmes-and-projects/en/

FAO. (2016). POST-HARVEST AND AGRO-INDUSTRY GOVERNMENT OF THE REPUBLIC OF THE UNION OF MYANMAR Formulation and Operationalization of National Action Plan for Poverty Alleviation and Rural Development through Agriculture (NAPA) Ministry of Agriculture, Livestock and Ir. (June).

FAO. (2019). *Handbook for Farmer Field School on Climate Smart Agriculture in coastal/delta zone, Myanmar*.

Fernandez-Moran, R., Al-Yaari, A., Mialon, A., Mahmoodi, A., Al Bitar, A., De Lannoy, G., ... Wigneron, J. P. (2017). SMOS-IC: An alternative SMOS soil moisture and vegetation optical depth product. *Remote Sensing*, *9*(5), 1–21. doi: 10.3390/rs9050457

Frenken, K. (2012). *Irrigation in Southern and Eastern Asia in figures. AQUASTAT Survey - 2011*. Retrieved from http://www.fao.org/docrep/016/i2809e/i2809e.pdf

Grant, J. P., Wigneron, J. P., De Jeu, R. A., Lawrence, H., Mialon, A., Richaume, P., ... Kerr, Y. (2016). Comparison of SMOS and AMSR-E vegetation optical depth to four MODIS-based vegetation indices. *Remote Sensing of Environment*, *172*, 87–100. Retrieved from http://dx.doi.org/10.1016/j.rse.2015.10.021 doi: 10.1016/j.rse.2015.10.021

Gruber, A., De Lannoy, G., Albergel, C., Al-Yaari, A., Brocca, L., Calvet, J. C., ... Wagner, W. (2020). Validation practices for satellite soil moisture retrievals: What are (the) errors? *Remote Sensing of Environment*, *244*(May), 111806. Retrieved from https://doi.org/10.1016/j.rse.2020.111806 doi: 10.1016/j.rse.2020.111806

Gruber, A., Dorigo, W., Zwieback, S., Xaver, A., & Wagner, W. (2013). Characterizing Coarse-Scale Representativeness of in situ Soil Moisture Measurements from the International Soil Moisture Network. *Vadose Zone Journal*, *12*(2), vzj2012.0170. doi: 10.2136/vzj2012.0170

Heathman, G. C., Cosh, M. H., Han, E., Jackson, T. J., McKee, L., & McAfee, S. (2012). Field scale spatiotemporal analysis of surface soil moisture for evaluating point-scale in situ networks. *Geoderma*, *170*, 195–205. Retrieved from http://dx.doi.org/10.1016/j.geoderma.2011.11.004 doi: 10.1016/j.geoderma.2011.11.004

Hemshorn de Sanchez, A. L. (2018). Vegetation Optical Depth: Its potential as an agricultural drought indicator. A case study on pepper fields in Indonesia. , 84.

Holmes, T. R., De Jeu, R. A., Owe, M., & Dolman, A. J. (2009). Land surface temperature from Ka band (37 GHz) passive microwave observations. *Journal of Geophysical Research Atmospheres*, *114*(4). doi: 10.1029/2008JD010257

Htway, O., & Matsumoto, J. (2011). Climatological onset dates of summer monsoon over Myanmar. *International Journal of Climatology*, *31*(3), 382–393. doi: 10.1002/joc.2076

Iksal, M. (2020). The researcher's complete guide to soil moisture. , *21*(1), 1–38.

Jackson, T. J., Bindlish, R., Cosh, M. H., Zhao, T., Starks, P. J., Bosch, D. D., ... Leroux, D. (2012). Validation of soil moisture and Ocean Salinity (SMOS) soil moisture over watershed networks in the U.S. *IEEE*

Transactions on Geoscience and Remote Sensing, *50*(5 PART 1), 1530–1543. doi: 10.1109/TGRS.2011.2168533

JICA. (2013). Report of Data Collection Survey on Agriculture Sector in the Republic of the Union of Myanmar: Final Report. (December), 167.

Kang, C. S., Kanniah, K. D., & Alvin Lau, M. S. (2016). *Microwave remote sensing for soil moisture estimation in tropical regions - A review and SMOS L2 products validation* (Vol. 12) (No. 2).

Kang, C. S., Kanniah, K. D., Kerr, Y. H., & Cracknell, A. P. (2016). Analysis of in-situ soil moisture data and validation of SMOS soil moisture products at selected agricultural sites over a tropical region. *International Journal of Remote Sensing*, *37*(16), 3636–3654. Retrieved from http://dx.doi.org/10.1080/01431161.2016.1201229 doi: 10.1080/01431161.2016.1201229

Kattler, N. (2017). Validation and applicability of soil moisture data from Myanmar. *Thesis*.

Kerr, Y. H., Waldteufel, P., Wigneron, J. P., Martinuzzi, J. M., Font, J., & Berger, M. (2001). Soil moisture retrieval from space: The Soil Moisture and Ocean Salinity (SMOS) mission. *IEEE Transactions on Geoscience and Remote Sensing*, *39*(8), 1729–1735. doi: 10.1109/36.942551

Liu, Y., Yang, Y., & Yue, X. (2018). Evaluation of satellite-based soil moisture products over four different continental in-situmeasurements. *Remote Sensing*, *10*(7). doi: 10.3390/rs10071161

Mascaro, G., Ko, A., & Vivoni, E. R. (2019). Closing the Loop of Satellite Soil Moisture Estimation via Scale Invariance of Hydrologic Simulations. *Scientific Reports*, *9*(1), 1–8. doi: 10.1038/s41598-019-52650-3

Meesters, A. G. C. A., Jeu, R. A. M. D., & Owe, M. (2005). Analytical Derivation of the Vegetation Optical Depth From the Microwave Polarization Difference Index. (July 2014), 10–13. doi: 10.1109/LGRS.2005.843983

METER GROUP. (2017). ZL6. , *5*(1), 1–8.

METER GROUP. (2019). Teros 11/12. , 30.

Mialon, A., Wigneron, J. P., De Rosnay, P., Escorihuela, M. J., & Kerr, Y. H. (2012). Evaluating the L-MEB model from long-term Microwave measurements over a rough field, SMOSREX 2006. *IEEE Transactions on Geoscience and Remote Sensing*, *50*(5 PART 1), 1458–1467. doi: 10.1109/TGRS.2011.2178421

Mo, T., Choudhury, B. J., Schmugge, T. J., Wang, J. R., & Jackson, T. J. (1982). A model for microwave emission from vegetation-covered fields. *Journal of Geophysical Research*, *87*(C13), 11229–11237. doi: 10.1029/JC087iC13p11229

Montzka, E. C., Cosh, M., Nickeson, J., Camacho, F., Montzka, A. C., Cosh, M., … Wigneron, J.-p. (2020). Soil Moisture Product Validation Good Practices Protocol. (October). doi: 10.5067/doc/ceoswgcv/lpv/sm.001

Nachtergaele, F., Velthuizen, H. V., Verelst, L., Batjes, N., Dijkshoorn, K., Engelen, V. V., … Shi, X. (n.d.). Harmonized World Soil Database.

Naing, M. M. (2007). Paddy field irrigation systems in Myanmar. *RAP Publication*.

Owe, M., de Jeu, R., & Holmes, T. (2008). Multisensor historical climatology of satellite-derived global land surface moisture. *Journal of Geophysical Research: Earth Surface*, *113*(1), 1–17. doi: 10.1029/2007JF000769

Parinussa, R. M., Holmes, T. R. H., & Jeu, R. A. M. D. (2012). Soil Moisture Retrievals From the WindSat Spaceborne Polarimetric Microwave Radiometer. , *50*(7), 2683–2694.

Park, C. H., Jagdhuber, T., Colliander, A., Lee, J., Berg, A., Cosh, M., … Wulfmeyer, V. (2020). Parameterization of vegetation scattering Albedo in the Tau-Omega model for soil moisture retrieval on croplands. *Remote Sensing*, *12*(18). doi: 10.3390/RS12182939

Parrens, M., Zakharova, E., Lafont, S., Calvet, J. C., Kerr, Y., Wagner, W., & Wigneron, J. P. (2012). Comparing soil moisture retrievals from SMOS and ASCAT over France. *Hydrology and Earth System Sciences*, *16*(2),

423–440. doi: 10.5194/hess-16-423-2012

Saleh, K., Wigneron, J. P., Waldteufel, P., de Rosnay, P., Schwank, M., Calvet, J. C., & Kerr, Y. H. (2007). Estimates of surface soil moisture under grass covers using L-band radiometry. *Remote Sensing of Environment*, *109*(1), 42–53. doi: 10.1016/j.rse.2006.12.002

Scanlon, T., Pasik, A., Dorigo, W., Jeu, R. d., Hahn, S., Schalie, R. v. d., … Preimesberger, W. (2020). ESA Climate Change Initiative Plus - Soil Moisture Algorithm Theoretical Baseline Document (ATBD) D2.1 Version 04.7. *ESA Bulletin, Version4.7*(D2.1 Version 04.7), 73.

van de Griend, A. A., & Wigneron, J. P. (2004). On the measurement of microwave vegetation properties: Some guidelines for a protocol. *IEEE Transactions on Geoscience and Remote Sensing*, *42*(10), 2277–2289. doi: 10.1109/TGRS.2004.832243

van der Schalie, R., Parinussa, R. M., Renzullo, L. J., van Dijk, A. I., Su, C. H., & de Jeu, R. A. (2015). SMOS soil moisture retrievals using the land parameter retrieval model: Evaluation over the mUrrumbidgee Catchment, southeast Australia. *Remote Sensing of Environment*, *163*, 70–79. doi: 10.1016/j.rse.2015.03.006

Wang, J. R., & Choudhury, B. J. (1980). Remote sensing of soil moisture content over bare fields at 1.4 GHz frequency. , *86*, 5277–5282.

Xaver, A., Zappa, L., Rab, G., Pfeil, I., Vreugdenhil, M., Hemment, D., & Arnoud Dorigo, W. (2020). Evaluating the suitability of the consumer low-cost Parrot Flower Power soil moisture sensor for scientific environmental applications. *Geoscientific Instrumentation, Methods and Data Systems*, *9*(1), 117–139. doi: 10.5194/gi-9-117-2020

Zonneveld, W. (2018). Validation of satellite obtained soil moisture with in-situ soil moisture sensor data and volumetric soil moisture samples in Bago , Myanmar . *Thesis*(October).

A

Fieldwork & Manual

(a) Measuring

(b) Inserting sensors

(c) Sensor placed in ground

(d) Settling with water

(e) Installation with staff

(f) On-site testing of sensors

Figure A.1: Installation loggers and sensors

(a) Front (b) Side (c) Bottom

Figure A.2: ZL6 with extra weather protection

Figure A.3: Infiltration test

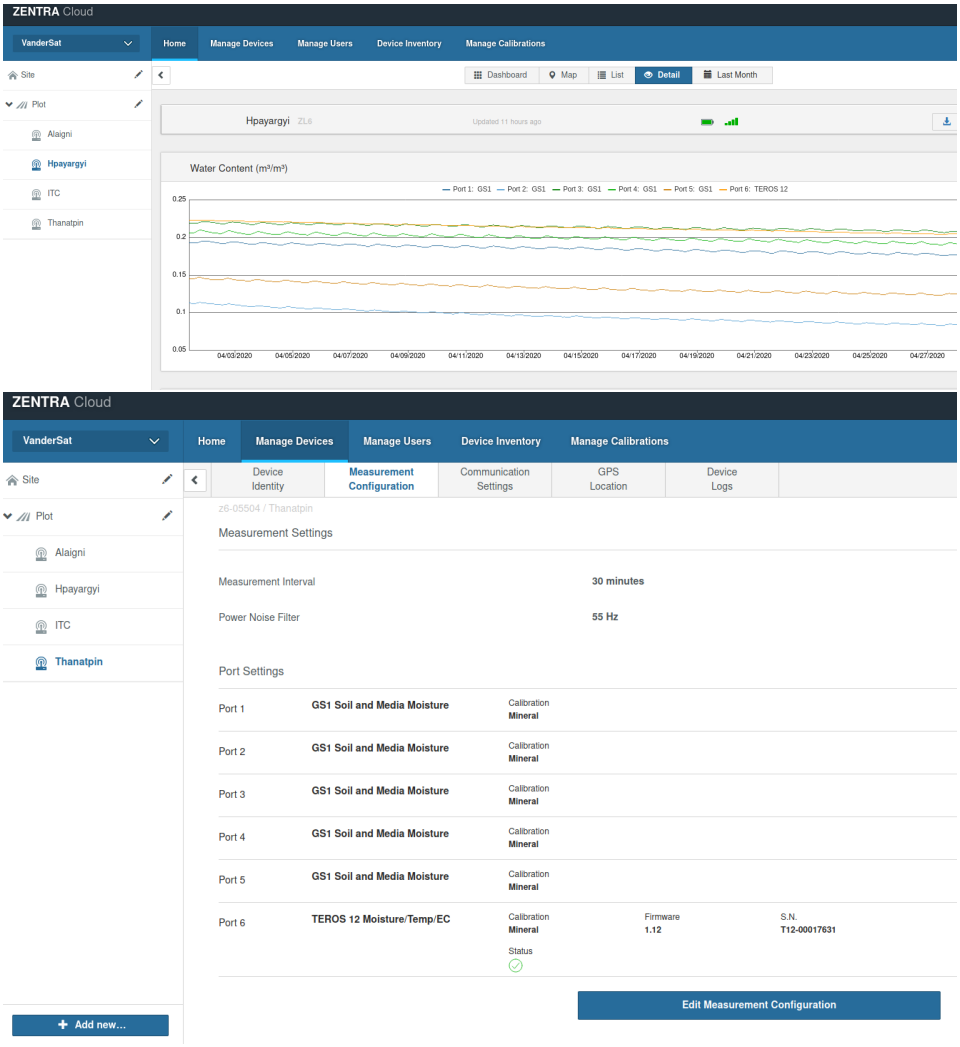

Figure A.4: Interface Zentra cloud

Manual

Soil moisture network Bago, Myanmar

Contents

Dear reader, this manual is set up to instruct you when using the ZL6 datalogger that was installed in February 2020 in Bago. First some important information and functions will be given:

Before going to the site make sure to bring the following:

- A laptop with the Zentra Utility software installed, see section 2.2
- Micro-USB cable, see Figure 5.
- The bitumen paint and tape, see section 3
- An umbrella to protect the device during rain.

All the loggers have a test button, see Figure 1, if the logger does not respond to connection attempts or does not appear to be working, press this button. After completing the self-tests, the ZL6 will indicate success or failure by lighting either the green or red status light.
Lights near the TEST button indicate the status of the ZL6. A green light is labeled OK and a red light is labeled ERROR. There are several possible status states:

- The green light gives a short, single blink every 5 s to indicate the ZL6 is configured to log sensor data.
- The green light blinks slowly (1 s on, then 1 s off), to indicate the logger is communicating to a computer or using the cellular module.
- The green light and red light blink together during self-test procedures (after pressing the TEST button or pulling the battery tab).
- The solid green lightor red lightt at the end of the self-test sequence indicates the results of the tests.
- The lights remain off if the logger measurement interval is set to Off (not logging).

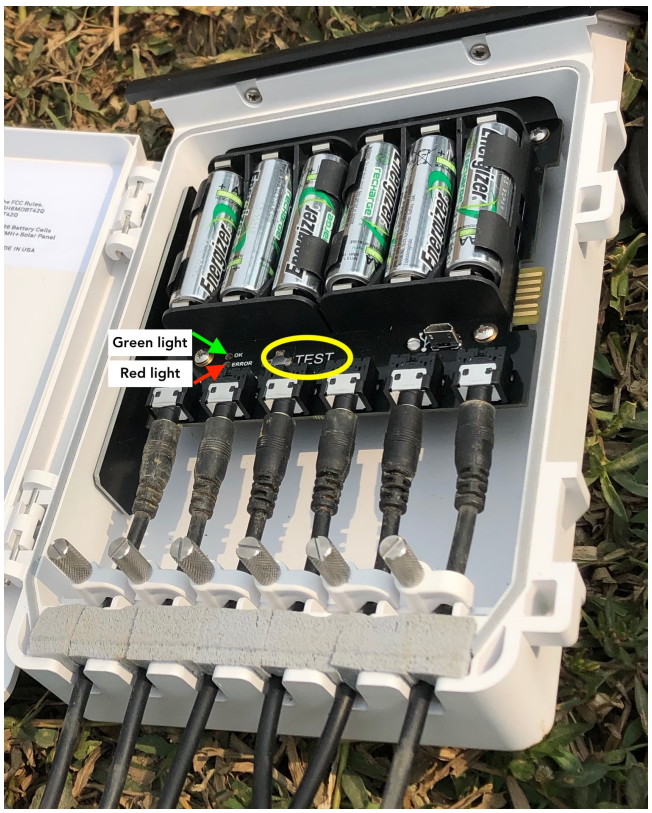

Figure 1: ZL6 logger test button and lights

If you have any question regarding this manual or if the sensor or zentra utility is not working, please contact: idekat@vandersat.com or tvanderhorst@vandersat.com

1 Locations and Materials

1.1 Locations

The in-situ network was placed within a radius of approximately 20km from Bago City, Myanmar, see Figure 2 and the coordinates. In Figure 3 the loggers can be seen at each location.

Irrigation Technology Centre (ITC)	17.3143° N, 96.4520° E
Hpa Yar Gyi	17.4661° N, 96.5303° E
Alaigni	17.2630° N, 96.3465° E
Tha Nat Pin	17.2912° N, 96.5731° E

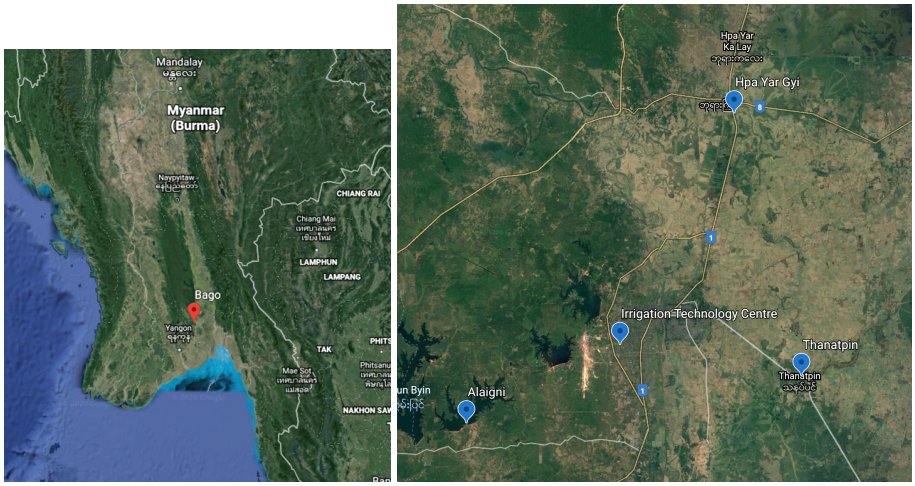

Figure 2: Locations

Figure 3: Loggers at each location

1.2 Materials

ZL6 datalogger

The ZL6 data logger stores and sends the measured data. The logger is equipped with a solar panel in the black area on top. The ZL6 interior can be seen in Figure 4. The logger contains a battery holder for 6 rechargeable NiMH batteries, 6 ports for sensors and a micro-USB port for communication with a laptop. The interior also containts a test button and two status lights.

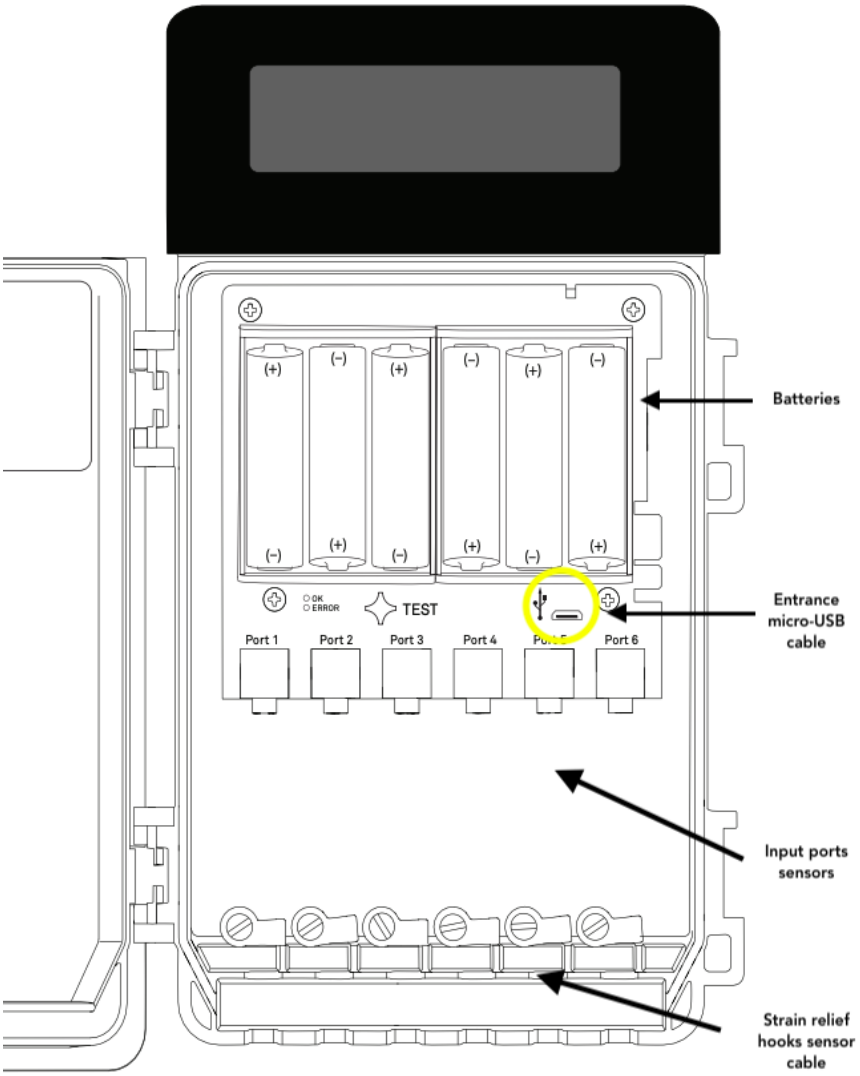

Figure 4: ZL6 interior

Sensors: GS1 and TEROS12 and **Micro-usb cable**
These materials can be seen in Figure 5. The sensor is installed into the ground and plugged in to the ports of the ZL6 logger. The micro-USB cable is used to connect to a laptop. see Figure 4 where the sensor and micro-USB can be plugged in.

Figure 5: Example sensor(left) and micro-USB (right)

2 Zentracloud en Zentra Utility

2.1 Zentra Cloud

The measurements of the sensors are being be uploaded once a day to the Zentra cloud. This cloud is a data management software that works together with the ZL6 datalogger. The cloud is accessible at any time and has a user friendly interface, see figure 6. Information about the devices, calibrations, the upload and measurement times and more can be found and reconfigured at any time. Measurements of every half hour,starting end February, can be found and downloaded. The soil moisture measurements are given in volumetric water content (VWC), in m^3/m^3. Volumetric water content represents the ratio of water volume to soil volume in a given soil. The temperature is given in degrees Celsius. For access to the cloud please contact us.

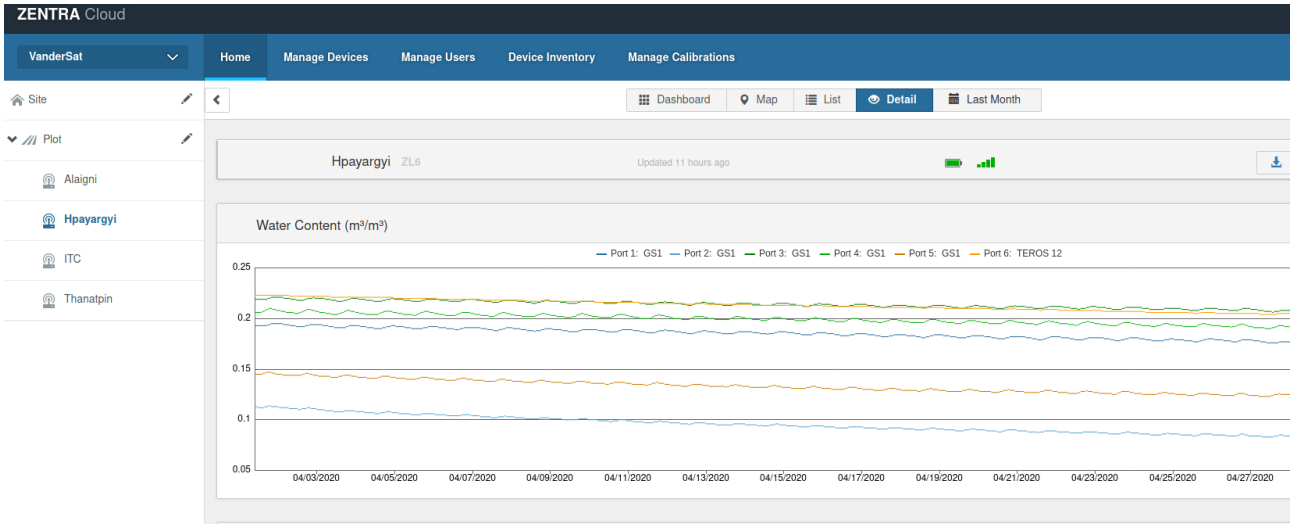

Figure 6: Interface Zentra cloud

2.2 Zentra Utility

The zentra utility can be downloaded from the ZL6 webpage (metergroup.com/zl6-support), see the figure below.

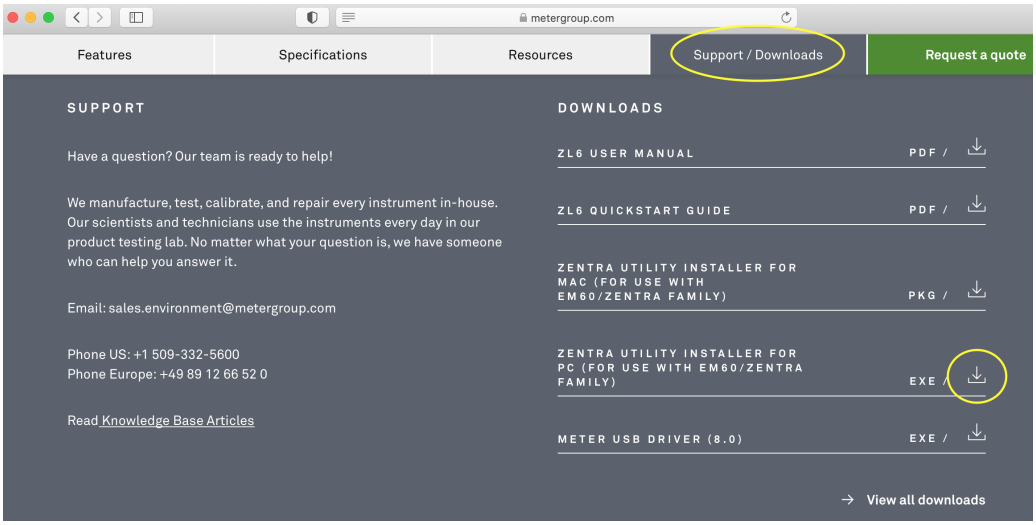

Figure 7: Download Zentra Utility

Function of the zentra utility:

- set all logger configuration parameters,
- test ZL6 and ZL6 Pro cellular communications,
- make real-time sensor measurements (scan sensors),
- create Excel files with sensor data, and
- upload data to Zentra Cloud.

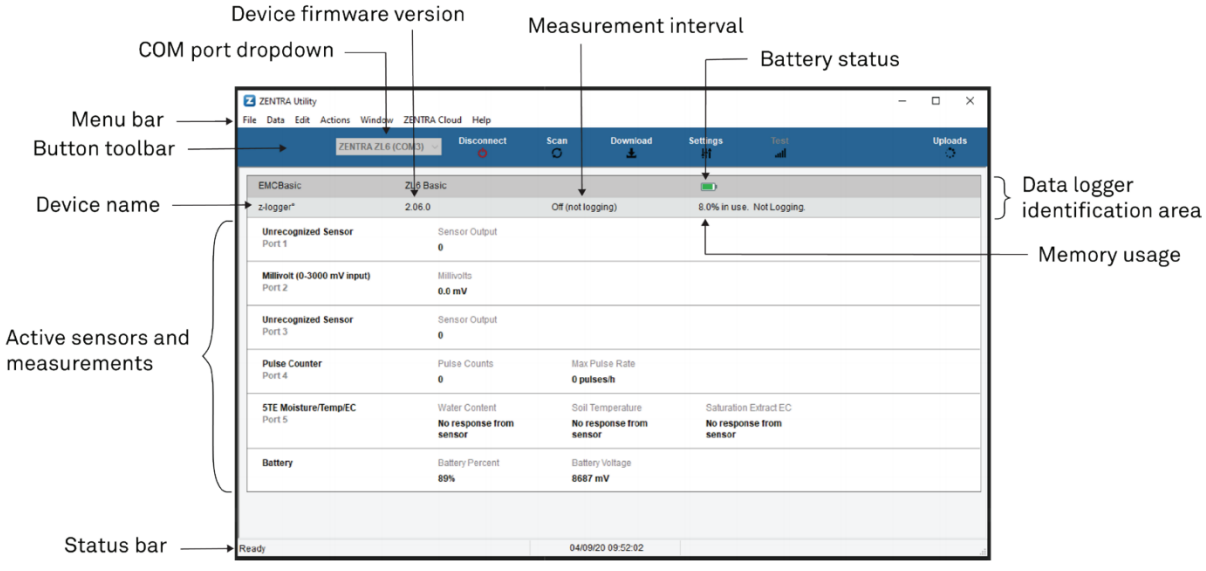

Figure 8: Zentra Utility interface

In figure 8 the interface of the Zentra utility can be seen, the following functions can be used:

- COM port dropdown menu: Lists USB devices connected to the computer.
- Connect/Disconnect: Click the Connect button to attempt to connect to the device currently selected in the COM port dropdown menu. Click the Disconnect button to disconnect from the currently connected logger.

- Scan: Queries the connected ZL6 for the current sensor readings and updates the active sensors and measurements area.
- Download: Downloads all data that has been collected on the ZL6 since the last time a download from the selected logger.
- Settings: Opens the Manage Settings dialog.
- Test: Opens the Cellular Communication Test dialog.
- Uploads: Uploads ZL6 data to Zentra Cloud, if login credentials have been added.

3 Maintenance and Protection

For the quick maintenance, which should be done once a month, please check the following:

- Logger is still attached to mounting post in upright position
- Logger is completely closed
- All 6 sensors are connected
- Solar panel is clean and not covered
- Protection is still intact

When the logger needs to be opened for data collection or reset, please do the following:

- Check if the interior is dry
- Verify that the sensor ports are clean and that the sensors are making good contact with the ports.
- Replace the batteries when it is needed.
- Inspect the battery holders to ensure they are clean and free of corrosion

NOTE: Do not mix NiMH and alkaline batteries together. Do not mix new and old batteries together.

When the interior is wet, please carefully dry the wet parts. If you have a desiccant packet available please put this inside the logger and then close it firmly en protect it.

Protection
Due to the heavy weather conditions in Bago, especially during the monsoon season it is important to keep the logger protected. The logger is designed to be durable, but is not fully waterproof. Following protection will create an extra layer of protection.

Whenever the work with the logger is done, firmly close the device. Use the bitumen tape to go over all the grooves and finish it with a layer of bitumen tape. See the figures below for the example.

(a) Front (b) Side (c) Bottom

Figure 9: ZL6 with extra weather protection

4 Manual data collection

The saved sensor data can be downloaded using the following steps:

1. Open the logger carefully, removing bitumen where needed.
2. Connect the logger to a laptop using the micro-USB cable, see Figure 5 and Figure 4 for the cable and entrance.
3. Choose the appropriate COM port from the dropdown list, see Figure 10
4. Click connect, see Figure 10
5. Click download on the button toolbar, see Figure 10
6. Edit the file name in the save dialog, with the correct time and date.
7. Select the location where the file will be saved on your computer and click save
8. Close and protect the logger as described in section 3.
9. Send the data via email to the person that requested it.

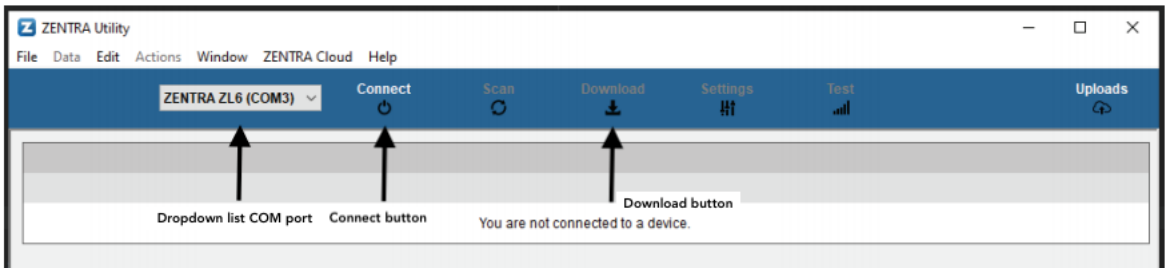

Figure 10: Button toolbar Zentra utility

5 Clearing SIM card's Network Blacklist

Connecting to the logger over USB allows special commands that will clear the SIM blacklist. This action should re-enable cellular connections.

Running a Carrier Connect test:
In ZENTRA Utility, go to Actions in the menu bar, see Figure 8 and choose **List Cellular Carriers**. If you see (forbidden) after your carriers in the area, see Figure 11, please follow the steps below.

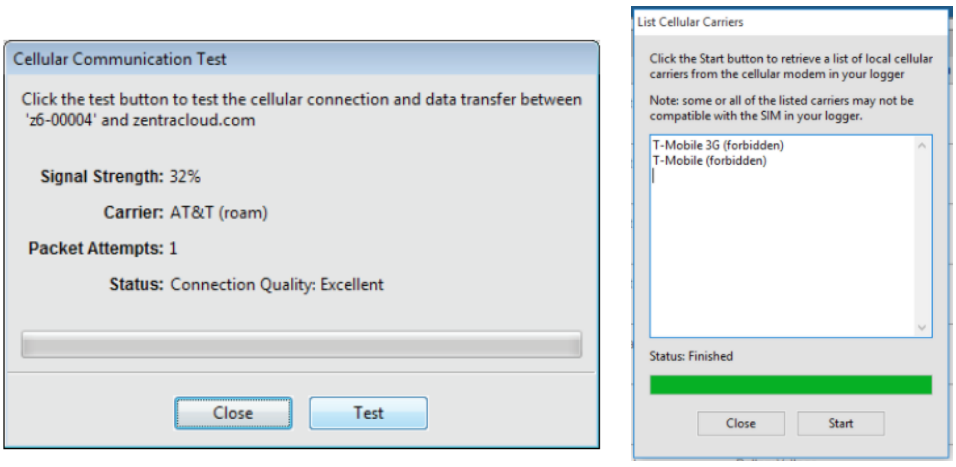

Figure 11: Carrier communication test and xxample list of cellular carriers

The following steps will clear the network blacklist stored on the data logger's SIM. These steps require you to connect to the logger over USB and send special commands through the **terminal** built-in to the zentra utility.

Running a command means typing the word in the terminal. Put your cursor on a blank line under the last ">" sign and type in your command, then press enter. In Figure 12 an example can be seen for the steps below, your screen should look something like this.

1. Connect the logger to a computer with a USB cable and connect to the COM port corresponding to the logger, see Figure 10
2. Go to window on the menu bar and select **Show Terminal**
3. Confirm that you have connected correctly by running the command: show
4. Make sure the cellular profile is set correctly. Run the following command: set -profile 202
5. The logger should return "OK". You only need to run this command once per logger.
6. Type the following to make sure the profile setting is correct: get -profile The logger should return "202".
7. Start up the cellular module so that we can interact with the SIM card: gsm -init
8. Wait 20 seconds for the module to continue starting up. Then type: gsm -fplmn
9. The logger will likely respond with something that looks like: 130184FFFFFFFFFFFFFFFFF OK It may respond with the following FFFFFFFFFFFFFFFFFFFFFFF OK
10. Before shutting of the cellular module, make sure that the SIM allowed a network connection (wait 15 seconds after the last command). Then turn off the cellular with: gsm -off

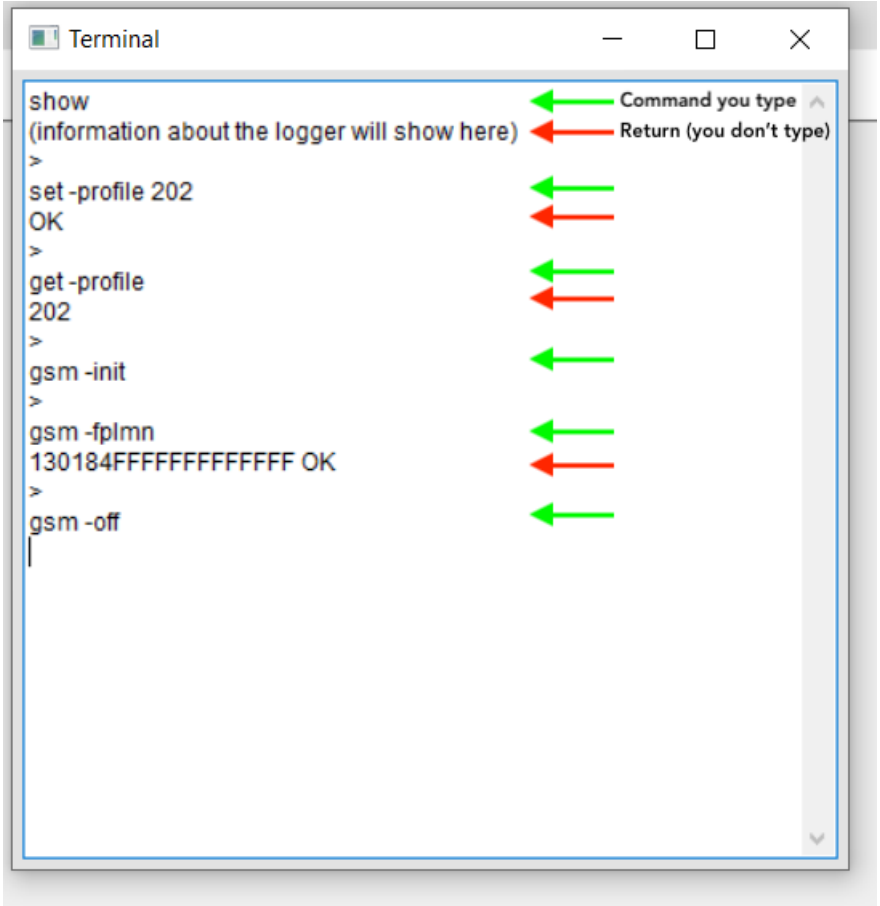

Figure 12: Example of running command in the terminal

B

International Soil Moisture Network

Both in-situ networks that were discussed in this report were added to the ISMN. To continue to collaboration with the ISMN the data of the in-situ network from 2020 must be send out regularly, ideally on half year basis. The documented below provide the metdata information that is required by the ISMN. The data can be downloaded from the ZentraCloud where Teije van der Horst (VanderSat) has acces to. The result should be emailed to ismn@geo.tuwien.ac.at and irene.himmelbauer@geo.tuwien.ac.at. The last updates was send in March 2021. A half yearly ISMN Statisics Report will be send out to all the contributors, sharing information about the network and its usage. In the paper (Dorigo et al., 2021) the latest update on the ISMN can be found, including the VDS (VanderSat) network.

In order to become a data provider, you are asked to **supply general information** about your **Network**, but also **Station** and **Data** related descriptions.

We require personal information such as Name and E-Mail of a contact person to be able to clarify data related issues and provide you with reports about data usage every 6 months.

All the information provided will be **stored in our database**, and can be accessed by registered users through the Advanced Download option.

This information is displayed on the ISMN website (1).

Some information are **mandatory** (*), while others are **optional** and up to your discretion.

General	
Network Name*,1	VanderSat
Network Abbreviation*,1	VDS
Abstract/description of network1	These networks have been installed to validate satellite soil moisture products over complex tropical regions.
Status (operational, closed, etc)1	Operational
Country*,1	Myanmar
Continent1	Asia
Operational start date*	First network-> aproxx 01/06/2017 second network->27/02/2020
Operational end date	First network-> aproxx 24/07/2018 second network-> Still measuring
Network Type (campaign, project, meteo, ...)*,1	Satellite validation project
Citation/Reference1	
URL to Data	
URL to Network1	
Acknowledgement	
EPSG Code to identify the Coordinate Reference System	

Contact person(s)	
Full name*,1	Ileen de Kat
Position/task*	Researcher
Phone	
E-mail*	idekat@vandersat.com
Address	
Organistaion(s) name*,1	VanderSat
Organisation(s) abbreviation	VDS
Role of organisation(s) (data measuring, data preparation, ...)	Satellite observed water data. Globally. Daily.
Address	
URL	https://www.vandersat.com/

* mandatory
1 shown on the ISMN website

Figure B.1: Metdata 2017 and 2020 network

In order to become a data provider, you are asked to **supply general information** about your **Network**, but also **Station** and **Data** related descriptions.

All the information provided will be **stored in our database**, and can be accessed by registered users through the Advanced Download option.

This information is displayed on the ISMN website (1).

Some information is **mandatory** (*), while others are **optional** and up to your discretion.

	station1	station2	station3	station4
General				
Name*,1	Irrigation Technology Centre	Hpayargyi	Alaigni	Thanatpin
Abbreviation*,1	ITC	Hpa	Al	Tha
Quality flag (checked, unchecked, etc)				
Comments				
Location				
Location (EPSG: 4326 WGS 84 / Lat/lon)*,1	17.3144/96.4519	17.4661/96.5302	17.2630/96.3465	17.2921/96.5731
Location (original coordinate system)*				
Altitude (m asl)*	1,3	0,8	0,8	1,5
Image/photo				
Image name				
Image description				
Image file				
Image creation date				

* mandatory
1 shown on the ISMN website

Figure B.2: Metdata 2017 and 2020 network

Data implentable in the ISMN						
Soil moisture (different depths)*,1						
Meteorological variables: soil temperature and soil suction (different depths), surface temperature, air temperature, precipitation, snow depth, snow water equivalent,1						
Soil properties: porosity, bulk density, organic matter content, texture (different depths, mandatory when SM is provided not in volumetric definition)*						
Site properties: land cover, land use, climate class						
station1	**dataset1**	**dataset2**	**dataset3**	**dataset4**	**dataset5**	
Irrigation Technology Centre						
Variable						
Quantity Name (e.g. soil moisture)*,1	Soil moisture	Soil moisture	Soil moisture	Soil moisture	Soil moisture	
Definition (e.g volumetric soil moisture)*,1	Volumetric soil moisture	Volumetric soil moisture	Volumetric soil moisture	Volumetric soil moisture	Volumetric soil moisture	
Unit (SI) (e.g. m3m-3)*,1	m3m-3	m3m-3	m3m-3	m3m-3	m3m-3	
Sensor						
Name*,1	Port 1	Port 2	Port 3	Port 4	Port 5	
Description						
Reference Document (e.g. URL)	http://publications.d	http://publication	http://publications.de	http://publications.deca	http://publications.decagon.com/Manuals/14640_GS1_Web.pdf	
Producer	Decagon	Decagon	Decagon	Decagon	Decagon	
Type	GS1	GS1	GS1	GS1	GS1	
Sensor position (horizontal/vertical)*,1	vertical	Horizontal	Horizontal	Horizontal	Horizontal	
Depth (if measured horizontally, "from" and "to" are identical)						
From*,1	0,01	0,1	0,1	0,2	0,2	
To*,1	0,1	0,1	0,1	0,2	0,2	
Dataset						
Acquisition time (UTC Shift)*	6:30	6:30	6:30	6:30	6:30	Data was collected each half hour during the measurement period.
Quality flag (CEOS flags or own definition)						
Measured/Interpolated Flag						
station2	**dataset1**	**dataset2**	**dataset3**	**dataset4**	**dataset5**	
Hpayargyi						
Variable						
Quantity Name (e.g. soil moisture)*,1	Soil moisture	Soil moisture	Soil moisture	Soil moisture	Soil moisture	
Definition (e.g volumetric soil moisture)*,1	Volumetric soil moisture	Volumetric soil moisture	Volumetric soil moisture	Volumetric soil moisture	Volumetric soil moisture	
Unit (SI) (e.g. m3m-3)*,1	m3m-3	m3m-3	m3m-3	m3m-3	m3m-3	
Sensor						
Name*,1	Port 1	Port 2	Port 3	Port 4	Port 5	
Description						
Reference Document (e.g. URL)	http://publications.d	http://publication	http://publications.de	http://publications.deca	http://publications.decagon.com/Manuals/14640_GS1_Web.pdf	
Producer	Decagon	Decagon	Decagon	Decagon	Decagon	
Type	GS1	GS1	GS1	GS1	GS1	
Sensor position (horizontal/vertical)*,1	Vertical	Horizontal	Horizontal	Horizontal	Horizontal	
Depth (if measured horizontally, "from" and "to" are identical)						
From*,1	0,01	0,1	0,1	0,2	0,2	
To*,1	0,1	0,1	0,1	0,2	0,2	
Dataset						
Acquisition time (UTC Shift)*	6:30	6:30	6:30	6:30	6:30	Data was collected each half hour during the measurement period.
Quality flag (CEOS flags or own definition)						
Measured/Interpolated Flag						

Figure B.3: Metdata 2017 and 2020 network

station3	**dataset1**	**dataset2**	**dataset3**	**dataset4**	**dataset5**	
Alaigni						
Variable						
Quantity Name (e.g. soil moisture)*,1	Soil moisture	Soil moisture	Soil moisture	Soil moisture	Soil moisture	
Definition (e.g volumetric soil moisture)*,1	Volumetric soil moisture	Volumetric soil moisture	Volumetric soil moisture	Volumetric soil moisture	Volumetric soil moisture	
Unit (SI) (e.g. m3m-3)*,1	m3m-3	m3m-3	m3m-3	m3m-3	m3m-3	
Sensor						
Name*,1	Port 1	Port 2	Port 3	Port 4	Port 5	
Description						
Reference Document (e.g. URL)	http://publications.d	http://publication	http://publications.de	http://publications.deca	http://publications.decagon.com/Manuals/14640_GS1_Web.pdf	
Producer	Decagon	Decagon	Decagon	Decagon	Decagon	
Type	GS1	GS1	GS1	GS1	GS1	
Sensor position (horizontal/vertical)*,1	Vertical	Horizontal	Horizontal	Horizontal	Horizontal	
Depth (if measured horizontally, "from" and "to" are identical)						
From*,1	0,01	0,1	0,1	0,2	0,2	
To*,1	0,1	0,1	0,1	0,2	0,2	
Dataset						
Acquisition time (UTC Shift)*	6:30	6:30	6:30	6:30	6:30	Data was collected each half hour during the measurement period.
Quality flag (CEOS flags or own definition)						
Measured/Interpolated Flag						
station4	**dataset1**	**dataset2**	**dataset3**	**dataset4**	**dataset5**	
Thanatpin						
Variable						
Quantity Name (e.g. soil moisture)*,1	Soil moisture	Soil moisture	Soil moisture	Soil moisture	Soil moisture	
Definition (e.g volumetric soil moisture)*,1	Volumetric soil moisture	Volumetric soil moisture	Volumetric soil moisture	Volumetric soil moisture	Volumetric soil moisture	
Unit (SI) (e.g. m3m-3)*,1	m3m-3	m3m-3	m3m-3	m3m-3	m3m-3	
Sensor						
Name*,1	Port 1	Port 2	Port 3	Port 4	Port 5	
Description						
Reference Document (e.g. URL)	http://publications.d	http://publication	http://publications.de	http://publications.deca	http://publications.decagon.com/Manuals/14640_GS1_Web.pdf	
Producer	Decagon	Decagon	Decagon	Decagon	Decagon	
Type	GS1	GS1	GS1	GS1	GS1	
Sensor position (horizontal/vertical)*,1	Vertical	Horizontal	Horizontal	Horizontal	Horizontal	
Depth (if measured horizontally, "from" and "to" are identical)						
From*,1	0,01	0,1	0,1	0,2	0,2	
To*,1	0,1	0,1	0,1	0,2	0,2	
Dataset						
Acquisition time (UTC Shift)*	6:30	6:30	6:30	6:30	6:30	Data was collected each half hour during the measurement period.
Quality flag (CEOS flags or own definition)						
Measured/Interpolated Flag						

Figure B.4: Metdata 2017 and 2020 network

Data implentable in the ISMN
Soil moisture (different depths)*,1
Meteorological variables: soil temperature and soil suction (different depths), surface temperature, air temperature, precipitation, snow depth, snow water equivalent,1
Soil properties: porosity, bulk density, organic matter content, texture (different depths, mandatory when SM is provided not in volumetric definition)*
Site properties: land cover, land use, climate class

station1	dataset1	dataset2	dataset3	dataset4	dataset5	dataset6	dataset7	dataset8
Irrigation Technology Centre								
Variable								
Quantity Name (e.g. soil moisture)*,1	Soil moisture	Soil moisture	Soil moisture	Soil moisture	Soil moisture	Soil moisture	Soil temperature	EC
Definition (e.g volumetric soil moisture)*,1	Volumetric soil moisture	Volumetric soil moisture	Volumetric soil moisture	Volumetric soil moisture	Volumetric soil moisture	Volumetric soil moisture	Soil temperature	Saturation extract EC
Unit (SI) (e.g. m3m-3)*,1	m3m-3	m3m-3	m3m-3	m3m-3	m3m-3	m3m-3	°C	mScm-1
Sensor								
Name*,1	Sensor 1	Sensor 2	Sensor 3	Sensor 4	Sensor 5	Sensor 6		
Description								
Reference Document (e.g. URL)	http://publications.d	http://publication	http://publications.de	http://publications.deca	http://publications.(	https://www.metergroup.com/environment/products/teros-12/		
Producer	Decagon	Decagon	Decagon	Decagon	Decagon	Metergroup		
Type	GS1	GS1	GS1	GS1	GS1	TEROS12		
Sensor position (horizontal/vertical)*,1	vertical	Horizontal	Horizontal	Horizontal	Horizontal	Horizontal		
Depth (if measured horizontally, "from" and "to" are identical)								
From*,1	0,01	0,1	0,2	0,1	0,2	0,2		
To*,1	0,1	0,1	0,2	0,1	0,2	0,2		
Dataset								
Acquisition time (UTC Shift)*	6:30	6:30	6:30	6:30	6:30	6:30		
Quality flag (CEOS flags or own definition)								
Measured/Interpolated Flag								

station2	dataset1	dataset2	dataset3	dataset4	dataset5	dataset6	dataset7	dataset8
Hpayargyl								
Variable								
Quantity Name (e.g. soil moisture)*,1	Soil moisture	Soil moisture	Soil moisture	Soil moisture	Soil moisture	Soil moisture	Soil temperature	EC
Definition (e.g volumetric soil moisture)*,1	Volumetric soil moisture	Volumetric soil moisture	Volumetric soil moisture	Volumetric soil moisture	Volumetric soil moisture	Volumetric soil moisture	Soil temperature	Saturation extract EC
Unit (SI) (e.g. m3m-3)*,1	m3m-3	m3m-3	m3m-3	m3m-3	m3m-3	m3m-3	°C	mScm-1
Sensor								
Name*,1	Sensor 1	Sensor 2	Sensor 3	Sensor 4	Sensor 5	Sensor 6		
Description								
Reference Document (e.g. URL)	http://publications.d	http://publication	http://publications.de	http://publications.deca	http://publications.(	https://www.metergroup.com/environment/products/teros-12/		
Producer	Decagon	Decagon	Decagon	Decagon	Decagon	Metergroup		
Type	GS1	GS1	GS1	GS1	GS1	TEROS12		
Sensor position (horizontal/vertical)*,1	Horizontal	Horizontal	Horizontal	Horizontal	Vertical	Horizontal		
Depth (if measured horizontally, "from" and "to" are identical)								
From*,1	0,2	0,1	0,2	0,1	0,01	0,2		
To*,1	0,2	0,1	0,2	0,1	0,1	0,2		
Dataset								
Acquisition time (UTC Shift)*	6:30	6:30	6:30	6:30	6:30	6:30		
Quality flag (CEOS flags or own definition)								
Measured/Interpolated Flag								

Figure B.5: Metdata 2017 and 2020 network

station3	dataset1	dataset2	dataset3	dataset4	dataset5	dataset6	dataset7	dataset8
Alaigni								
Variable								
Quantity Name (e.g. soil moisture)*,1	Soil moisture	Soil moisture	Soil moisture	Soil moisture	Soil moisture	Soil moisture	Soil temperature	EC
Definition (e.g volumetric soil moisture)*,1	Volumetric soil moisture	Volumetric soil moisture	Volumetric soil moisture	Volumetric soil moisture	Volumetric soil moisture	Volumetric soil moisture	Soil temperature	Saturation extract EC
Unit (SI) (e.g. m3m-3)*,1	m3m-3	m3m-3	m3m-3	m3m-3	m3m-3	m3m-3	°C	mScm-1
Sensor								
Name*,1	Sensor 1	Sensor 2	Sensor 3	Sensor 4	Sensor 5	Sensor 6		
Description								
Reference Document (e.g. URL)	http://publications.d	http://publication	http://publications.de	http://publications.deca	http://publications.(	https://www.metergroup.com/environment/products/teros-12/		
Producer	Decagon	Decagon	Decagon	Decagon	Decagon	Metergroup		
Type	GS1	GS1	GS1	GS1	GS1	TEROS12		
Sensor position (horizontal/vertical)*,1	Horizontal	Horizontal	Horizontal	Horizontal	Vertical	Horizontal		
Depth (if measured horizontally, "from" and "to" are identical)								
From*,1	0,2	0,1	0,2	0,1	0,01	0,2		
To*,1	0,2	0,1	0,2	0,1	0,1	0,2		
Dataset								
Acquisition time (UTC Shift)*	6:30	6:30	6:30	6:30	6:30	6:30		
Quality flag (CEOS flags or own definition)								
Measured/Interpolated Flag								

station4	dataset1	dataset2	dataset3	dataset4	dataset5	dataset6	dataset7	dataset8
Thanatpin								
Variable								
Quantity Name (e.g. soil moisture)*,1	Soil moisture	Soil moisture	Soil moisture	Soil moisture	Soil moisture	Soil moisture	Soil temperature	EC
Definition (e.g volumetric soil moisture)*,1	Volumetric soil moisture	Volumetric soil moisture	Volumetric soil moisture	Volumetric soil moisture	Volumetric soil moisture	Volumetric soil moisture	Soil temperature	Saturation extract EC
Unit (SI) (e.g. m3m-3)*,1	m3m-3	m3m-3	m3m-3	m3m-3	m3m-3	m3m-3	°C	mScm-1
Sensor								
Name*,1	Sensor 1	Sensor 2	Sensor 3	Sensor 4	Sensor 5	Sensor 6		
Description								
Reference Document (e.g. URL)	http://publications.d	http://publication	http://publications.de	http://publications.deca	http://publications.(	https://www.metergroup.com/environment/products/teros-12/		
Producer	Decagon	Decagon	Decagon	Decagon	Decagon	Metergroup		
Type	GS1	GS1	GS1	GS1	GS1	TEROS12		
Sensor position (horizontal/vertical)*,1	Horizontal	Horizontal	Horizontal	Horizontal	Vertical	Horizontal		
Depth (if measured horizontally, "from" and "to" are identical)								
From*,1	0,2	0,1	0,2	0,1	0,01	0,2		
To*,1	0,2	0,1	0,2	0,1	0,1	0,2		
Dataset								
Acquisition time (UTC Shift)*	6:30	6:30	6:30	6:30	6:30	6:30		
Quality flag (CEOS flags or own definition)								
Measured/Interpolated Flag								

Figure B.6: Metdata 2017 and 2020 network

variable	flag category	flag	flag is set if following condition is met
soil moisture	C - reported value exceeds output format field size	C01	soil moisture < 0.0 m^3/m^3
		C02	soil moisture > 0.6 m^3/m^3
		C03	soil moisture > saturation point (derived from HWSD parameter values)
	D - questionable/dubious - geophysical based	D01	in situ soil temperature(*) < 0°C
		D02	in situ air temperature < 0°C
		D03	GLDAS soil temperature(*) < 0°C
		D04	soil moisture shows peaks without precipitation event (in situ) in the preceeding 24 hours
		D05	soil moisture shows peaks without precipitation event (GLDAS) in the preceeding 24 hours
	D - questionable/dubious - spectrum based	D06	a spike is detected in soil moisture spectrum
		D07	a negative jump is detected in soil moisture spectrum
		D08	a positive jump is detected in

variable	flag category	flag	flag is set if following condition is met
			soil moisture spectrum
		D09	low constant values (for a minimum time of 12 hours) occur in soil moisture spectrum
		D10	saturated plateau (for a minimum time length of 12 hours) occurs in soil moisture spectrum
			(*) at corresponding depth layer
soil temperature	C - reported value exceeds output format field size	C01	soil temperature < -60°C
		C02	soil temperature > 60°C
soil surface temperature	C - reported value exceeds output format field size	C01	soil surface temperature < -60°C
		C02	soil surface temperature > 60°C
air temperature	C - reported value exceeds output format field size	C01	air temperature < -60°C
		C02	air temperature > 60°C
precipitation	C - reported value exceeds output format field size	C01	precipitation < 0 mm/h
		C02	precipitation > 100 mm/h
soil suction	C - reported value exceeds output format field size	C01	soil suction < 0 kPa
		C02	soil suction > 2500 kPa

variable	flag category	flag	flag is set if following condition is met
snow water equivalent	C - reported value exceeds output format field size	C01	snow water equivalent < 0 mm
snow depth	C - reported value exceeds output format field size	C01	snow depth < 0 mm
all dynamic variables		M	parameter value missing
		G	good

C

Additional plots

Intercomparison plots

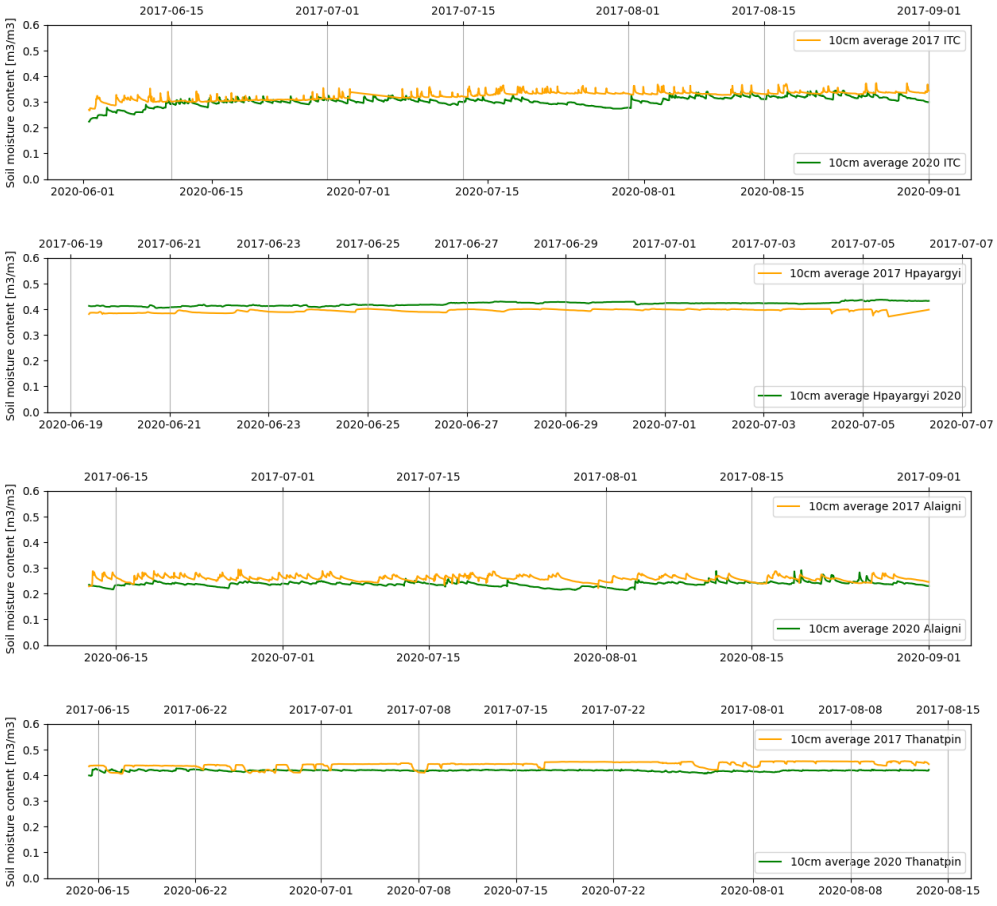

Figure C.1: Visual comparison of the measured soil moisture content by the 2017 in-situ network and the 2020 in-situ network

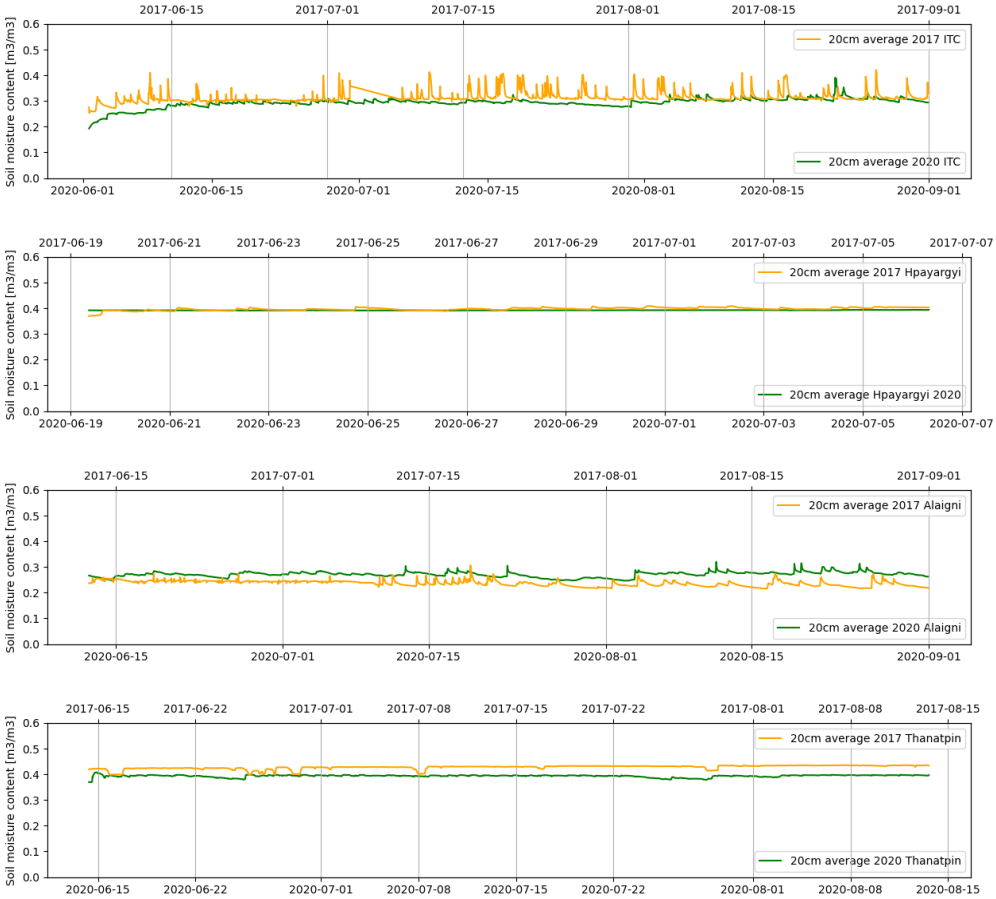

Figure C.2: Visual comparison of the measured soil moisture content by the 2017 in-situ network and the 2020 in-situ network

Sensitivity plots

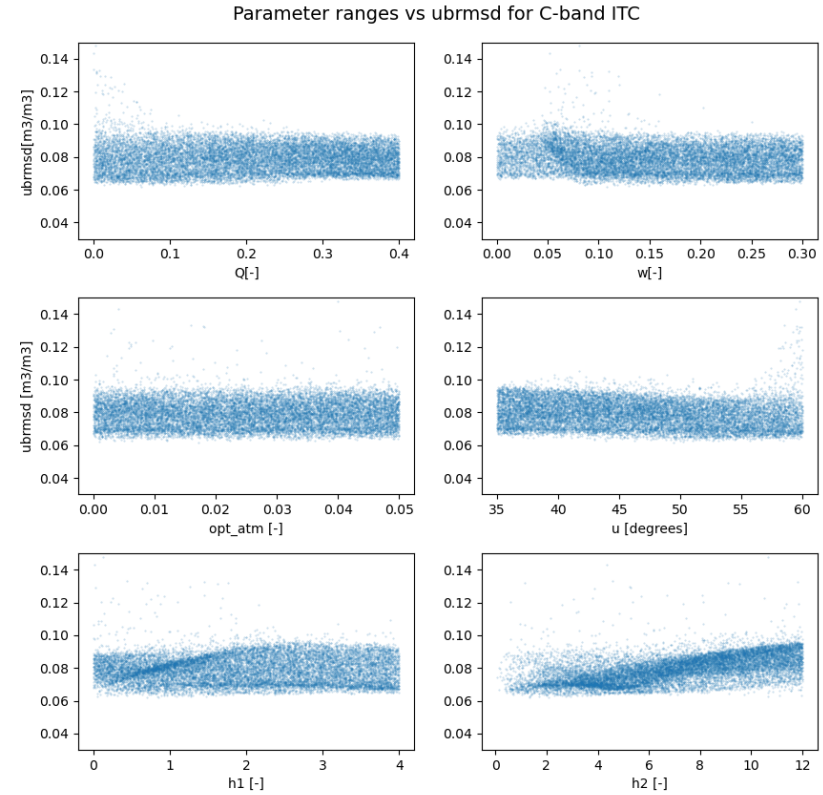
Parameter ranges vs ubrmsd for C-band ITC
ubrmsd[m3/m3]
Q[-]
w[-]
ubrmsd [m3/m3]
opt_atm [-]
u [degrees]
h1 [-]
h2 [-]

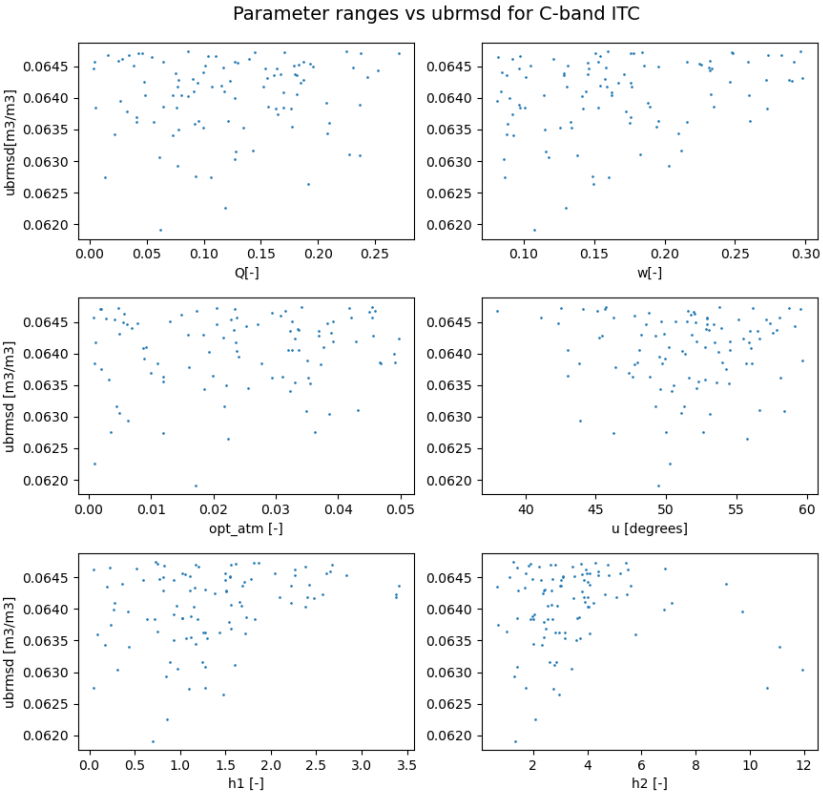
Parameter ranges vs ubrmsd for C-band ITC
ubrmsd[m3/m3]
Q[-]
w[-]
ubrmsd [m3/m3]
opt_atm [-]
u [degrees]
h1 [-]
h2 [-]

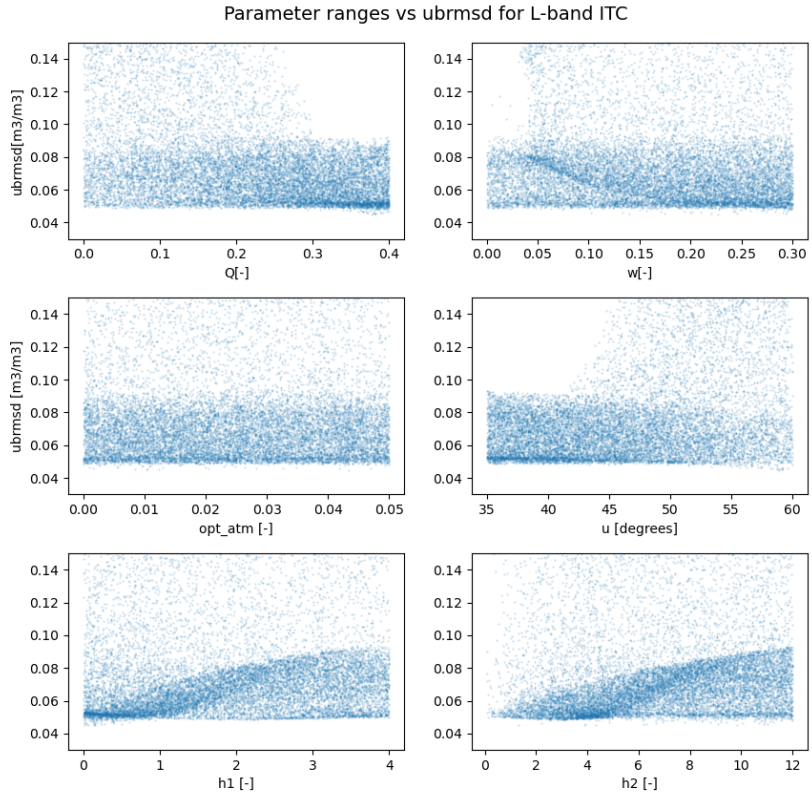
Parameter ranges vs ubrmsd for L-band ITC
ubrmsd[m3/m3]
Q[-]
w[-]
ubrmsd [m3/m3]
opt_atm [-]
u [degrees]
h1 [-]
h2 [-]

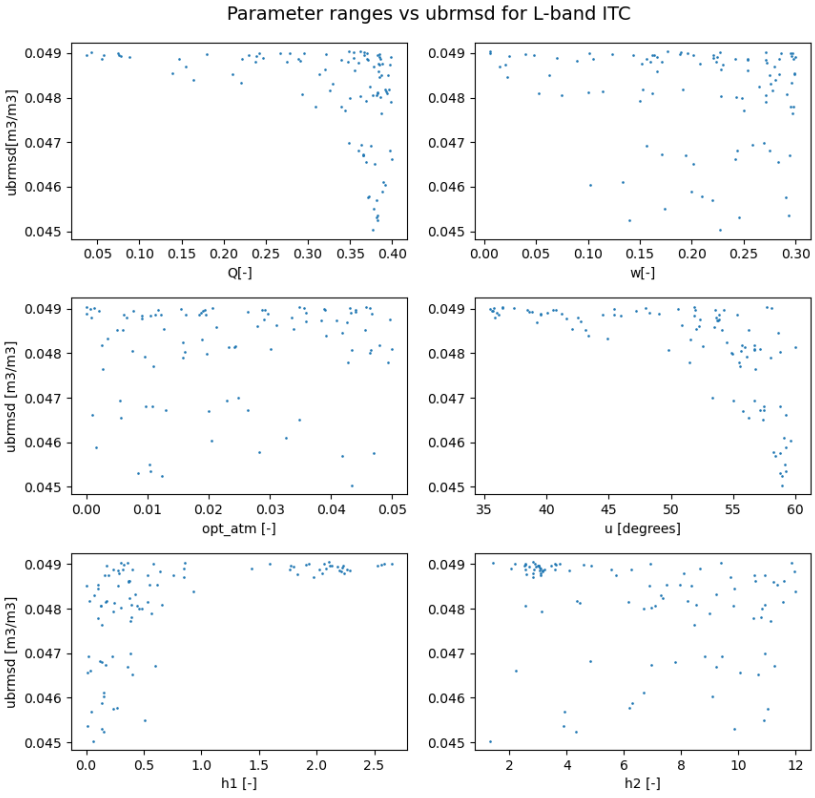
Parameter ranges vs ubrmsd for L-band ITC
ubrmsd[m3/m3]
Q[-]
w[-]
ubrmsd [m3/m3]
opt_atm [-]
u [degrees]
h1 [-]
h2 [-]

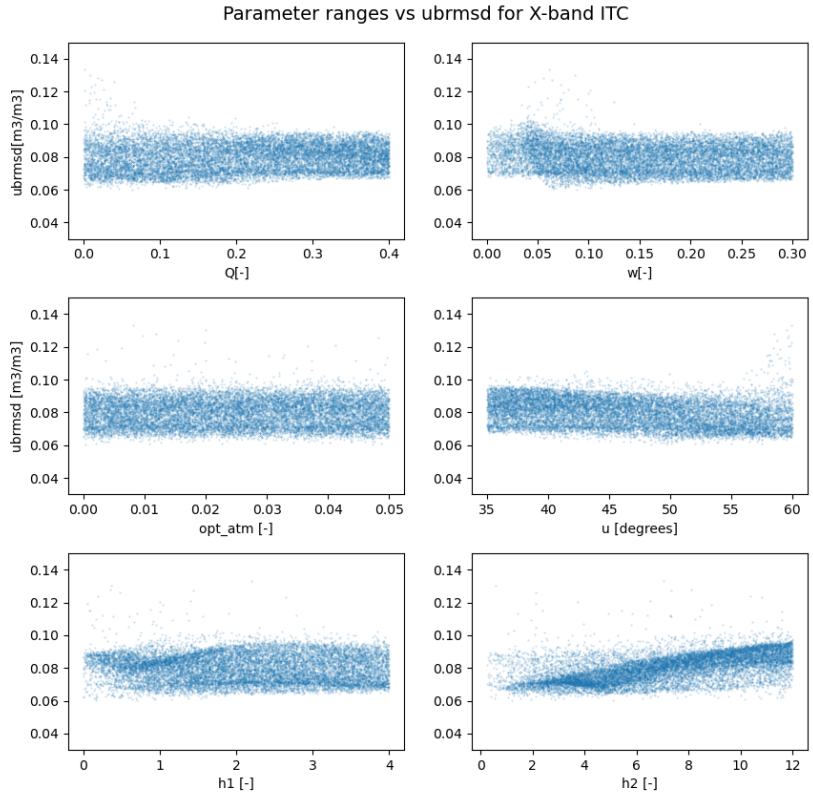
Parameter ranges vs ubrmsd for X-band ITC
ubrmsd[m3/m3]
Q[-]
w[-]
ubrmsd [m3/m3]
opt_atm [-]
u [degrees]
h1 [-]
h2 [-]

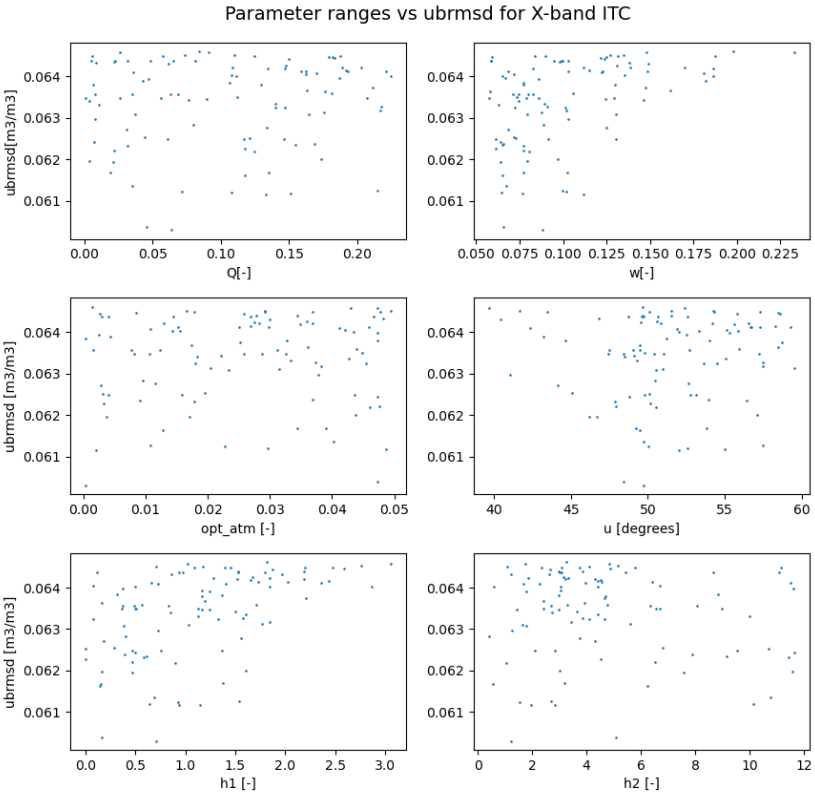
Parameter ranges vs ubrmsd for X-band ITC
ubrmsd[m3/m3]
Q[-]
w[-]
ubrmsd [m3/m3]
opt_atm [-]
u [degrees]
h1 [-]
h2 [-]

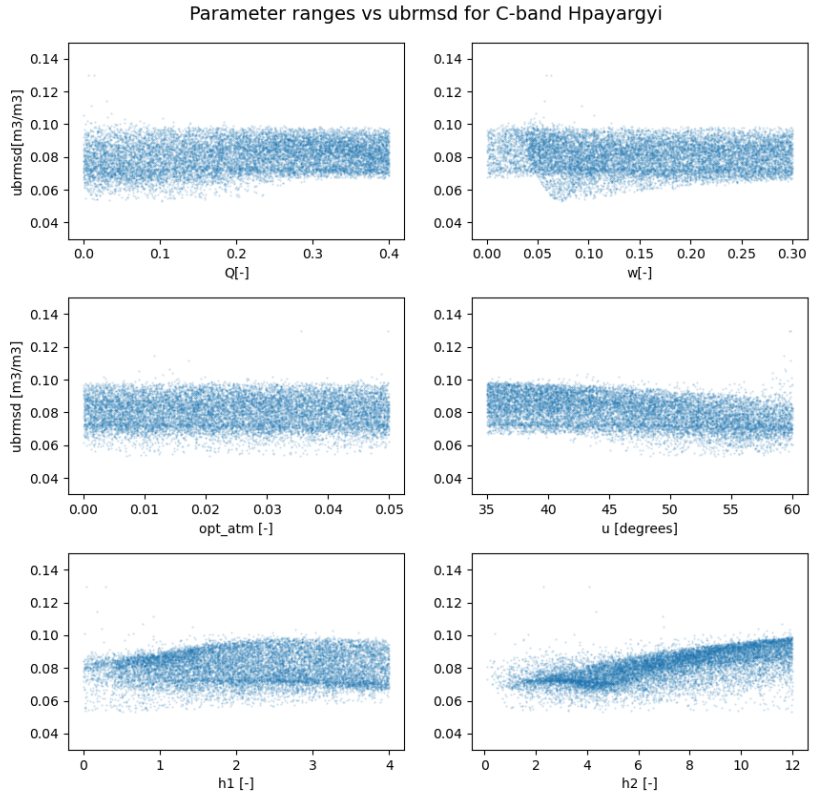
Parameter ranges vs ubrmsd for C-band Hpayargyi
ubrmsd[m3/m3]
Q[-]
w[-]
ubrmsd [m3/m3]
opt_atm [-]
u [degrees]
h1 [-]
h2 [-]

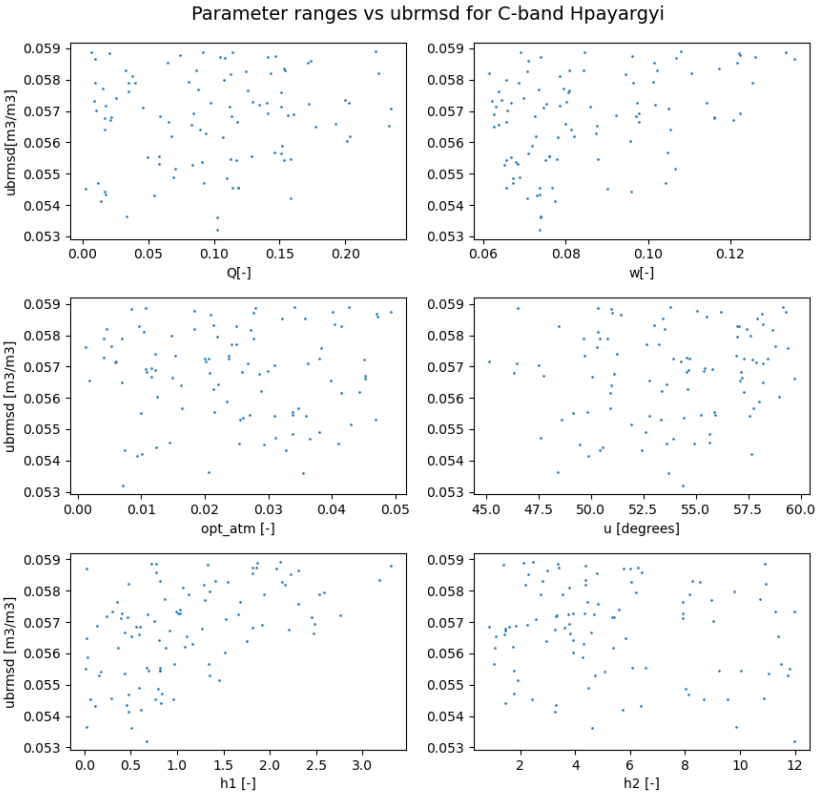
Parameter ranges vs ubrmsd for C-band Hpayargyi
ubrmsd[m3/m3]
Q[-]
w[-]
ubrmsd [m3/m3]
opt_atm [-]
u [degrees]
h1 [-]
h2 [-]

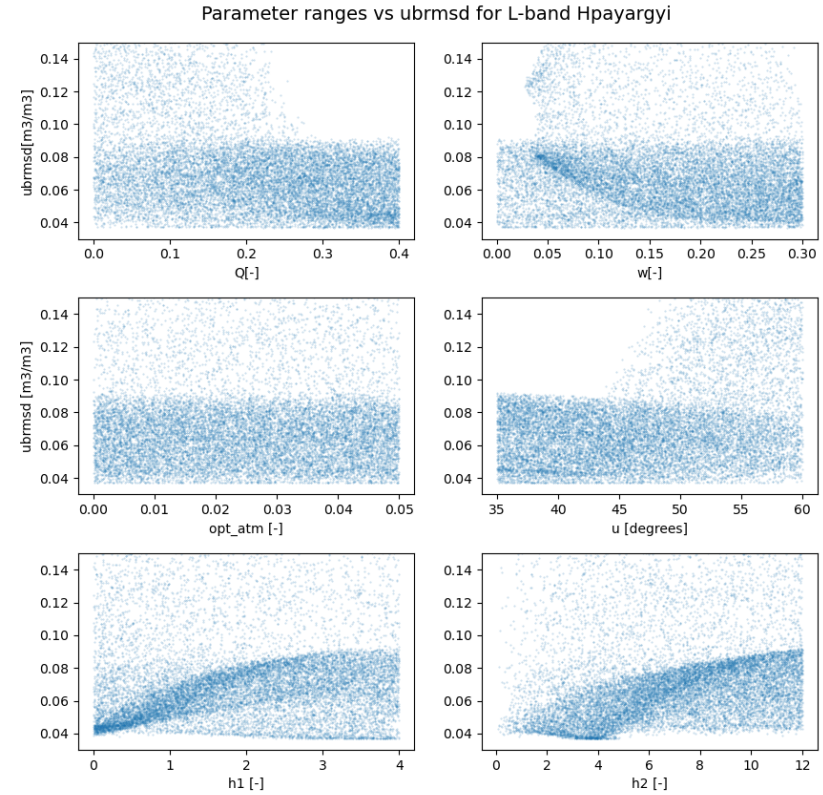
Parameter ranges vs ubrmsd for L-band Hpayargyi
ubrmsd[m3/m3]
Q[-]
w[-]
ubrmsd [m3/m3]
opt_atm [-]
u [degrees]
h1 [-]
h2 [-]

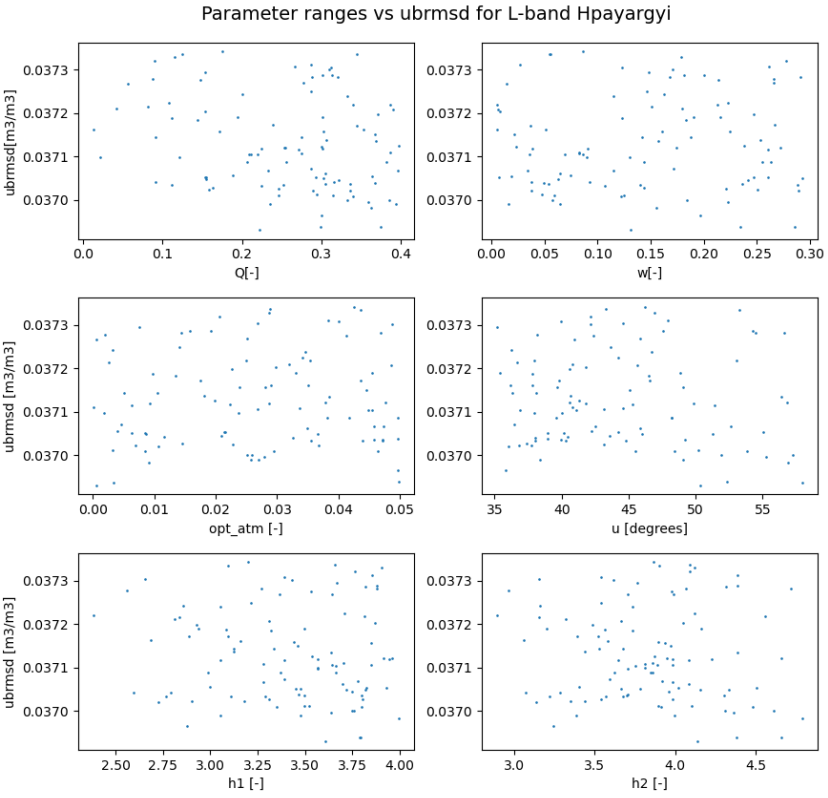
Parameter ranges vs ubrmsd for L-band Hpayargyi
ubrmsd[m3/m3]
Q[-]
w[-]
ubrmsd [m3/m3]
opt_atm [-]
u [degrees]
h1 [-]
h2 [-]

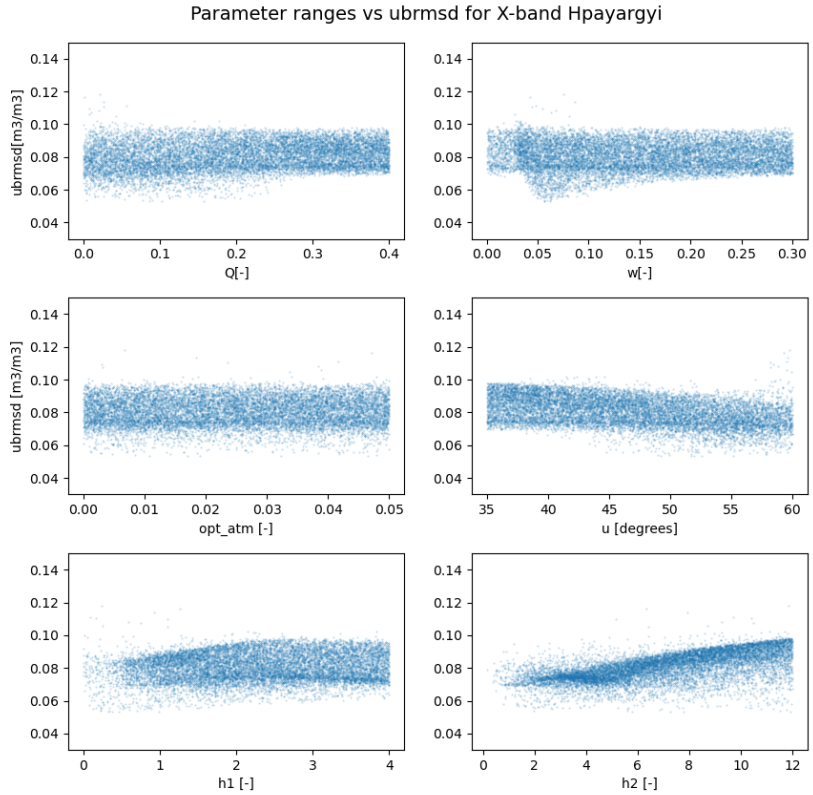
Parameter ranges vs ubrmsd for X-band Hpayargyi
ubrmsd[m3/m3]
Q[-]
w[-]
ubrmsd [m3/m3]
opt_atm [-]
u [degrees]
h1 [-]
h2 [-]

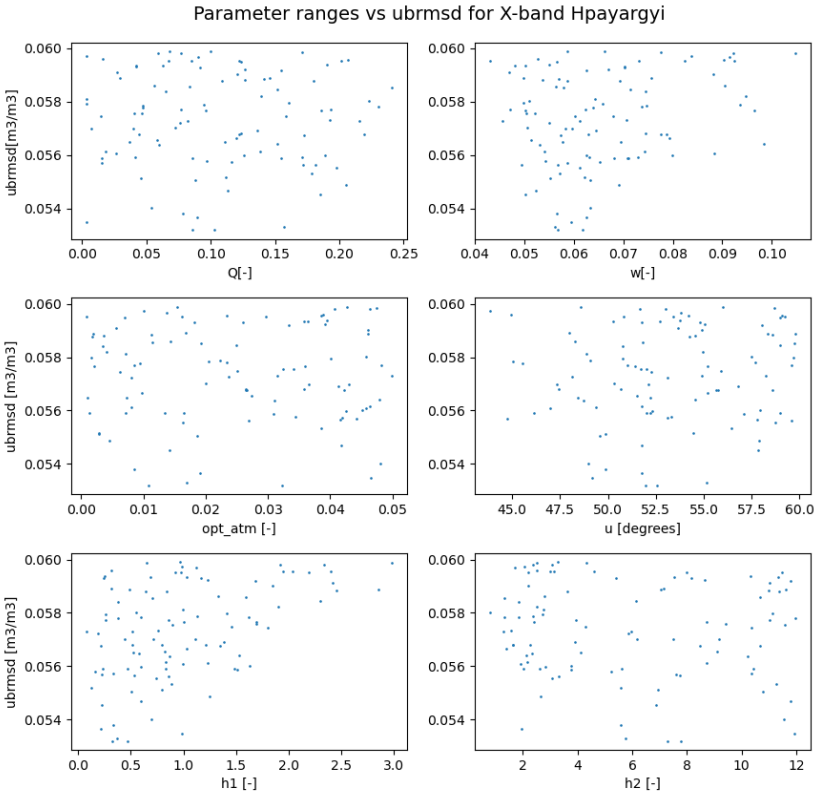
Parameter ranges vs ubrmsd for X-band Hpayargyi
ubrmsd[m3/m3]
Q[-]
w[-]
ubrmsd [m3/m3]
opt_atm [-]
u [degrees]
h1 [-]
h2 [-]

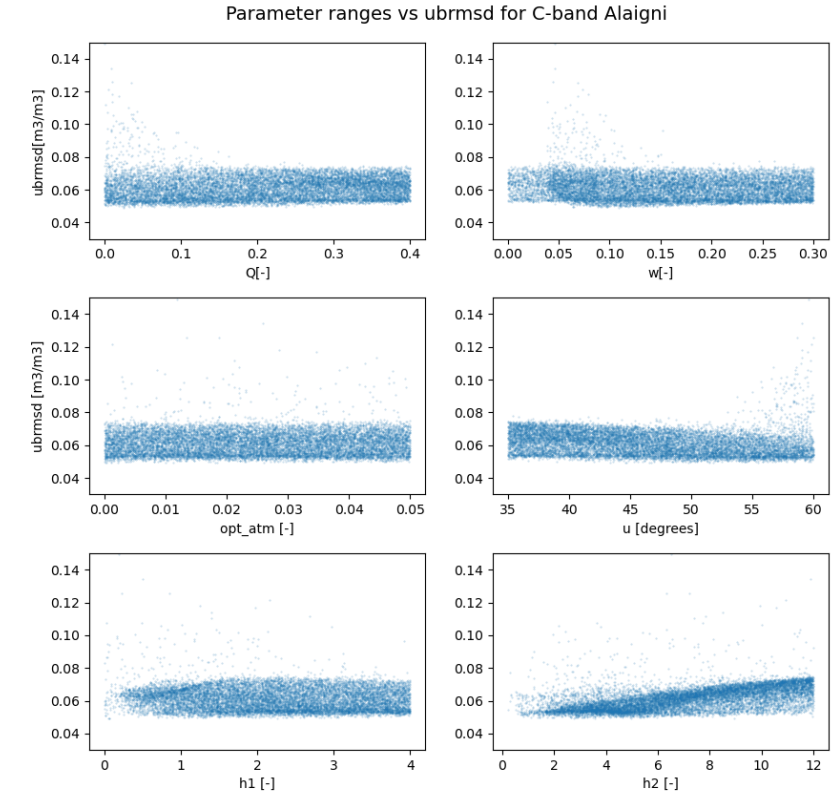
Parameter ranges vs ubrmsd for C-band Alaigni
ubrmsd[m3/m3]
Q[-]
w[-]
ubrmsd [m3/m3]
opt_atm [-]
u [degrees]
h1 [-]
h2 [-]

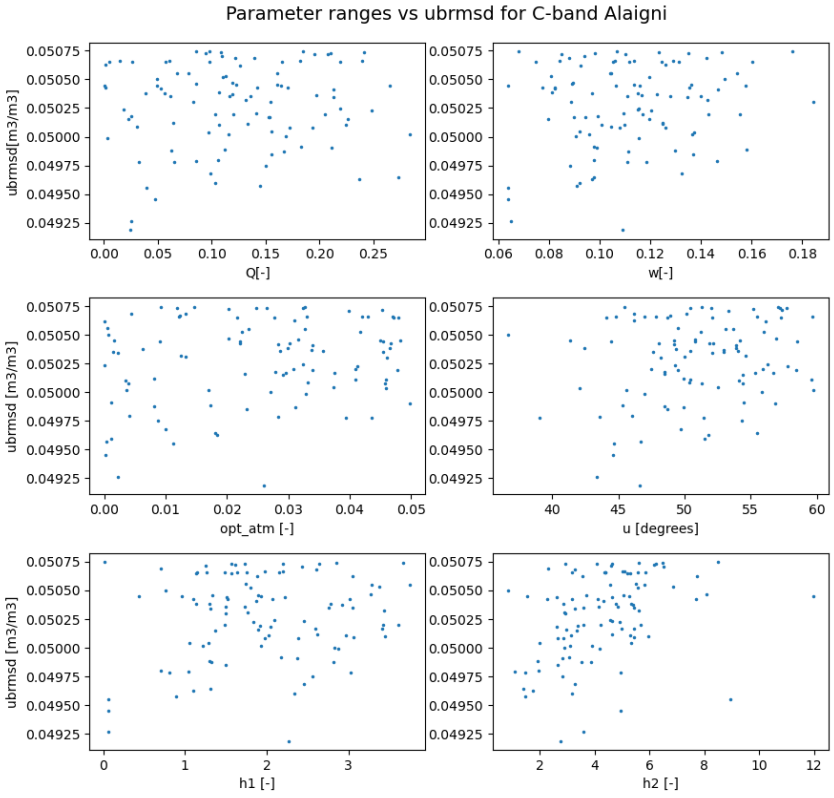
Parameter ranges vs ubrmsd for C-band Alaigni
ubrmsd[m3/m3]
Q[-]
w[-]
ubrmsd [m3/m3]
opt_atm [-]
u [degrees]
h1 [-]
h2 [-]

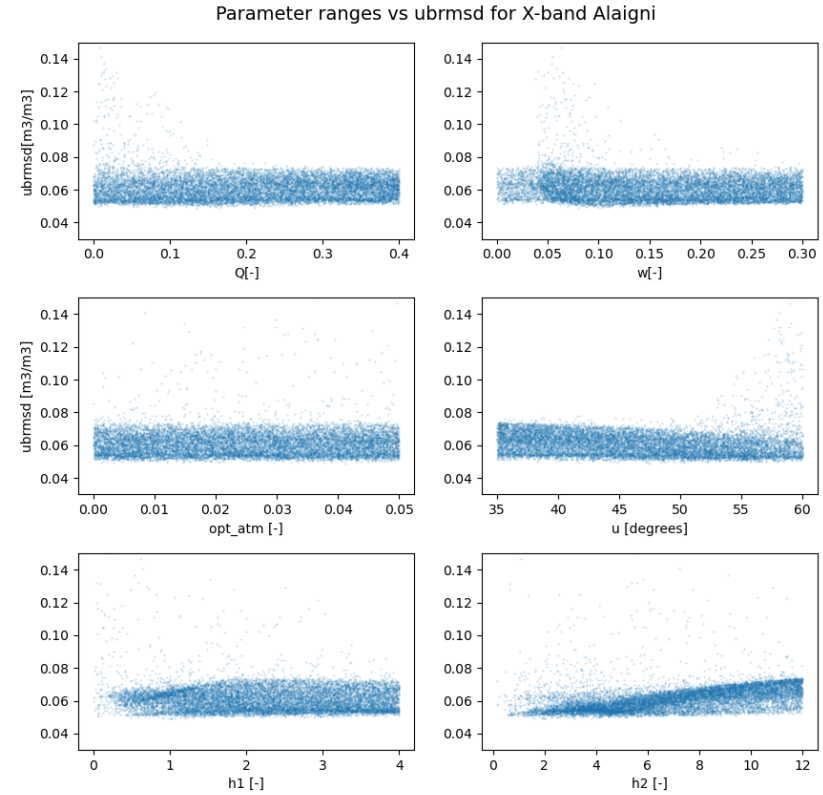
Parameter ranges vs ubrmsd for X-band Alaigni
ubrmsd[m3/m3]
Q[-]
w[-]
ubrmsd [m3/m3]
opt_atm [-]
u [degrees]
h1 [-]
h2 [-]

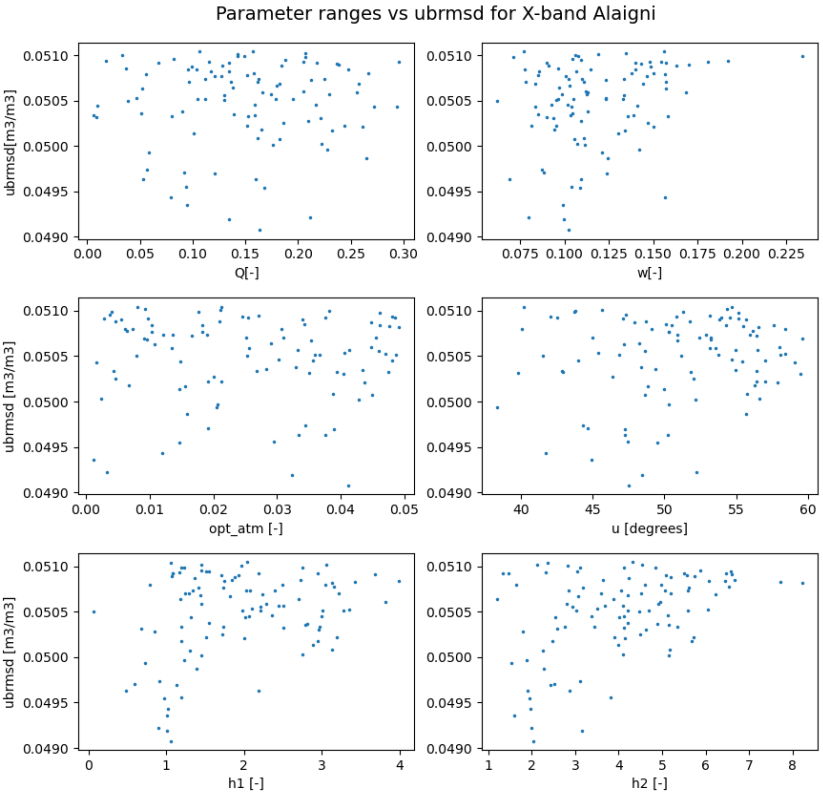
Parameter ranges vs ubrmsd for X-band Alaigni
ubrmsd[m3/m3]
Q[-]
w[-]
ubrmsd [m3/m3]
opt_atm [-]
u [degrees]
h1 [-]
h2 [-]

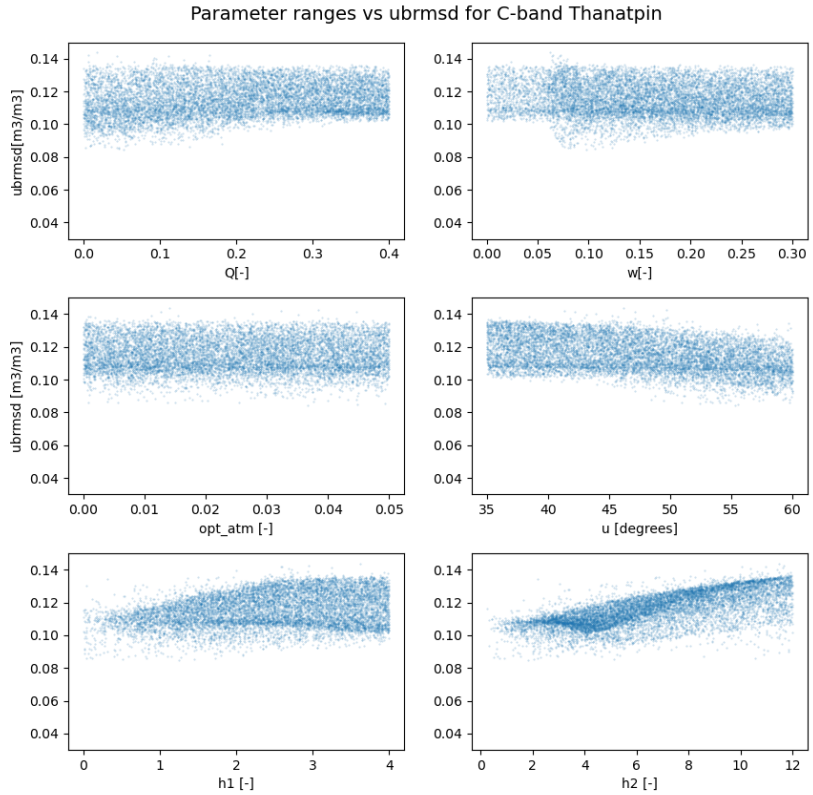
Parameter ranges vs ubrmsd for C-band Thanatpin
ubrmsd[m3/m3]
Q[-]
w[-]
ubrmsd [m3/m3]
opt_atm [-]
u [degrees]
h1 [-]
h2 [-]

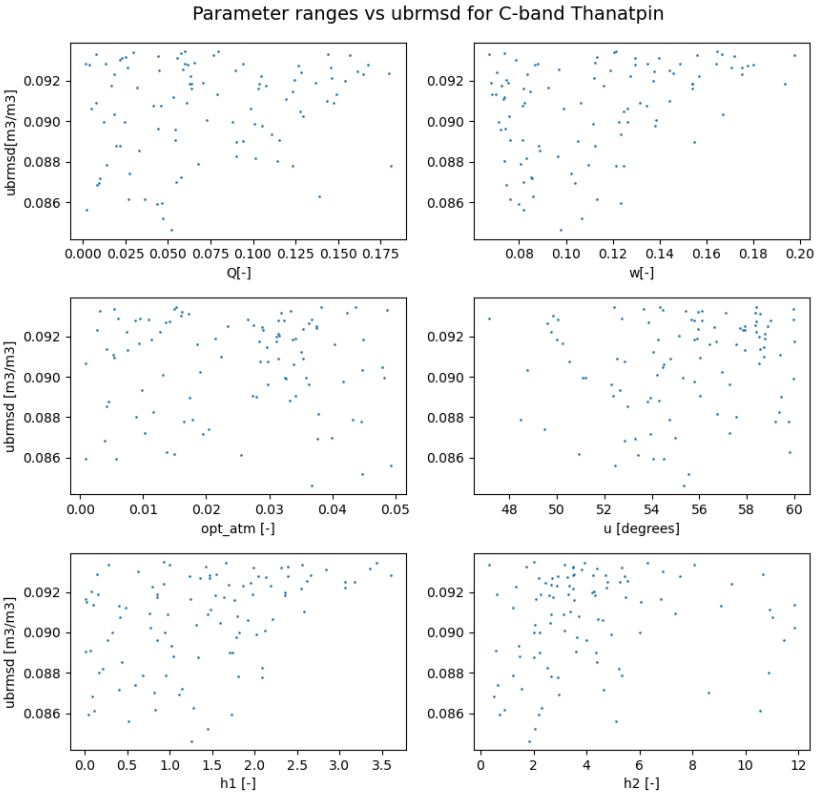
Parameter ranges vs ubrmsd for C-band Thanatpin
ubrmsd[m3/m3]
Q[-]
w[-]
ubrmsd [m3/m3]
opt_atm [-]
u [degrees]
h1 [-]
h2 [-]

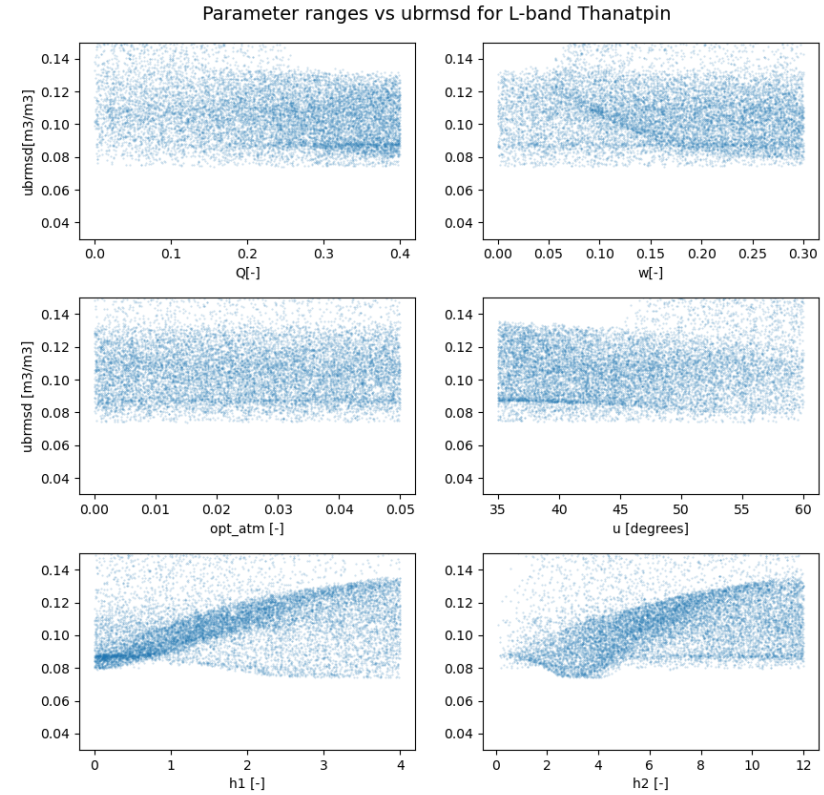
Parameter ranges vs ubrmsd for L-band Thanatpin
ubrmsd[m3/m3]
Q[-]
w[-]
ubrmsd [m3/m3]
opt_atm [-]
u [degrees]
h1 [-]
h2 [-]

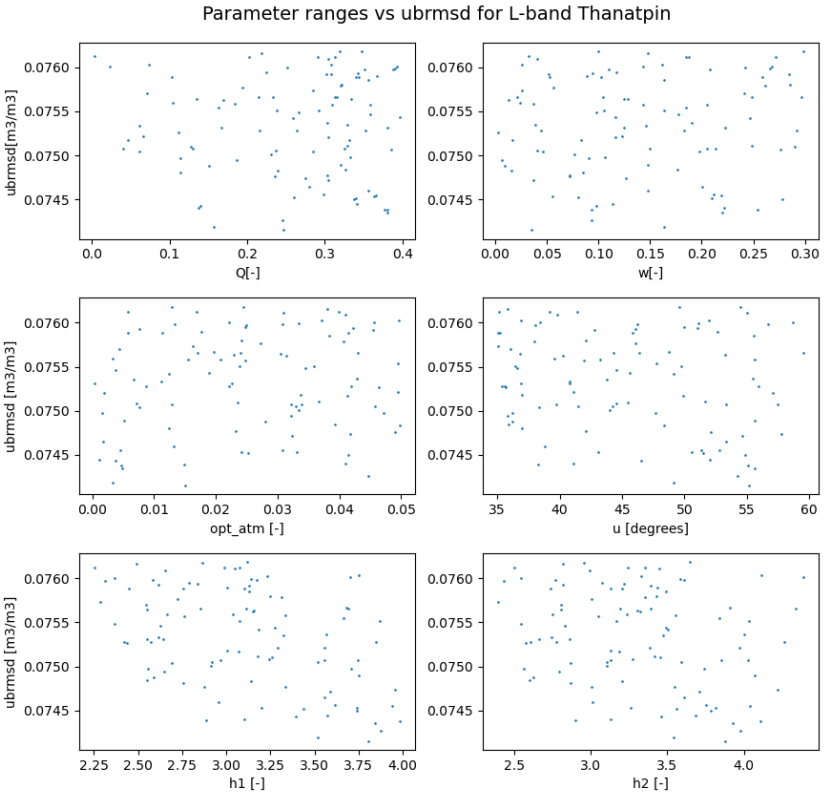
Parameter ranges vs ubrmsd for L-band Thanatpin
ubrmsd[m3/m3]
Q[-]
w[-]
ubrmsd [m3/m3]
opt_atm [-]
u [degrees]
ubrmsd [m3/m3]
h1 [-]
h2 [-]

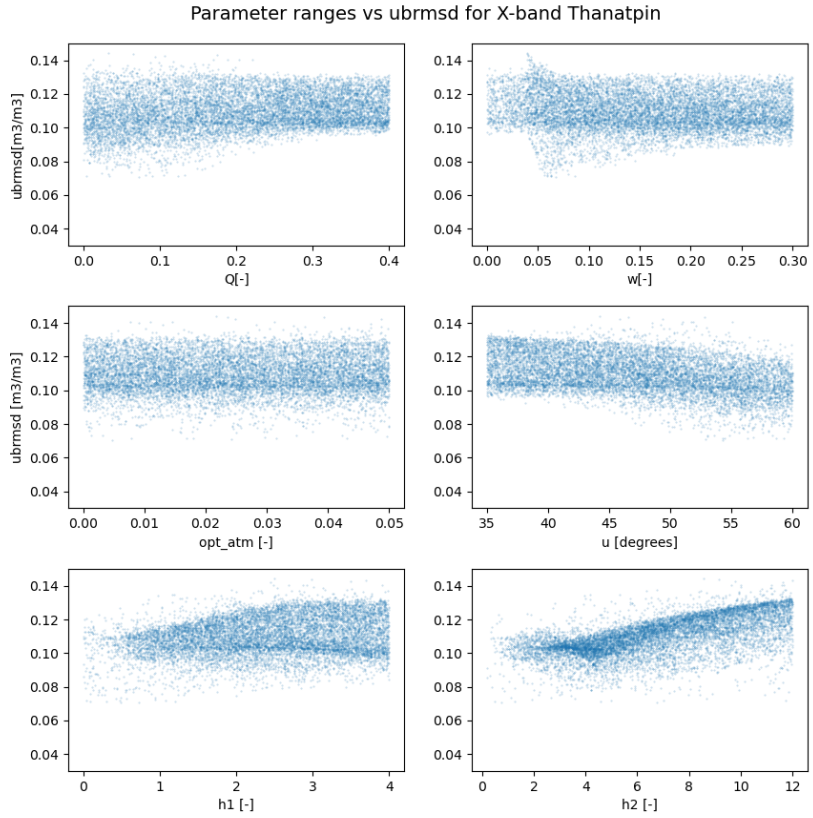
Parameter ranges vs ubrmsd for X-band Thanatpin
ubrmsd[m3/m3]
Q[-]
w[-]
ubrmsd [m3/m3]
opt_atm [-]
u [degrees]
h1 [-]
h2 [-]

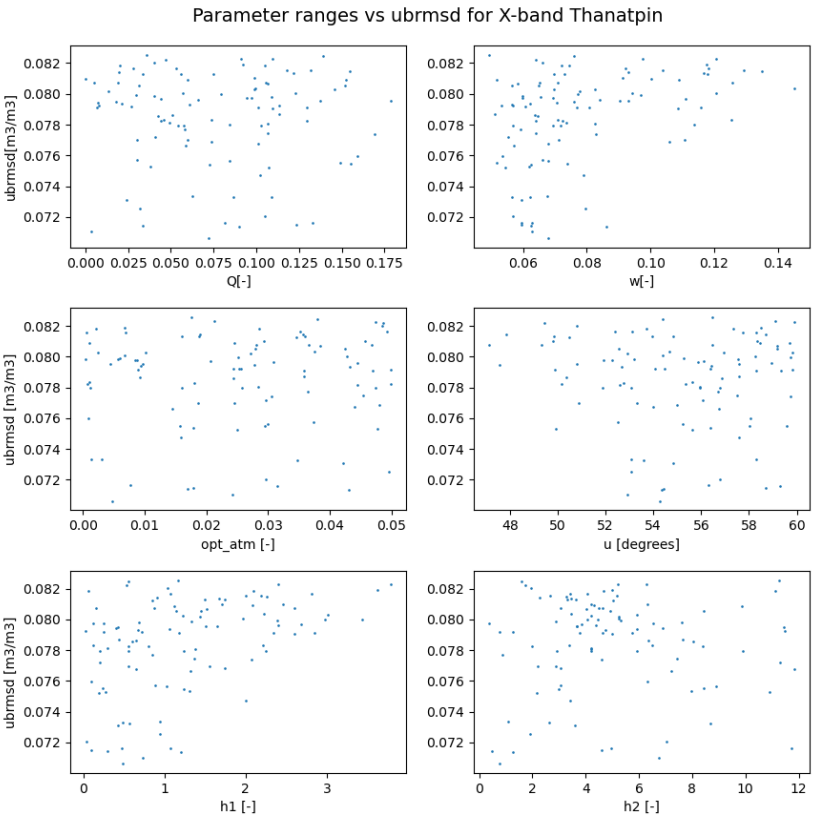
Parameter ranges vs ubrmsd for X-band Thanatpin
ubrmsd[m3/m3]
Q[-]
w[-]
ubrmsd [m3/m3]
opt_atm [-]
u [degrees]
h1 [-]
h2 [-]